STRATEGIES TO IMPROVE MALARIA DIAGNOSTICS AT THE POINT OF CARE BY UNDERSTANDING PROTEIN BEHAVIOR AND DEVELOPING LOW-RESOURCE DNA DETECTION METHODS

By

Anna Lynn Bitting

Dissertation

Submitted to the Faculty of the

Graduate School of Vanderbilt University

in partial fulfillment of the requirements

for the degree of

DOCTOR OF PHILOSOPHY

in

Chemistry

May 2017

Nashville, Tennessee

Approved:

David W. Wright, Ph.D.

David E. Cliffel, Ph.D.

Janet E. Macdonald, Ph.D.

Raymond L. Mernaugh, Ph.D.

ACKNOWLEDGEMENTS

As I look back at my graduate school career, I am proud of how much I have accomplished and how far I have grown, but of course I could not have done it without a lot of help and support. First of all, I have to thank my advisor, Professor David Wright. Your mentorship and advice have helped me become a better scientist and learn to tell the "story" of my research. I would also like to thank my committee members, Professors David Cliffel, Janet Macdonald, and Ray Mernaugh. I appreciate your scientific advice, support, and mentorship. I must also thank my frequent collaborator Professor Rick Haselton. Your alternative perspective on research has helped me think abstractly.

I also have to thank my fellow Wright Lab members, both past and present. From talking to other graduate students at Vanderbilt and at other universities, I know that not every lab is as supportive and fun as ours. We have such a diverse set of knowledge in the lab, and everyone is always willing to share their expertise, bounce ideas around, and tear down and rebuild exam talks. I feel so lucky to have met you crazy folks, and I'm especially lucky to call so many of you my friends as well as colleagues. Keersten – I couldn't have asked for a better rotation mentor, and I'm so happy we became friends as well. Getting through grad school was a lot less scary with your help and guidance. Jenny – From Live on the Green to watching Nashville the TV show, we had a ton of fun. You helped me learn to take some things in life a little less seriously, and for that I am grateful. Wes – Baymate! Thanks for hashing out experiments with me and motivating me when I needed a kick in the ass. I'm so thankful for your encouragement. Also, thanks for putting up with my messy desk and aversion to direct sunlight. Stevie – I learned so

much about our lab culture from you, and I've tried to emulate your example as a senior grad student. Thank you for being a supportive colleague and friend, and for being blunt when necessary. Chris – Thanks for being my first baymate and helping me gain direction in my first year. Your advice was invaluable. Alexis – I'm glad I've gotten to know you better over the last few years, especially because your sass, wisdom, and Starbucks/CVS runs help keep lab fun. Your gold nanoparticle knowledge is priceless; thank you for sharing some of it with me. Christine – Thank you for keeping the lab going and organized, and stepping up when necessary. Thanks for editing all my documents and being a great friend. Lauren – Thanks for being funny, kind, and level-headed, and for making me go to Devil's Pool. Adam – I always appreciate your unique outlook, your peptide synthesizer wisdom, your sass, and the gossip you bring from downstairs. Andrew – Your positive outlook is a great addition to the lab, and you're a great fun activities chairperson. We're all rooting for you, so get better soon buddy. Tom – Thanks for keeping the LFA operation running and bringing in a valuable "outsider" perspective to the lab. It's been so much fun working with you. Becca – You were such a great role model of how to work hard in lab, and I know you'll achieve great things in your career. Nick – Thanks for imparting your DNA and CD knowledge to me, as well as advice on paper-writing and figure-making. Kim – Thanks for being a great labmate and always the voice of reason in debates. Abraham – You were a source for great conversation and philosophical discussion, and crazy stories. Thanks for the fun times. Joseph, Danielle, Lwiindi, and Mindy – Thanks for letting me work with VZNIGHT. Traveling to Zambia was a great life experience and I really appreciate the chance to be a part of it. Armin, Megan, and Carson – I'm so glad you guys chose the Wright Lab. Your dedication and fun spirits make me confident in the future of the lab. Finally, I would like to thank our honorary lab member, the 8th floor custodian, Greg. Your encouraging words

never failed to pick me up when I was down, and I can only hope to find friends as positive as you when I leave here.

There were many other members of the chemistry department who influenced my time here, but a few in particular stick out. Bobby and Jeremy – I had so much fun living with you. Thanks for adopting me and letting me join in all the wacky adventures and trivia time, and for being overall great friends. Evan – It took us a few years to really become friends, but I'm so glad we did. Thanks for smokin' meats and sharing the delicious results with your neighbors.

Dave – I'm so happy I found you. Thank you for supporting me, caring for me, and making me laugh these last two and a half years.

Last but certainly not least, to my family – Thanks for loving and supporting me throughout my long school career. I love you.

TABLE OF CONTENTS

LIST OF TABLES

LIST OF FIGURES

CHAPTER I

INTRODUCTION: MALARIA DIAGNOSTICS IN THE MODERN WORLD

In 2000, the United Nations made a set of Millennium Development Goals (MDGs) to guide an international partnership to reduce extreme poverty worldwide by 2015.[1] One of the targets of the MDGs was focused on halting and reversing the incidence of malaria by 2015, which has been met.[2] The World Health Organization (WHO) estimates that between 2000 and 2015, malaria incidence has decreased by 37% and malaria death rates have decreased by 60%. Furthermore, in 2000 malaria was the leading cause of death for children under 5 in sub-Saharan Africa, but by 2015 it was fourth. While this is certainly progress, malaria remains endemic in 91 countries in Africa, Asia, and the Americas[3] (**Figure 1.1**[3]). The World Health Organization

Countries endemic for malaria, 2016
Countries not endemic for malaria, 2000
Countries endemic in 2000, no longer endemic in 2016
Not applicable
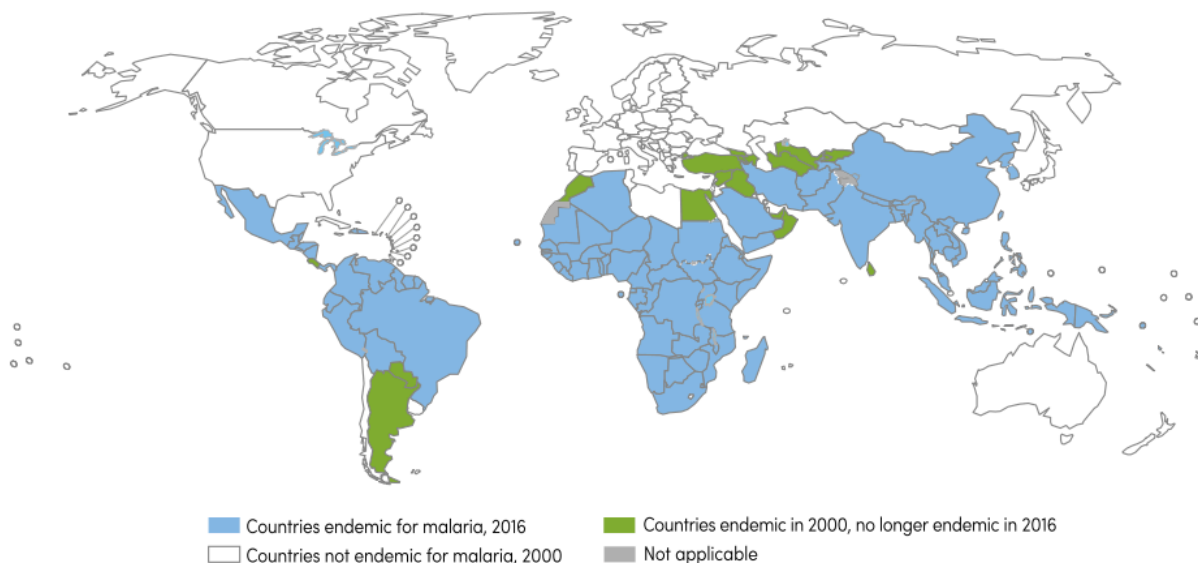
Figure 1.1.[3] *Map showing worldwide prevalence of malaria in 2016 compared to 2000.*

estimates that there were 214 million malaria cases and 438,000 malaria deaths in 2015, with roughly 88% of these cases and deaths occurring in sub-Saharan Africa, followed by Southeast Asia. It is clear that while progress is being made towards malaria elimination, this disease still remains a major health concern in tropical regions of the world.

Biology of the Malaria Parasite

Malaria in humans is caused by the *Plasmodium* parasite, transmitted by *Anopheles* mosquitos. There over 100 *Plasmodium* species, but only four species are known to cause malaria in humans, with a fifth species beginning to infect humans as well. The others infect various other mammals, birds, and even reptiles. The main species causing human malaria are *P. falciparum*, *P. vivax*, *P. ovale*, and *P. malariae*.[4] *P. falciparum* is the predominant species in Africa, though it is found in subtropical and tropical areas worldwide. It is also one of the most virulent malaria species. *P. vivax* is most common in Asia and Latin America, though it is found in some areas of Africa. This species, along with *P. ovale*, has a dormant liver stage as part of its life cycle, which can cause relapses months or years after the initial illness if not treated effectively. *P. ovale* is very similar to *P. vivax* but is found mostly in West Africa and the Western Pacific islands. *P. malariae* is found worldwide, and can cause lifelong chronic infection and kidney disease if left untreated.[5]

A malaria parasite infects two hosts, humans and female *Anopheles* mosquitos, during its full lifecycle (**Figure 1.2**[6]). When an infected female *Anopheles* mosquito bites a human and takes a blood meal, she also injects *Plasmodium* sporozoites into the human's bloodstream. These sporozoites infect the liver, where they can mature into schizonts, rupture, and release merozoites. This liver stage can last for several days or a few weeks, and results in a delay

between the mosquito bite and the development of symptoms. *P. vivax* and *P. ovale* sporozoites can also become dormant hypnozoites in the liver, and can re-activate to complete their lifecycle weeks, months, or years after the initial mosquito bite.[7] Once merozoites are released, they infect red blood cells and become trophozoites, also known as the ring stage. The trophozoites mature into schizonts that rupture, releasing merozoites again. This asexual replication is known as the erythrocytic cycle, and it is responsible for producing the symptoms of the disease. Trophozoites in the blood stage can also become gametocytes, which are ingested by a female *Anopheles* mosquito that bites an infected human. In the stomach of the mosquito, the gametocytes undergo sexual reproduction and generate zygotes, which mature into elongated, motile ookinetes. The ookinetes develop into oocysts after invading the wall of the mosquito midgut, and the oocysts grow until they rupture and release sporozoites. The sporozoites then travel to the mosquito salivary glands, where they can be injected into another human host and continue the transmission cycle.[8]
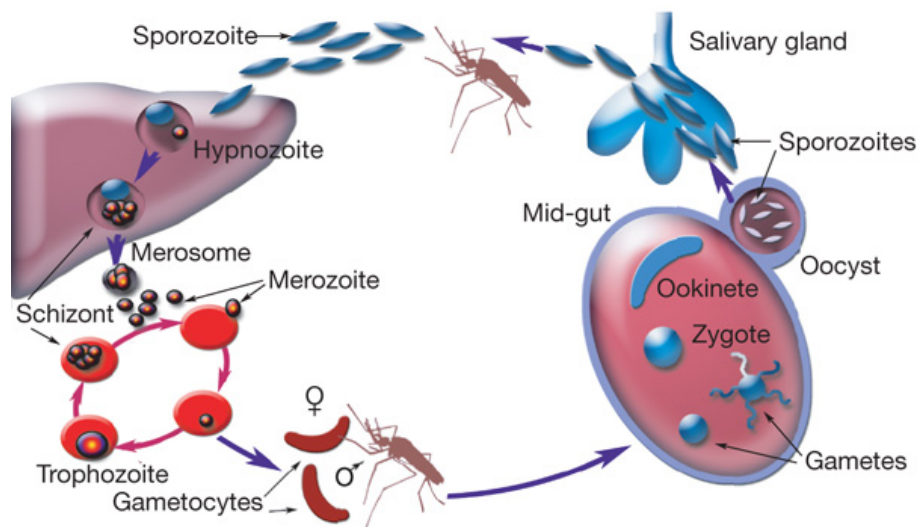
Figure 1.2.[6] *Simplified life cycle of the malaria parasite.*

Understanding this parasite biology is necessary to effectively diagnose, treat, and ultimately eliminate the transmission of malaria. Because malaria is caused by a parasite, there are many biomarkers available to diagnose its presence. The parasite itself can be a biomarker when analyzing blood via microscopy, and any proteins or DNA sequences produced by the parasite but not by humans can be used as biomarkers as well. In order to use these biomarkers most effectively, however, we must understand how the parasite, its protein expression levels, and its DNA concentrations change during the course of its lifecycle. We must also understand how the body deals with these biomarkers after the infection has been cleared. For example, several countries have reported gene deletions in *P. falciparum* for the protein biomarker *Pf*HRP2. In these regions, it would be inappropriate to use a *Pf*HRP2 test for the detection of *P. falciparum*. In regions where *Pf*HRP2 is a common biomarker, the protein has been shown to persist in a patient's blood for several weeks after parasite clearance.[9] This indicates that *Pf*HRP2 should not be used to monitor treatment effectiveness. Malaria diagnostics will have to account for these biological realities and others as the global community moves toward the WHO goal of malaria elimination.

Current Malaria Diagnostic Landscape

To guide the work of malaria elimination campaigns through 2030, the World Health Organization has released a new Global Technical Strategy (GTS) for Malaria.[10] As mentioned above, malaria is currently endemic in 95 countries. The WHO sets goals in the Global Technical Strategy to eliminate malaria from at least 10 of these countries by 2020, and at least 35 of these countries by 2030. Several of these countries are within five years of reaching their goal of malaria elimination, defined as zero new locally-transmitted infections in a geographical area. In

order to actually achieve the goals set out by WHO, the GTS outlines three "pillars" for future action. The first pillar is to "ensure universal access to malaria prevention, diagnosis, and treatment" and this is to be supported with expanded research in these areas as well.[10] While preventing and treating malaria are obvious steps toward elimination, the utility of diagnostic tests are not always apparent, even to those in the malaria community.

The most apparent reason for the need for diagnostic tests for malaria lies in the fact that malaria shares its main symptoms of fatigue, nausea, joint pain, and fever with many other diseases.[11] Therefore, diagnostics are necessary to determine the particular illness for a patient presenting with fever so that the patient can receive accurate and timely treatment. If a patient is incorrectly diagnosed with malaria based on clinical symptoms alone, they will be given antimalarial drugs that will not treat their actual illness, delaying effective treatment and allowing that illness to possibly become more serious. Diagnostic tests are also important for patients that do have malaria, because they help determine the most effective treatment available. *P. falciparum* and *P. vivax* may be treated with different combinations of drugs, because the liver stage hypnozoites of *P. vivax* must also be eliminated, so it is important to determine the species of infection.[7] *P. falciparum* resistance to the drug artemisinin has been documented in five counties in Southeast Asia, and the responsible gene mutation has been recently discovered.[3,12,13] There are no point-of-care tests for this mutation, but they will be necessary in the future for accurate treatment. Like *P. falciparum*, *P. vivax* has also developed resistance to certain drugs in certain areas, so treatment may change depending on the geographical area where the infection was acquired.[11]

The diagnosis of *P. vivax* malaria in general is expected to become more important as *P. falciparum* transmission is eliminated.[14] Most current malaria control efforts are focused on sub-

Saharan Africa, where *P. falciparum* is most present and causes the most deaths, but *P. vivax* is most prevalent in Southeast Asia and South America, where it is estimated to have caused 13.8 million cases of malaria in 2015.[2] Currently, rapid diagnostic tests that detect *P. vivax* lack the sensitivity, stability, and availability of those that detect *P. falciparum*.[14–16] This is especially important to address because *P. vivax* infections tend to show low parasitemia in comparison to *P. falciparum* infections.[7,16] There are also currently no diagnostic tests to detect the presence of hypnozoites in a patient's liver, which would be extremely helpful to monitor treatment and prevent relapses of *P. vivax*. Currently, the only "radical cure" drug for *P. vivax* that kills blood stage parasites as well as hypnozoites is primaquine, but yet another diagnostic is needed in this case to determine if the drug is safe to use for each individual patient.[7] Primaquine causes severe, often fatal, hemolytic anemia in patients with glucose-6-phosphate dehydrogenase (G6PD) deficiency, which is a common genetic abnormality ranging from 3 to 30% frequency in tropical areas.[17] Tests for G6PD deficiency require complex procedures and are expensive, so often a patient's G6PD status is unknown. In these cases, the risk of administering primaquine must be balanced with the benefit of eliminating the risk of relapse. A point-of-care G6PD test will ultimately be necessary to control and eliminate *P. vivax*.

As the world moves towards malaria elimination, it will become imperative to diagnose low parasitemia infections of all malaria species. Especially in low-transmission areas, it is quite common for people to be infected with low-density parasitemia that does not produce symptoms and is undetectable with typical field diagnostic tests.[10,14] These asymptomatic individuals can still transmit the disease to mosquitos, however, and unknowingly contribute to sustaining the parasite by acting as a disease reservoir.[11,18,19] There is debate about the parasitemia cut-off between asymptomatic and symptomatic infections, but it is generally accepted that

asymptomatic infections occur at parasite densities of 200 p/μL or less. This threshold can vary

by individual, however, partly due to immunological differences in infected individuals, and

partly due to the complexities of the parasite lifecycle. While high parasitemia generally

correlates with disease severity, the densities of circulating parasites and sequestered parasites

can change depending on the lifecycle stage of the parasites and their synchronicity.[20] Even

though asymptomatic infections are by definition difficult to diagnose, it is necessary to diagnose

and treat these infections in order to reach the goal of malaria elimination.

Diagnostic Method	LOD	Biomarker	Cost	Time
Light Microscopy	5 – 20 parasites/μL	Parasites	$$	30 minutes
PCR	0.1 – 5 parasites/μL	Genetic material	$$$$	2 – 4 hours
Rapid Diagnostic Tests	100 – 200 parasites/μL	Protein	$	20 minutes

Figure 1.3. *Various malaria diagnostic techniques.*

Current diagnostics detect malaria parasites using proteins, nucleic acids, or the parasite

itself as biomarkers (**Figure 1.3**). The current "gold standard" diagnostic technique is

microscopy, where a stained blood sample is examined under a microscope to count the parasites

present. Microscopy is a much more accessible diagnostic technique than PCR, because even

small rural health clinics can often afford a small microscope, slides, and stain. However,

technical expertise is still required for an accurate diagnosis, so the necessary training for clinicians can increase the overall cost of the test. This technique also has a variable limit of detection due to its dependence on the skill of the microscopist. The most sensitive diagnostic technique available is polymerase chain reaction (PCR), which can detect DNA from parasite densities of 1 p/μL or less, depending on the assay. While this limit of detection is ideal for diagnosing asymptomatic infections, the technique is not ideal for most settings. PCR is an expensive, time-consuming technique that requires great technological expertise to perform correctly. This means that PCR is most often reserved for research laboratories or large, regional hospitals, and it is not commonly used at the point of care. To overcome these technical and monetary obstacles, rapid diagnostic tests (RDTs) were developed in the 1990s as an accessible diagnostic technique for the point of care. These tests detect parasite proteins, and have a variable limit of detection depending on the manufacturer and the particular biomarker protein. Despite this variability, RDTs have become one of the most widely-used diagnostic tests for malaria due to their portability, ease of use, and relatively low cost.

Protein-based RDTs fill a need and have many advantages for malaria diagnostics at the point of care, but they also come with disadvantages. RDTs typically detect either *Pf*HRP2, a protein specific to *P. falciparum*, or *p*LDH, a protein found in all malaria species, or a combination of the two. This means that RDTs can aid in determining the species of infection for a patient, but only to a degree. If the patient is tested using a multiplex test, it can determine if the infection is *P. falciparum* or non-*falciparum*, but all *P. vivax*, *P. malariae*, and *P. ovale* infections will be grouped together as non-*falciparum*. If the test only detects one protein, it can provide even more limited information. For example, a negative result with a *Pf*HRP2 test could mean that the patient does not have malaria at all, or that the patient is infected with a non-

falciparum species. Results from multiplex tests are further complicated because *p*LDH tests tend to be less sensitive and have higher limits of detection than *Pf*HRP2 tests. This introduces uncertainty in test results, along with past manufacturing issues that caused certain RDT brands to perform much worse than other brands. There is still a place for protein-based malaria diagnostics, but it is clear that there are continuing issues to address in order to make these tests reliable and informative at the point of care.

In comparison to protein, DNA can provide clinicians with much more diagnostically relevant information. Multiplex PCR assays have been developed to detect every species of malaria infecting humans, which eliminates the uncertainty of a positive *p*LDH test result.[21–23] Sequence-specific DNA tests can also be used to test for G6PD deficiency[24] and genes which confer drug resistance[13], both important problems that have been unaddressed by current diagnostics. Furthermore, PCR has been used to detect malaria DNA in patient saliva several times, which is promising for DNA diagnostics as non-invasive tests that do not require a blood sample.[22,25–27] However, as mentioned above, DNA diagnostic tests are currently limited in their reliance on PCR amplification because DNA is typically present in samples in very low concentrations. DNA tests hold high potential for malaria diagnostics, but the gap between high-resource hospital laboratories and low-resource health clinics must be bridged in order to make DNA analysis a robust, accessible diagnostic option for the point of care.

Scope of this work

The current diagnostics listed above must be improved, and new diagnostics must be developed, in order to meet the challenges for malaria elimination described above. Current protein-based RDTs must be improved or redesigned in order to lower the limit of detection.

DNA-based diagnostics can be used to test for species of infection, drug resistance, G6PD deficiency, and low-parasitemia infections, but they are too expensive and technically difficult to be used at the point of care. This dissertation focuses on understanding the issues facing current diagnostic and investigates strategies to improve them. Chapters II and III focus on protein-based diagnostics, while Chapters IV and V move on to DNA-based diagnostics as an ultimately more useful and versatile diagnostic format. **Chapter II** discusses the optimization of a transition metal-based detection strategy for the protein biomarker *Pf*HRP2 as an alternative to typical antibody-based diagnostics. **Chapter III** investigates the structural changes in *Pf*HRP2 when the protein binds to heme, and explores the effects of these changes on antibody binding to the protein. These two chapters also discuss the issues associated with protein-based malaria diagnostics.

Chapter IV moves forward into DNA-based malaria diagnostics, as they can provide a wider variety of information necessary for effective malaria control. This chapter describes a DNA extraction method that was developed in order to simplify sample processing for DNA diagnostics. The method was then incorporated into an automated extraction device to further simplify the process, and then combined with in-line PCR to allow for sample-to-answer DNA diagnostics with minimal user interaction. Finally, **Chapter V** describes the development of a DNA-based RDT and an enzyme-free pre-amplification strategy which eliminates the need to run PCR before the RDT. Taken as a whole, this work follows the research goals of the malaria community, which was previously focused on further understanding and improving current protein diagnostics. In the past few years, however, the community realized that DNA diagnostics have the potential to be more robust and provide more detailed information than protein, but DNA diagnostics are currently hindered by their reliance on expensive, technically

challenging PCR. While this work cannot completely fill the need for new, easily accessible

malaria diagnostics, it can provide new tools and understanding to work towards the goal of

malaria elimination.

References

(1)   UN Millennium Project. UN Millennium Project | Goals, targets & indicators

http://www.unmillenniumproject.org/goals/gti.htm (accessed Jan 18, 2017).

(2)   World Health Organization. *World Malaria Report 2015*; 2015.

(3)   World Health Organization (WHO). *World Malaria Report 2016*; 2016.

(4)   Centers for Disease Control and Prevention. CDC - Malaria - About Malaria - Biology -

Malaria Parasites https://www.cdc.gov/malaria/about/biology/parasites.html (accessed Jan

18, 2017).

(5)   Collins, W. E.; Jeffery, G. M. *Clin. Microbiol. Rev.* **2007**, *20*, 579–592.

(6)   Winzeler, E. A. *Nature* **2008**, *455*, 751–756.

(7)   Global Malaria Progamme. *Control and Elimination of Plamodium Vivax Malaria - A

Technical Brief*; 2015.

(8)   Centers for Disease Control and Prevention. CDC - Malaria - About Malaria - Biology

https://www.cdc.gov/malaria/about/biology/index.html (accessed Jan 18, 2017).

(9)   Mayxay, M.; Pukrittayakamee, S.; Chotivanich, K.; Looaresuwan, S.; White, N. J. *Trans.

R. Soc. Trop. Med. Hyg.* **2001**, *95*, 179–182.

(10)   World Health Organization. *Glob. Tech. Strateg. Malar. 2016 - 2030* **2015**, 1–35.

(11)   World Health Organization. *Guidelines for the Treatment of Malaria*; 2015.

(12)   Straimer, J.; Gnadig, N. F.; Witkowski, B.; Amaratunga, C.; Duru, V.; Ramadani, A. P.;

Dacheux, M.; Khim, N.; Zhang, L.; Lam, S.; Gregory, P. D.; Urnov, F. D.; Mercereau-Puijalon, O.; Benoit-Vical, F.; Fairhurst, R. M.; Menard, D.; Fidock, D. A. *Science (80-.)*. **2015**, *347*, 428–431.

(13)   Isozumi, R.; Uemura, H.; Kimata, I.; Ichinose, Y.; Logedi, J.; Omar, A. H.; Kaneko, A. *Emerg. Infect. Dis.* **2015**, *21*, 490–492.

(14)   The malERA CGoDD. *PLoS Med.* **2011**, *8*, e1000396.

(15)   World Health Organization; Special Programme for Research and Training in Tropical Diseases; Foundation for Innovative New Diagnostics; Centers for Disease Control and Prevention. *Malaria Rapid Diagnostic Test Performance: Results of WHO Product Testing of Malaria RDTs: Round 3 (2010 - 2011)*.; 2011.

(16)   Baird, J. K.; Valecha, N.; Duparc, S.; White, N. J.; Price, R. N. *Am. J. Trop. Med. Hyg.* **2016**, *95*, 35–51.

(17)   Ashley, E. a; Recht, J.; White, N. J. *Malar. J.* **2014**, *13*, 418.

(18)   Bousema, T.; Okell, L.; Felger, I.; Drakeley, C. *Nat. Rev. Microbiol.* **2014**, *12*, 833–840.

(19)   Vinetz, J. M.; Gilman, R. H. *Am. J. Trop. Med. Hyg.* **2002**, *66*, 639–640.

(20)   Laishram, D. D.; Sutton, P. L.; Nanda, N.; Sharma, V. L.; Sobti, R. C.; Carlton, J. M.; Joshi, H. *Malar. J.* **2012**, *11*, 29.

(21)   Rougemont, M.; Van Saanen, M.; Sahli, R.; Hinrikson, H. P.; Bille, J.; Jaton, K. *J. Clin. Microbiol.* **2004**, *42*, 5636–5643.

(22)   Putaporntip, C.; Buppan, P.; Jongwutiwes, S. *Clin. Microbiol. Infect.* **2011**, *17*, 1484–1491.

(23)   Perandin, F.; Manca, N.; Calderaro, A.; Piccolo, G.; Galati, L.; Ricci, L.; Medici, M. C.; Arcangeletti, M. C.; Snounou, G.; Dettori, G.; Chezzi, C. *J. Clin. Microbiol.* **2004**, *42*,

1214–1219.

(24)   Domingo, G. J.; Satyagraha, A. W.; Anvikar, A.; Baird, K.; Bancone, G.; Bansil, P.;
       Carter, N.; Cheng, Q.; Culpepper, J.; Eziefula, C.; Fukuda, M.; Green, J.; Hwang, J.;
       Lacerda, M.; McGray, S.; Menard, D.; Nosten, F.; Nuchprayoon, I.; Oo, N. N.;
       Bualombai, P.; Pumpradit, W.; Qian, K.; Recht, J.; Roca, A.; Satimai, W.; Sovannaroth,
       S.; Vestergaard, L.; Von Seidlein, L. *Malar. J.* **2013**, *12*, 1–12.

(25)   Nwakanma, D. C.; Gomez Escobar, N.; Walther, M.; Crozier, S.; Dubovsky, F.; Malkin,
       E.; Locke, E.; Conway, D. J. *J. Infect. Dis.* **2009**, *199*, 1567–1574.

(26)   Mharakurwa, S.; Simoloka, C.; Thuma, P. E.; Shiff, C. J.; Sullivan, D. J. *Malar. J.* **2006**,
       5, 103.

(27)   Pooe, O. J.; Shonhai, A.; Mharakurwa, S. *African J. Microbiol. Res.* **2011**, *5*, 5120–5126.

CHAPTER II

ON-PARTICLE DETECTION OF *PLASMODIUM FALCIPARUM* [H]ISTIDINE-RICH
PROTEIN 2 BY A "SWITCH-ON" IRIDIUM(III) PROBE[1]

Introduction

Detection of molecular biomarkers via colorimetric and fluorescent signaling is important

for a wide range of biochemical applications from molecular tracking to diagnostics.[2,3] Low-

molecular weight organic dyes are the most commonly used reagents in biological studies.[4,5]

Unfortunately, these organic fluorophores are subject to photobleaching, typically show small

stokes shifts and have broad, often overlapping, emission spectra. Enzymatic labeling of

biomolecular scaffolds is widely used in immunoassays and western blots for quantification of a

specific antigen.[6] Despite production of an amplifying, highly detectable colorimetric signal, the

enzymes and their substrates can be sensitive to light, environmental conditions and non-specific

protein interferents. Further, many cofactors or co-reagents, such as hydrogen peroxide, used in

these reactions do not have long shelf lives. An alternative has been the use of inorganic

fluorescent probes, including quantum dots and metal-based emissive complexes.

Quantum dots are semiconducting nanocrystals that emit visible light based on their

composition and size. Electron-hole pairs, known as excitons, formed during excitation

recombine and releases photons in narrow, long-lived symmetric energy bands.[7] Tuning the size

and surface functionalization of quantum dots allows them to be used for multiplexed detection

of biomolecules. However, surface defects trap excitons and prevent light emission, which leads

to reduced quantum yield as well as the "blinking" phenomena common to quantum dot

methods. Originally developed as nuclear magnetic resonance (NMR) and magnetic resonance

14

imaging (MRI) reagents, metal lanthanide complexes have recently been used for immunoassays and cellular imaging. These probes are marked by long lifetimes and large Stokes shifts, but the intricate synthetic pathways necessary for probe stability limit their use in biological settings.[8,9]

An alternative class of signaling probes is based on emissive transition-metal complexes. The light emitting properties of cyclometalated Ir(III) have been studied in various applications, including organic light emitting diodes (OLEDs),[10–12] oxygen sensing,[13] catalysis,[14] and cell staining.[15] Cyclometalated Ir (III) complexes are characterized by thermal and chemical stability, large Stokes shifts, long lifetimes, high quantum efficiency and photostability.[16,17] Recently, Ma and coworkers demonstrated that cyclometalated Ir(III) complexes of the form $[Ir(C^\wedge N)_2(solv)_2]^+$ selectively bind histidine and histidine containing peptides.[15,18] When irradiated with long wave UV light, these complexes are non-emissive in their solvento state. In the presence of histidine, the associated solvent molecules are displaced as the histidine binds the metal center. Due to this ligand substitution, metal ligand charge transfer (^{3}MLCT) and ligand centered transfer (^{3}LC) pathways are activated resulting in an intense blue-green phosphorescent signal is released as the triplet excited state electron relaxes to the ground state.[11,16]

Enzyme linked immunosorbent assays (ELISAs) is a common method for the immunological detection of disease biomarkers. Regulation of histidine rich proteins have been associated with several diseases including liver cirrhosis, cancer and thrombic disorders.[19] For malaria, *Plasmodium falciparum* Histidine Rich Protein 2 (*Pf*HRP2) has long been validated as a major biomarker of malarial infection. *Pf*HRP2 is a 67 kDa protein comprised of 34% histidine, is secreted by the parasite into the blood of the host.[20] The primary amino acid structure of this protein is marked by characteristic AHHAHHAAD motifs, which have been shown to bind free metal ions[20] as well as heme complexes.[21] Immunochromatographic rapid diagnostic tests

(RDTs) have become important diagnostic tools in low-resource settings. Unfortunately, RDT efficacy is often limited by sample condition and purity, target concentration, manufacturing quality control, environmental conditions, and antibody failures.[22]

Metal-based phosphorescent probes are excellent candidates for the detection of this protein due to their selective, stabile and efficient emission properties. In this chapter, we elucidate the optimal reaction conditions (e.g. buffer, temperature, pH) as well as assess the detection limits of $[Ir(ppy)_2(H_2O)_2]^+$ (**Ir1**) toward BNT-II, a branched peptide mimic of *Pf*HRP2.[23] Using the optimized assay conditions, we demonstrate low nanomolar limits of detection when the recombinant HRP2 (rcHRP2) is bound to the surface of 50 μM magnetic Ni(II)NTA agarose particles in a solution-based ELISA format. This assay can be performed in less than 2 hours using simple, antibody-free reagents, as compared to traditional ELISAs that take 4-5 hours and require sensitive biological reagents.

Materials and Methods

Materials and Reagents

Dichlorotetrakis(2-(2-pyridinyl)phenyl)diiridium(III) (**diIr1**), silver trifluoromethanesulfonate (AgOTf), L-alanine (Ala), L-Histidine (His), L-Cystine (Cys), L-Tryptophan (Try), L-Valine (Val), L-Lysine (Lys), L-Isoleucine (Ile), L-Aspartic Acid (Asp), L-Phenylalanine (Phe), L-serine (Ser), bovine serum albumin (BSA), phosphate buffered saline (PBS) and 4-(2-hydroxyethyl)-1-piperazineethanesulfonic acid (HEPES) were purchased from Sigma-Aldrich. BNT-II was synthesized in the laboratory according to previously published methods.[23] Recombinant HRP2 (rcHRP2) was purchased from Immunology Consultants Laboratory Inc. Costar black and white polypropylene 96-well plates were purchased from

Fisher Scientific. 50 μM Ni(II)NTA magnetic agarose particles were purchased from Qiagen. All other reagents or buffers were purchased from either Sigma-Aldrich or Fisher Scientific.

Instrumentation

^{1}H NMR spectra of **Ir1** in CDCl$_3$ were recorded using a Bruker AV-400 instrument at 400 MHz. Electrospray ionization mass spectra (ESI-MS) of **Ir1** in MeOH were measured with a Finnigan LCQ ion trap LC-MS with ESI ionization. UV-visible spectra were recorded with an Agilent 8453 UV-Visible spectrophotometer. Phosphorescence measurements were recorded using a BioTek Synergy H4 microplate reader. Cyclic voltammetry (CV) measurements of 200 μM **Ir1** in degassed acetonitrile were recorded on a CHI1030 potentiostat (5 V/s scan rate). Glassy carbon was used as the working electrode and platinum wire as the counter electrode. Ag/AgCl was used as the reference electrode with ferrocene as the internal standard.

*Synthesis of Iridium(III) Complex **Ir1***

The complex Ir(ppy)$_2$(H$_2$O)$_2$$^+$, **Ir1**, was synthesized using a previously published method.[24] 50 μM **diIr1** was dissolved in 5mL of methylene chloride before the addition of 100 μM solution of AgOTf in methanol. The slurry was stirred for 1hr at room temperature. Afterwards, the slurry was filtered through Celite, and the filtrate was evaporated until 1-2 mL of filtrate remained. The remaining filtrate was lyophilized overnight yielding a bright yellow powder. ^{1}H NMR (400 MHz, CDCl$_3$, δ=ppm): 6.1047(H3A, doublet) 6.7061(H4A, triplet) 6.8631(H5A, triplet) 7.3657(H5B, doublet) 7.5236(H6A, doublet) 7.8926(H3B, H4B, overlapping resonances) 9.015(H6B, doublet); CV: E$_p$ (1.64V vs NHE) E$_h$ (1.569V vs NHE)

*Activity of **Ir1** against Amino Acids and Biomolecules*

Interactions between **Ir1** and various amino acids, peptides and proteins were elucidated by observing changes in the phosphorescent emission upon reacting 50 μM **Ir1** with these molecules. All reactions and titrations were performed in black 96-well plates at a total volume of 100 μL. 2.5 μL of 2 mM **Ir1** in methanol was added to 100 μL solutions of a given biomolecule to bring the final concentration of **Ir1** in each well to 50 μM.

*Amino Acid Selectivity of **Ir1***

50 μM of **Ir1** was incubated for 10 minutes with individual 100 μL solutions of the following amino acids: Ala, Asp, Cys, His, Ile, Lys, Ser, Try, and Val (n=3 for each amino acid). After the 10-minute incubation period, emission spectra of all amino acids were taken using the BioTek Synergy H4 plate reader (365ex/400-700em).

Optimization of In-Solution Assay Parameters

In order to optimize the reaction conditions for the assay, 50 μM **Ir1** was incubated with L-Histidine under various conditions (e.g. buffer type, pH, temperature, incubation time). Spectral scans (365ex/400-700em) and endpoint measurements (365ex/ 510em) were taken using the BioTek Synergy H4 plate reader.

In-Solution Limit of Detection of 6-His, BNT-II and rcHRP2

50 μM of **Ir1** was titrated with varying nanomolar concentrations of BNT-II and rcHRPII in order to determine the limit of detection for each biomolecule. After a 10-minute incubation period, spectral scans (365ex/400-700em) and endpoint measurements (365ex/ 510em) were

taken using the BioTek Synergy H4 plate reader. Limit of detection was defined as the value of x when $y = 3\sigma_{blank}$.

On-Particle Limit of Detection of BNT-II and rcHRP2

1 μM BNT-II and rcHRPII were serially diluted by half in HEPES Buffered Saline with Tween (HBST; 100 mM HEPES, 137 mM NaCl, pH 7.4, 0.25% Tween-20) and incubated with 10 μL of 50 μM Ni(II)NTA magnetic agarose particles for 15 minutes in a white 96 well plate (n=6; 100 μL for each concentration of BNT-II and rcHRPII). After the incubation period, the particles were washed 3 times with 250 μL of HBST using a 96 well plate magnetic rack. After washing, the particles were resuspended in 100 μL HBST and 2.5 μL of 2 mM **Ir1** was added to each well. The biomarker bound particles were incubated with **Ir1** for 60 minutes before endpoint measurements (365ex/ 510em) were taken using the BioTek Synergy H4 plate reader. Limit of detection was defined as the value of x when $y = 3\sigma_{blank}$. The statistical significance of the limit of detection of the on-bead assay to the in-solution assay was determined by an unpaired t-test using the Prism 5.0 graphing software.

Results and Discussion

*Physical and Spectroscopic Characteristics of **Ir1***

Synthesis and characterization of cyclometalated Ir(III) complexes have been studied for several years for a wide range of applications. Following the synthetic route outlined in **Figure 2.1**,[24] a bright yellow powder was obtained and characterized to be $[Ir(ppy)_2(H_2O)_2]^+$ (**Ir1**). The solvento-complex was synthesized by first splitting the chloride bridge in the $[Ir(ppy)_2(Cl)]_2$
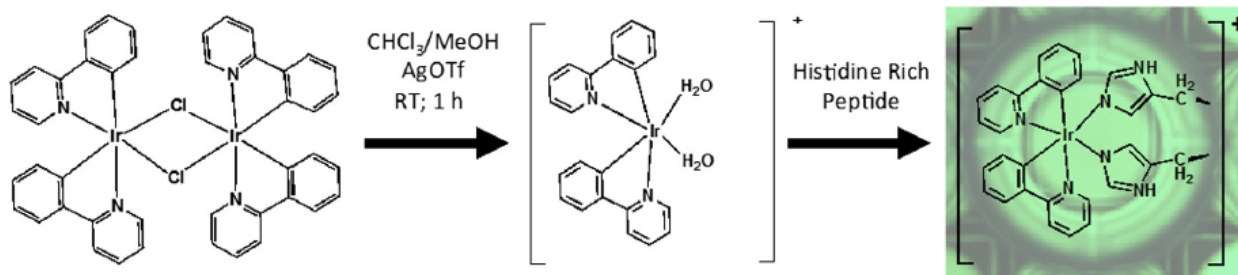
Figure 2.1. *Chloride bridge splitting reaction of dichlorotetrakis(2-(2-pyridinyl)phenyl)diiridium(III) (**diIr1**) to create the aquo complex Ir(ppy)₂(H₂O)₂⁺ (**Ir1**). The reaction is driven by precipitation of AgCl as an insoluble salt. On the addition of a histidine-containing peptide, the water molecules are displaced from the metal as the imidazole side chain binds.*

dimer by precipitation of the chloride in the form of an insoluble silver salt. Water molecules

associate to the metal center to form a stable cationic complex. ^{1}H NMR,[24] ESI and CV[14]

confirmed formation of **Ir1** (**Appendix A, SI Figure 2.1 to 2.3**). High energy absorption bands

were found in 200-300 nm region of the UV-Visible spectrum of 200 μM **Ir1** in methanol, while

weaker bands in the 350-500 nm region were assigned to metal-ligand charge transfer (^{1}MLCT

and ^{3}MLCT) and intraligand transitions (π-π^*) (**Appendix A, SI Figure 2.4**).[18] In solution, **Ir1**

exhibited no emissive properties upon excitation at 365 nm.
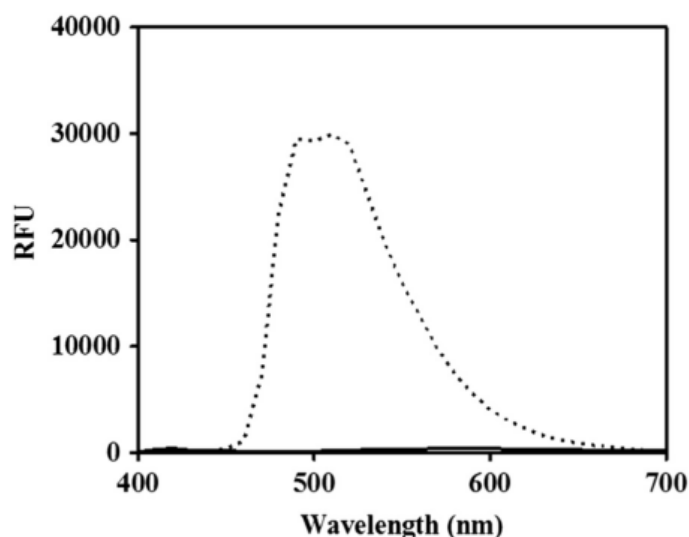
Figure 2.2. *Interaction of 200 μM of various amino acids (Cys, Ser, Asp, Glu, Phe, Lys, Arg, Tyr, Trp, and His) with 50 μM **Ir1** in 100 mM PBS. Signal in relative fluorescence units (RFU) from all amino acids besides histidine (dashed black trace) was negligible.*

*Optimization of **Ir1** Signal with L-Histidine*

The specificity of **Ir1** toward L-Histidine (L-His) was investigated to confirm complex specificity. After reacting **Ir1** with each of the 20 amino acids, only L-His coordinatation elicited a phosphorescent response at 510 nm (**Figure 2.2**), consistent with previously published results.[18] The water molecules are displaced from the Ir(III) metal center by ligand substitution with L-His to create an emissive bioconjugate. The strong σ_{donor} nature of the C^N ligands pushes electron density to the metal center. Upon binding histidine and excitation with 365nm UV light, the singlet excited state (^{1}MLCT/^{1}LC) of the Ir(III) bioconjugate undergoes intersystem crossing to the triplet excited state (^{3}MLCT) and "switches on" the phosphorescent signal at 510 nm.
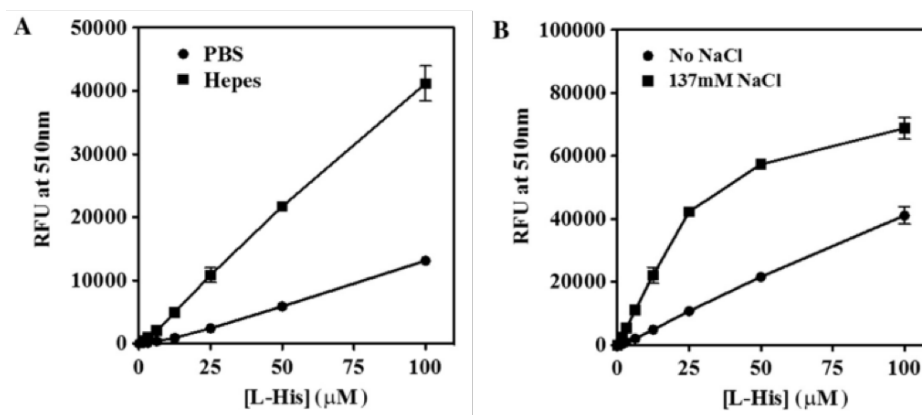
Figure 2.3. *A) Relative fluorescence signal intensity (RFU) of 50 µM **Ir1** with varying concentrations of L-His in 100 mM PBS and 100 mM HEPES buffers, B) Effect of adding 137 mM NaCl to 100 mM HEPES buffer on the signal intensity of 50 µM **Ir1** with varying L-His.*

It is well known that the solution environment can change the photophysical properties of an emitting compound.[25] Additionally, coordinating buffers, such as phosphate buffer, can complex with metal ions, leading to insoluble precipitates. Although previously published methods used similar iridium probes in phosphate buffer, it was noted that **Ir1**, if stored in phosphate buffered saline (PBS), gradually precipitated as a yellow solid. The bidentate

phosphate anion was likely displacing the water molecules and deactivating the Ir(III) complex via the formation of an insoluble salt. By switching to HEPES, a non-coordinating zwitterionic buffer, the signal response of **Ir1** to L-His increased 3-fold (**Figure 2.3A**). 137 mM NaCl was added to the HEPES buffer (HBS) to more closely mimic the salt concentration found in PBS solutions. This addition of salt increased the sensitivity of **Ir1** toward L-His by a factor of four (**Figure 2.3B**).

To further explore this shift toward signal saturation of **Ir1**/L-His conjugate in the presence of salt, the reaction kinetics of 10 μM L-His with **Ir1** in phosphate buffer (PB), PBS, HEPES, and HBS was monitored at 510 nm over the course of 2 hours (**Figure 2.4**). Both PBS and HBS showed a rapid increase in signal during the first 20 minutes of the reaction; however, signal began to stabilize after 30 minutes. A similar trend was seen in PB, but the saturated signal was approximately half of that from PBS. The reaction coordinate in HEPES deviated from the previous buffer systems in that the signal steadily increased over the course of 100 minutes. The effect of the coordinating phosphate anion on the loss of signal is apparent in the reaction of L-His with **Ir1** in PB alone versus HEPES.
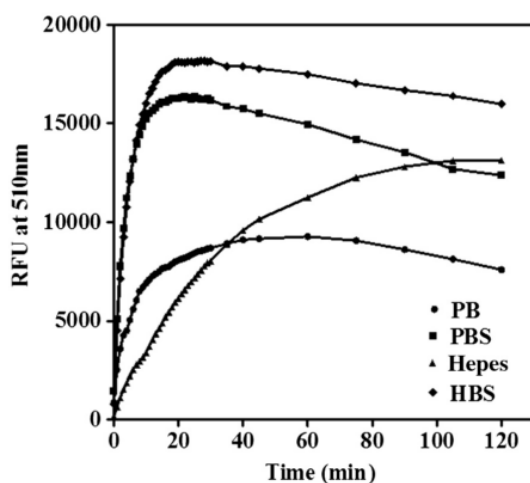
Figure 2.4. *Reaction kinetics of 10 μM L-His with 50 μM **Ir1** with various buffers.*

The presence of NaCl in both phosphate and HEPES buffers appeared to increase target complexation to **Ir1** when compared with their salt deficient counterparts. This is likely due to a kinetic salt effect that the addition of NaCl to the buffer has the on the interaction between the probe and histidine.[26] In neutral buffer conditions, both **Ir1** and L-Histidine are positively charged and thus are slightly repelled from each other in solution. This is evidenced in the slow generation of signal in PB and HEPES buffer systems. The addition of negatively charged chloride ions forms a charge screen around the reactants as governed by the Debye-Huckel theory,[27] which in turn lowers the energy of the reactants and enhances the interaction between the two species as seen by the rapid increase in signal in the first 10 minutes in PBS and HBS. Given these results, the amino acid specificity of **Ir1** was then reanalyzed in HBS to ensure specificity to L-His alone was maintained (**Appendix A, SI Figure 2.5**).
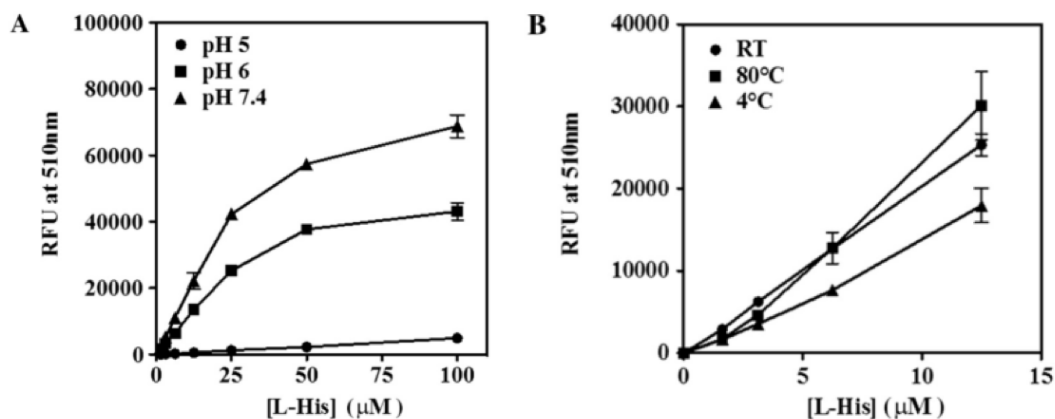
Figure 2.5. *Effect of A) varying pH and B) temperature on the relative fluorescence intensity (RFU) of L-His with 50 μM **Ir1** in 100 mM HBS.*

The effect of pH and temperature on signal generation was determined (**Figure 2.5A**). Below pH 6, very little signal was observed. However, above pH 6, signal from the **Ir1**/L-His conjugate reached saturation around 50 μM L-His. This correlation between intensity of signal

23

and pH is related to the pKa of histidine. In order for histidine to bind to the Ir(III) metal center, the nitrogen on the imidazole ring must be deprotonated. It was observed that signal intensity correlated directly to this "working" concentration of deprotonated histidine (**Appendix A, SI Figure 2.6**), calculated from the Henderson-Hasselbach equation. Below pH 6, there were fewer histidine molecules available for binding, which in turn reduced signal. Therefore, pH 7.4 was selected as the operational pH for HBS in the assay. When creating a diagnostic probe for possible use in a wide range of climates and conditions, operational temperature must be taken into account to ensure the diagnostic result will be consistent and independent of the environment. The signal response at room temperature (RT) and 80°C was not statistically different over a range of histidine concentrations ($p < 0.05$), but at 4°C the signal response decreased two-fold (**Figure 2.5B**). At lower temperatures, the complexation of L-histidine is likely slower than at temperatures above 25°C, resulting in less signal.

The optimized assay conditions for use of the **Ir1** probe was standardized to be 100mM HEPES buffer, pH 7.4 with 137 mM NaCl at temperatures at or above room temperature. At the assay conditions, the quantum yield of the **Ir1**/L-His conjugate agreed with previously published data (**Appendix A, SI Figure 2.7**).[18] In a field where antibody-coupled technologies are the current "gold-standard" for biomarker detection, the robust nature of **Ir1** offers a number of advantages as a diagnostic in probe low-resource settings.

*Development of Optimized **Ir1** Assay with a PfHRP2 Mimic*

With optimized reaction conditions, an assay was designed for the detection of the malaria biomarker HRPII. Optimization of the assay with L-Histidine as opposed to the whole protein allowed for fine-tuning of the basic buffer components prior to introducing the probe to a
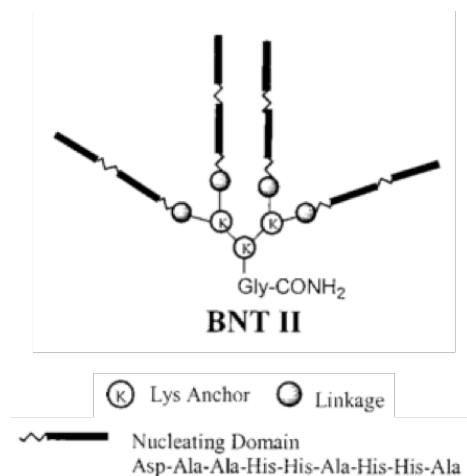
Figure 2.6. *Structure of the PfHRP2 mimic, BNT-II.*

more complex spatial environment. Initial experiments utilized BNT-II, a branched peptide

synthesized to mimic the primary repeating AHH/AHHAAD units characteristic of *Pf*HRPII,[23] as

the target (**Figure 2.6**). Comparing absolute signal generated on a molar basis, BNT-II yielded

higher signal response than L-His upon incubation with **Ir1** (**Figure 2.7A**). It was also noted that

upon comparing signal response versus concentration of total histidine, BNT-II, with 32 histidine

residues per molecule, the concentration of histidine necessary for signal saturation was reduced

16-fold from L-His (**Figure 2.7B**). Beyond 100 μM L-His, the signal leveled off as **Ir1** became

the limiting reagent. If all of the imidazole side chains in BNT-II were available to bind **Ir1,** the

two curves would overlap. Since we do not see this trend, we know stoichiometric signal

generation is not achieved in the BNT-II system. This could be the result of either non-

stoichiometric binding of **Ir1** to BNT-II or quenching of the bound probes. While we may

assume **Ir1** would preferentially bind adjacent histidine residues in the AHH motif, the probe

could bind across the alanine in the HAH region, effectively reducing the signal by a factor of 2

(**Appendix A, SI Figure 2.8**). Additionally, steric bulk around the lysine linker core of the
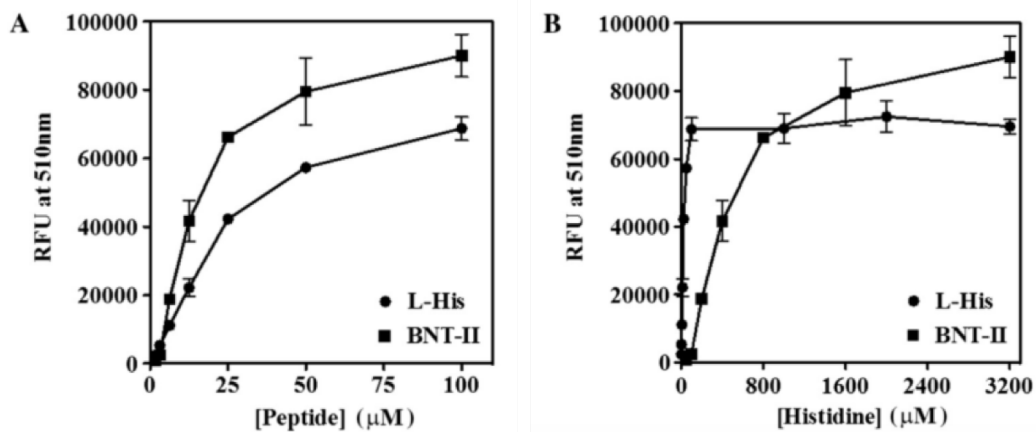
Figure 2.7. *A) Relative fluorescence intensity (RFU) of solution concentrations of L-His and BNT-II and B) Correlation between RFU and total histidine concentration in L-His and BNT-II.*

peptide may prevent iridium from assuming the correct coordination geometry for binding.[23] Aside from non-stoichiometric binding of the probe to the target, photophysical quenching could be occurring in the system. Because of the structure of BNT-II, any bound Ir(III) probes would be in close proximity in chemical space and triplet-triplet annihilation could occur.[28] This annihilation effect would cancel two excited triplet states in the Ir(III) bioconjugate and relax the energy back to the ground state. While quantum yield of BNT-II with **Ir1** was determined to be 8.3% (**Appendix A, SI Figure 2.7**) further analysis of this possible quenching effect is outside of the scope of this chapter.

Depending on the severity of infection, clinically relevant limits of detection of *Pf*HRP2 can fall in the low picomolar to low micromolar regime.[29] Using the optimized assay conditions, detection of the clinical biomarker recombinant HRP2 (rcHRP2) was assessed with the probe (**Figure 2.8**). When concentration of the protein was converted to concentration of total histidine, the titration curve was very similar to that of BNT-II, indicating that a similar loading/quenching effect is likely occurring in the rcHRP2/**Ir1** system (**Appendix A, SI Figure 2.9**). Regardless of

26

these effects, the limit of detection in solution was determined to be 54.8nM and 12.8nM for BNT-II and rcHRPII, respectively.
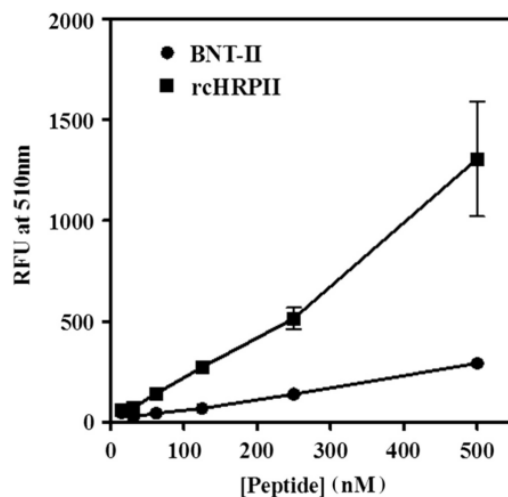
Figure 2.8. *Titration of nanomolar concentrations of BNT-II and rcHRP2 with 50 μM **Ir1** in HBS.*

Ir1 Assay for the On-Bead Detection of PfHRP2

With the advent of microparticle-based diagnostic tools, the ability to detect a target biomolecule on the surface of the particle becomes increasingly advantageous. Current methods for the detection of disease protein biomarkers rely heavily on antibody-based techniques such as enzyme linked immunosorbent assays (ELISAs) and gold nanoparticle conjugates.[30] ELISAs can achieve low picomolar limits of detection, but the entire assay takes 4-5 hours, relies on temperature and time-sensitive reagents, and requires specialized equipment and trained technicians. Due to the interesting optical and aggregation properties of colloidal gold nanoparticles (AuNPs), assays have recently emerged utilizing these colloids for protein biomarker detection.[31] Antibodies or metal-affinity ligands have been conjugated to the surface of the AuNPs for the capture and detection of proteins.[32] These conjugates are often used in the lateral flow rapid diagnostic tests manufactured for the detection of the malaria biomarker

27

*Pf*HRP2. Despite maintaining a low-resource design, the thermal instability of the antibody-AuNP conjugate impedes the accuracy of the assay.[33]
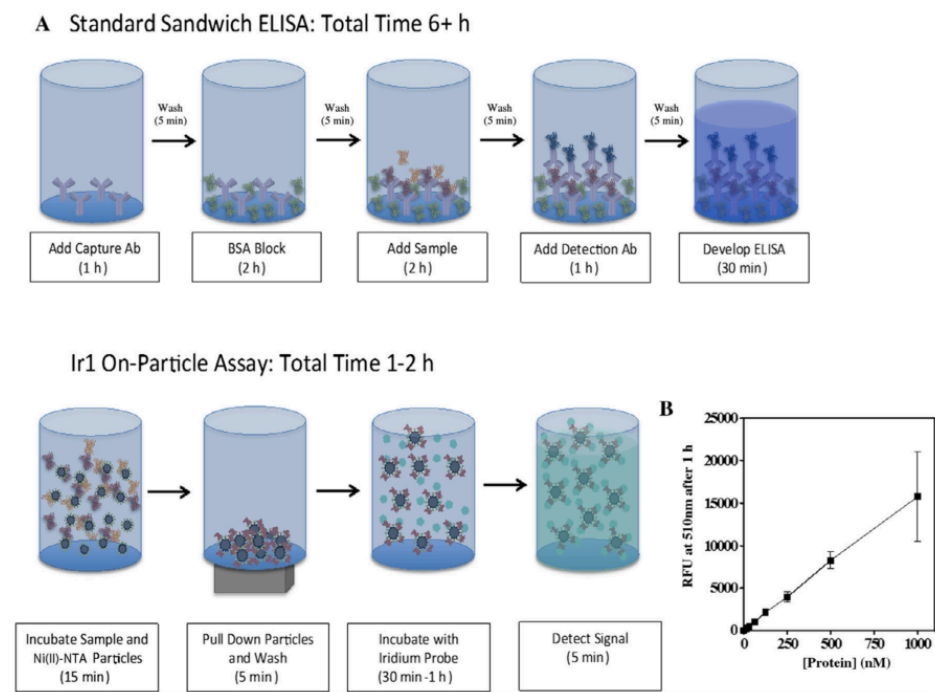
Figure 2.9. *A) Comparison of a standard sandwich ELISA format and the **Ir1** on-particle assay. B) Titration of nanomolar concentrations of rcHRP2 in the on-particle **Ir1** assay.*

In previous studies, 50 μM Ni(II)NTA magnetic agarose particles bind *Pf*HRP2 through the imidazole side chains and facilitate the purification of the biomarker away from contaminating blood proteins and cellular debris.[29] Many histidine residues would still be available for coordination to the iridium probe when the protein is bound to the surface of the particle. By labeling the bound histidine rich biomarker, we are effectively creating a solution-based sandwich ELISA assay that is complete in 1.5 hours without needing several hours of processing time and environmentally sensitive antibody reagents (**Figure 2.9A**). The use of magnetic particles to immobilize the target biomarker for processing is the key component for

the reduction of assay time. In a normal ELISA format, each reagent is immobilized on the well plate in 1-2 hour steps, and the plate must be washed extensively in between these steps to remove any unbound reagents. Our modified ELISA assay has fewer overall steps than a normal ELISA format however; magnetic particles can be intermixed with the sample for more efficient binding, and the particles can be pulled down to the bottom of the reaction chamber for fast washing.

Qualitatively, we were able to visualize the iridium on the surface of the particle under long-wave UV light (**Appendix A, SI Figure 2.10**). Optimal protein binding times increased from 10 minutes in the case of free protein in solution to 45 minutes for bead bound target (**Appendix A, SI Figure 2.11**). This is likely due to decreasing degrees of freedom of HRP2 to react with **Ir1** upon binding to the surface of the particle. Using the optimized assay conditions, the limit of detection for rcHRP2 on-particle was 14.5 nM (0.972 μg/mL), with no signal generated from the blank (**Figure 2.9B**). The linear range of the assay spans three orders of magnitude in the nanomolar regime. Beyond this range, the signal becomes saturated, likely due to quenching effects and/or the probe being the limiting reagent at increasing concentrations of target. The limit of detection for rcHRP2 in-solution and on-bead were statistically the same based on an unpaired t-test ($p = 0.731$), thus validating both the magnetic particle's binding capacity as well as the probes ability to detect the biomarker when immobilized on a surface.

Conclusion

This chapter describes the utility of a cyclometallated Ir(III) probe for the selective labeling and detection of the malarial biomarker *Pf*HRP2 on the surface of a magnetic particle. By first optimizing several assay parameters, the **Ir1** probe was used for the detection of low

nanomolar amounts of rcHRP2 bound to the surface of the particle. This type of on-particle assay

mimics that of a traditional ELISA design performed in a 96-well plate, but the assay is complete

in under two hours, due to the use of magnetic particles for biomarker immobilization,

processing and detection. While the limit of detection fell within the symptomatic range

required for the clinical diagnosis of malaria, detection of increasingly low picomolar levels of

*Pf*HRP2 has become necessary for the identification of asymptomatic patients, who serve as

transmission reservoirs for the disease. This is seen in comparing the curve of the presented on-

bead assay to a traditional ELISA for *Pf*HRP2 (**Appendix A, SI Figure 2.12**). In addition, **Ir1** is

specific for histidine but not for *Pf*HRP2. The presence of additional histidine containing

proteins, such as human serum albumin or histidine rich glycoprotein, could give false positives

for the proposed assay design. This was evidenced by background signal generated from the

surface of particles that were incubated with unspiked diluted plasma that was 6-fold higher

intensity than that of rcHRP2 (data not shown). Selective isolation of the target protein away

from contaminating proteins, using our recently published rapid extraction cassette,[29] would

greatly enhance this probe's utility in a field diagnosis setting. Additionally, several strategies

can be explored to achieve lower detection limits and specificity, comparable to that of a

traditional ELISA format, namely the creation of a branched histidine containing peptide that can

be conjugated to molecular recognition elements (MREs), such as antibodies or aptamers. By

coupling this peptide to an HRP2-specific MREs, we can simultaneously target HRP2 and

enhance the signal via the branched histidine motifs. These modifications to the probe would

push the magnetic particle based Ir(III) assay toward higher signal output for ease of biomarker

detection by the end user.

Acknowledgements

References

(1)   Davis, K. M.; Bitting, A. L.; Wright, D. W. *Anal. Biochem.* **2014**, *445*, 60–66.

(2)   Gubala, V.; Harris, L. F.; Ricco, A. J.; Tan, M. X.; Williams, D. E. *Anal. Chem.* **2012**, *84*, 487–515.

(3)   Kuzmenko, A.; Tankov, S.; English, B. P.; Tarassov, I.; Tenson, T.; Kamenski, P.; Elf, J.; Hauryliuk, V. *Sci. Rep.* **2011**, *1*, 51–57.

(4)   Sassolas, A.; Leca-Bouvier, B. D.; Blum, L. J. *Chem. Rev.* **2008**, *108*, 109–139.

(5)   Miyawaki, A.; Sawano, A.; Kogure, T. *Nat. Cell Biol.* **2003**, *Suppl*, S1-7.

(6)   Liu, M.; Jia, C.; Huang, Y.; Lou, X.; Yao, S.; Jin, Q.; Zhao, J.; Xiang, J. *Analyst* **2010**, *135*, 327–331.

(7)   Michalet, X.; Pinaud, F. F.; Bentolila, L. A.; Tsay, J. M.; Doose, S.; Li, J. J.; Sundaresan, G.; Wu, A. M.; Gambhir, S. S.; Weiss, S. *Science* **2005**, *307*, 538–544.

(8)   Thibon, A.; Pierre, V. C. *Anal. Bioanal. Chem.* **2009**, *394*, 107–120.

(9)   Steinkamp, T.; Karst, U. *Anal. Bioanal. Chem.* **2004**, *380*.

(10)   Holder, E.; Langeveld, B. M. W.; Schubert, U. S. *Adv. Mater.* **2005**, *17*, 1109–1121.

(11)   Wagenknecht, P. S.; Ford, P. C. *Coord. Chem. Rev.* **2011**, *255*, 591–616.

(12)   Lamansky, S.; Djurovich, P.; Murphy, D.; Abdel-Razzaq, F.; Lee, H.-E.; Adachi, C.; Burrows, P. E.; Forrest, S. R.; Thompson, M. E. *J. Am. Chem. Soc.* **2001**, *123*, 4304–4312.

(13)   Ho, M.-L.; Chen, Y.-A.; Chen, T.-C.; Chang, P.-J.; Yu, Y.-P.; Cheng, K.-Y.; Shih, C.-H.; Lee, G.-H.; Sheu, H.-S. *Dalt. Trans.* **2012**, *41*, 2592.

(14)   McDaniel, N. D.; Coughlin, F. J.; Tinker, L. L.; Bernhard, S. *J. Am. Chem. Soc.* **2008**, *130*, 210–217.

(15)   Ma, D.-L.; Wong, W.-L.; Chung, W.-H.; Chan, F.-Y.; So, P.-K.; Lai, T.-S.; Zhou, Z.-Y.; Leung, Y.-C.; Wong, K.-Y. *Angew. Chemie Int. Ed.* **2008**, *47*, 3735–3739.

(16)   You, Y.; Nam, W. *Chem. Soc. Rev.* **2012**, *41*, 7061.

(17)   Zhao, Q.; Yu, M.; Shi, L.; Liu, S.; Li, C.; Shi, M.; Zhou, Z.; Huang, C.; Li, F. *Organometallics* **2010**, *29*, 1085–1091.

(18)   Li, C.; Yu, M.; Sun, Y.; Wu, Y.; Huang, C.; Li, F. *J. Am. Chem. Soc.* **2011**, *133*, 11231–11239.

(19) Jones, A. L.; Hulett, M. D.; Parish, C. R. *Immunol. Cell Biol.* **2005**, *83*, 106–118.

(20) Panton, L. J.; McPhie, P.; Maloy, W. L.; Wellems, T. E.; Taylor, D. W.; Howard, R. J. *Mol. Biochem. Parasitol.* **1989**, *35*, 149–160.

(21) Schneider, E. L.; Marletta, M. A. *Biochemistry* **2005**, *44*, 979–986.

(22) Mabey, D.; Peeling, R. W.; Ustianowski, A.; Perkins, M. D. *Nat. Rev. Microbiol.* **2004**, *2*, 231–240.

(23) Ziegler, J.; Chang, R. T.; Wright, D. W. *J. Am. Chem. Soc.* **1999**, *121*, 2395–2400.

(24) Schmid, B.; Garces, F. O. *Inorg. Chem.* **1994**.

(25) Xu, J.; Yang, C.; Tong, B.; Zhang, Y.; Liang, L.; Lu, M. *J. Fluoresc.* **2013**, *23*, 865–875.

(26) Verity, B.; Bigger, S. W. *Int. J. Chem. Kinet.* **1996**, *28*, 919–923.

(27) Atkins, P. W. (Peter W.; De Paula, J. *Atkins' Physical Chemistry*; 8th ed.; W.H. Freeman: New York, 2006.

(28) Haneder, S. Correlation between electronic structure and light emission properties in phosphorescent emitters, Ludwig Maximilian Universitat Munchen, 2009.

(29) Davis, K. M.; Swartz, J. D.; Haselton, F. R.; Wright, D. W. *Anal. Chem.* **2012**, *84*, 6136–6142.

(30) Giljohann, D. A.; Mirkin, C. A. *Nature* **2009**, *462*, 461–464.

(31) Swartz, J. D.; Gulka, C. P.; Haselton, F. R.; Wright, D. W. *Langmuir* **2011**, *27*, 15330–15339.

(32) de Souza Castilho, M.; Laube, T.; Yamanaka, H.; Alegret, S.; Pividori, M. I. *Anal. Chem.* **2011**, *83*, 5570–5577.

(33) Bell, D.; Peeling, R. W. *Nat. Rev. Microbiol.* **2006**, *4*, S34–S38.

CHAPTER III

STRUCTURAL CHARACTERIZATION OF RECOMBINANT *Pf*HRP2 BINDING TO HEME
AND EFFECTS ON RAPID DIAGNOSTIC TEST PERFORMANCE

Introduction

Early diagnosis of malaria is a key element in elimination strategies because individuals with low parasite loads can still serve as transmission reservoirs.[1–4] However, the most common field diagnostic for malaria, rapid diagnostic tests, often show variable performance at low parasite densities.[5,6] Rapid diagnostic tests (RDTs) are often used in widespread malaria screening efforts to quickly and easily detect the malaria biomarker *Plasmodium falciparum* histidine-rich protein 2 (*Pf*HRP2) in a small drop of blood. However, there are many external factors that can adversely affect the performance of these tests in field diagnostic settings, such as heat degradation and humidity.[6] For several years, these tests suffered from poor manufacturing standards, and certain brands vastly outperformed other brands.[6] In order to inform purchasing decisions and enforce standards, the World Health Organization began a biannual review process for malaria RDTs which has improved the overall quality of tests available.[7] While the tests themselves have become more reliable, parasite evolution has affected their utility as well. *Pf*HRP2 protein sequence variations[8,9] and even gene deletion[10,11] have been reported in areas of Southeast Asia and South America, which means that even the best *Pf*HRP2 test will not be an effective malaria diagnostic in these areas. Current diagnostic developers are constantly trying to stay one step ahead of the parasite by investigating new diagnostics and working to improve the *Pf*HRP2 diagnostics that are already in use.

Assay developers use recombinant protein as a standard for assay validation. Recombinant proteins are produced using bacteria (typically *E. coli*) that have been genetically modified to produce the protein sequence of interest. After expression, the protein is purified from the bacteria and characterized, and it can be used in the same way as native protein. Recombinant proteins are also used in antibody production because the sequence and purity can be controlled more so than a native protein. However, because the protein sequence is not in its native environment, a recombinant protein often does not possess the same folding or three-dimensional structures as the native protein. This can be a problem when the correct secondary and tertiary structure of the protein is essential for assay function, as in antibody-based assays such as RDTs or enzyme-linked immunosorbent assays (ELISAs).

Past studies have indicated that *Pf*HRP2 may play a role in the parasite's heme detoxification process by binding free heme and promoting its crystallization into hemozoin.[12,13] During the parasite lifecycle, *Pf*HRP2 is excreted into circulating blood as the parasitized red blood cells burst, allowing the parasites to infect new red blood cells.[14] Circulating blood contains heme mostly in its protein-bound hemoglobin form, but data from our lab indicates that parasitized blood also contains ~10 μM free heme. These two observations together indicate that a blood sample used for *Pf*HRP2 detection will have some proportion of its *Pf*HRP2 bound to free heme. We hypothesize that heme-bound *Pf*HRP2 adopts a different conformation from free protein, and that this conformational change may affect protein binding to antibodies on an RDT. Previous studies have shown that binding heme alters the structure of rc*Pf*HRP2, but the effects of these changes have not been investigated.[15] This is especially a concern since native protein will be exposed to heme in blood as described above, but purified recombinant protein used for industrial antibody production will not be exposed to heme.

This chapter is focused on investigating the structure of *Pf*HRP2 and its relationship to the effectiveness of current RDTs. Specifically, we investigate the conformational changes of recombinant (rc) *Pf*HRP2 in the presence of heme using circular dichroism (CD), and the effects of these structural changes on antibody-based *Pf*HRP2 detection using ELISA and RDT formats. Understanding how the structure of rc*Pf*HRP2 changes with its environment can help us design more sensitive, effective diagnostic tests for malaria.

Materials and Methods

Materials and reagents

Various recombinant forms of *Pf*HRP2 (ITG and FCQ79) were obtained from PATH. CTK *Pf*HRP2 was purchased from CTK Biotech (Cat # A3000). Hemin chloride was purchased from MP Biomedicals, LLC (Cat # 198820). Zn(II)PPIX was purchased from Frontier Scientific (Cat # Zn625-9). Fisherbrand clear 96-well polystyrene plates were purchased from Fisher Scientific (Cat # 12565501). The 2mm microcell CD cuvette was purchased from Aviv Biomedical (Cat # 1301-101000-2) and used with a microcell spacer also purchased from Aviv Biomedical (Cat # 0021-100190-1). Spectra-Por Micro Float-A-Lyzer $100 - 200\ \mu$L $8 - 10$ kDa MWCO dialysis devices were purchased from Fisher Scientific (Cat # 08-607-075). Amicon Ultra 0.5 mL 3 kDa MWCO centrifugal filters were purchased from Millipore (Cat # UFC500324). Antibodies for the *Pf*HRP2 ELISA were purchased from Abcam Inc. (Cat # ab9206 and ab30384). Paracheck Pf RDTs were acquired from Orchid Biomedical Systems (Cat # 30301025). SD Bioline Malaria Ag Pf RDTs were purchased from Standard Diagnostics Inc. (Cat # 05FK50). ICT Pf RDTs were purchased from IDT Diagnostics (Cat # ML01). All other reagents and buffers were purchased from either Sigma-Aldrich or Fisher Scientific.

Instrumentation

Absorbance measurements were taken using a Synergy H4 microplate reader and a

NanoDrop ND-1000 spectrophotometer. Circular dichroism measurements were recorded using

an Aviv Model 215 CD Spectrometer. RDT signal measurements were taken using a Qiagen

ESEQuant Lateral Flow Reader.

Absorbance Titrations

ITG rc*Pf*HRP2 was buffer exchanged to 20 mM potassium phosphate buffer, pH 7, (PB)

using Zeba 7K MWCO Spin Desalting Columns. Absorbance spectra of blank PB and 5 μM ITG

rc*Pf*HRP2 were taken from 250 – 700 nm in a UV-transparent 96-well plate. The rc*Pf*HRP2

wells were brought to 15 μM heme by adding 2.86 μL of 1mM hemin in 100 mM NaOH to the

samples, which were then mixed and incubated at room temperature for 15 minutes before

another absorbance spectrum was recorded. Hemin additions, incubation, and absorbance

measurements were continued until 18 molar equivalents of hemin had been added to the protein

samples. For comparison, absorbance spectra were recorded for the same concentrations of

hemin in PB without protein present.

Circular Dichroism Spectroscopy of Various rcPfHRP2 Proteoforms

ITG rc*Pf*HRP2 was buffer exchanged to 20 mM potassium phosphate buffer, pH 7, (PB)

using Zeba 7K MWCO Spin Desalting Columns. Protein concentration (typically 3 – 5 μM) was

determined by measuring A_{220} using a NanoDrop ND-1000 spectrophotometer. Circular

dichroism spectra of samples and blanks were recorded from 185 – 260 nm with wavelength step

0.5 nm and 3 scans per sample using a 2 mm pathlength microcell in an Aviv Model 215 CD Spectrometer. 1 mM hemin in 100 mM NaOH was added to each protein sample in 3 molar equivalent increments. After each addition, the solution was pipetted to mix and allowed to incubate at room temperature for 15 minutes before another CD scan was run. Data was averaged, smoothed, and background subtracted using Aviv 215 CD software. These experiments were repeated using additions of 1 mM Zn(II)PPIX in 100 mM NaOH in place of hemin additions, and using additions of 100 mM NaOH alone to control for volume effects.

After 15 molar equivalents of heme was added to certain samples, they were subjected to dialysis or centrifugal filtration to determine if observed structural changes were reversible. For dialysis, Micro Float-A-Lyzer 8 – 10 MWCO dialysis devices were used according to the manufacturer's instructions. Briefly, the membrane was first soaked in 10% ethanol for 10 minutes to remove glycerin before being flushed thoroughly with DI water. Next, after all air was removed from the device, 100 μL of heme-bound protein sample was added to the device. The device was placed in 100 mL of PB, which was stirred for 22 hours with buffer changes at 2 hours, 6 hours, and 10 hours. Sample was retrieved from the device and analyzed via CD as above. For centrifugal filtration, Amicon Ultra 3K MWCO centrifugal filters were used according to the manufacturer's instructions. Briefly, 75 μL of heme-bound protein sample was added to the device along with 400 μL PB. The filter was centrifuged for 30 minutes at 14,000g and the filtrate was discarded. 400 μL PB was added to the filter and centrifuged twice more. Finally, the filter device was flipped over into a new collection tube and centrifuged for 2 minutes at 1,000g to collect the sample. The sample volume was 35 μL due to the concentration effect of the filter, so 40 μL PB was added to bring the sample to an adequate volume for CD analysis, and the sample was analyzed via CD as above.

Temperature experiments were conducted via CD in two ways. First, a full spectrum was taken as above for samples of rc*Pf*HRP2 with and without heme, both at room temperature and at 85°C. Then, a temperature step experiment was run by subjecting rc*Pf*HRP2 samples to gradual, controlled temperature change, and recording CD data at 222 nm every 1°C.

Rapid Diagnostic Test Studies

The effect of heme on the detection of varying amounts of rc*Pf*HRP2 was tested using 3 RDT brands. Various concentrations of ITG rc*Pf*HRP2 in PBS were prepared, both with and without 10.64 molar equivalents of heme in solution. The samples that included heme were allowed to incubate for 15 minutes at room temperature before testing. All samples were run in triplicate on 3 different RDT brands (Paracheck, SD Bioline, and ICT Pf) according to manufacturer instructions. RDT signal was measured using a Qiagen ESEQuant LFA Reader with channel and type set to E1/D2 and reflective, respectively.

The effect of heme concentration on the detection of a single rc*Pf*HRP2 concentration was also tested using SD Bioline RDTs. Several samples of 28.2 nM ITG rc*Pf*HRP2 were prepared with varying molar equivalents of heme added and allowed to incubate for 15 minutes at room temperature. All samples were run in triplicate on SD Bioline RDTs according to the manufacturer's instructions. RDT signal was measured using a Qiagen ESEQuant LFA Reader with channel and type set to E1/D2 and reflective, respectively.

ELISA Studies

An in-house ELISA was used to quantify rc*Pf*HRP2 binding to antibodies.[16] A 100 μL solution of 1 μg/mL IgM anti-HRP2 (Abcam ab9206) in 1X PBS was added to each well of a

Immulon 2 HB 96-well plate, which was then sealed with Parafilm and allowed to incubate for 1 hour on an orbital shaker. After incubation, the plate was washed 3 times with 300 μL of 1X PBS containing 0.1% Tween-20 (PBST). Next, 300 μL of a solution of PBST with 5% BSA (by weight) was added to each well and incubated for 2 hours. The plate was then washed three times with PBST before adding 100 μL per well of the standard curve, controls and samples. The standard curve consisted of ITG rc*Pf*HRP2 serially diluted from 5 pM to 0.078 pM in PBST with 0.1% BSA. Samples consisted of 0.5 pM, 1 pM, or 3 pM ITG rc*Pf*HRP2 in PBST with 0.1% BSA that had been incubated with various molar equivalents of heme for 15 mintues prior to ELISA analysis. The standards and samples were incubated for 2 hours, after which the plate was washed four times with PBST. Next, a 100 μL solution of 0.5 μg/mL IgG anti-HRP2 with HRP (Abcam ab30384) in PBST containing 0.5% BSA was added to each well and incubated for 1 hour while protected from light. The plate was then washed five times prior to development. 100μL of TMB One solution was added to each well and developed for 10 minutes in low light. The reaction was quenched with 100 μL of 2 M H_2SO_4. The absorbance at 450 nm was measured using a BioTek Synergy H4 microplate reader.

Results and Discussion

Effect of protein binding on heme absorbance

Absorbance spectra measurements were used to confirm that heme in solution will bind to rc*Pf*HRP2. When heme absorbance is measured in phosphate buffer with no protein present, the spectrum shows a broad absorbance peak from 300 – 450 nm, centered at 370 nm (**Figure 3.1A**). As expected, the signal intensity is related to the heme concentration in solution. When heme absorbance is read in the presence of 5 μM rc*Pf*HRP2, a sharp Soret peak appears at 410

nm (**Figure 3.1B**). The appearance of this sharp red-shifted peak indicates that heme is coordinated to the protein.[17] Furthermore, when the peak absorbance at 410 nm is plotted against heme concentration added to the protein, a linear trend is observed until 15 molar equivalents of heme have been added to the protein (**Figure 3.1C**). When 18 molar equivalents of heme are added to the protein, the Soret peak has the same intensity as the sample with 15 molar equivalents. This indicates that the protein can bind up to 15 heme molecules at pH 7 to reach saturation, consistent with previous literature.[15]
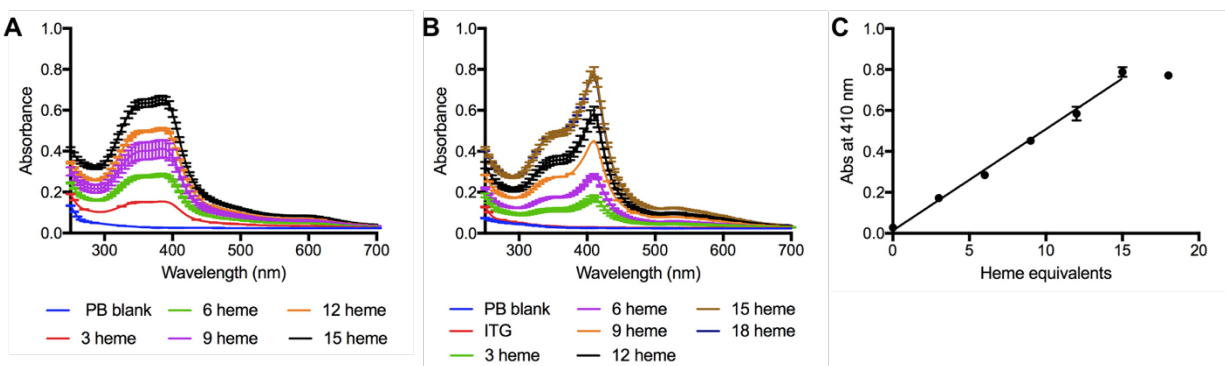
Figure 3.1. *Absorbance spectra of varying concentrations of heme presented as molar equivalents relative to protein A) in PBS alone and B) incubated with 5 μM rcHRP2 in PBS. C) Linear trend of the Soret peak absorbance at 410 nm with increasing heme.*

Effect of heme binding on protein CD spectra

Circular dichroism was used to investigate the three-dimensional structure of several rc*Pf*HRP2 variants at pH 7. These samples were then titrated with heme to observe structural changes resulting from heme binding to the protein. Tag-free variants of the protein such as ITG (**Figure 3.2A**) and FCQ79 (**Figure 3.2B**) produce spectra with a sharp, deep peak at 203 nm and a very shallow, wide shoulder centered around 222 nm. The peak at 203 nm is indicative of a strongly random-coil structure[18,19], meaning that the protein is mostly globular without a

41

classically defined structure. As heme is added to the protein, however, the peak at 203 nm become less intense and shifts closer to 210 nm, while the broad band at 222 nm becomes more intense. The shape of the spectrum after 15 molar equivalents of heme have been added to the protein is strongly indicative of an α-helical structure[18,19], especially for the FCQ79 variant where the peak intensity ratio is nearly 1:1. These results, combined with the absorbance data above, suggest that binding more heme molecules causes rc*Pf*HRP2 to adopt a more rigid helical structure compared to its native, mostly unstructured state.
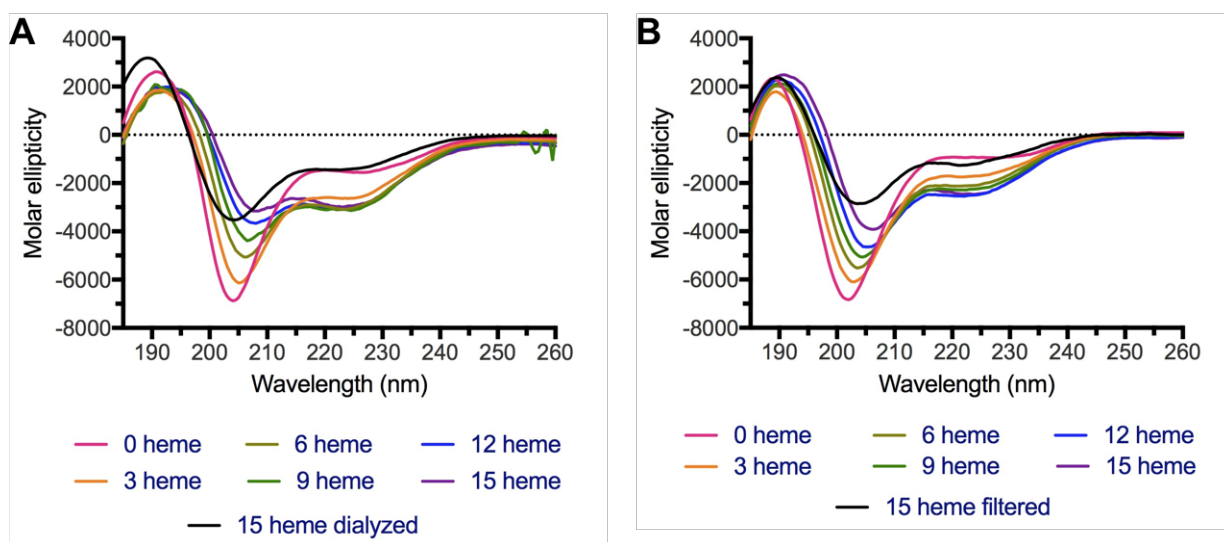
Figure 3.2. *Circular dichroism (CD) spectra of heme titrated into solutions of A) ITG rcPfHRP2 and B) FCQ79 rcPfHRP2 in 20 mM phosphate buffer, pH 7. Each graph also shows a spectrum for the same sample after A) dialysis or B) centrifugal filtration. Heme is labeled as molar equivalents relative to protein concentration.*

To determine if the observed structural changes in untagged rc*Pf*HRP2 were reversible, protein samples were filtered after heme addition and then re-analyzed via CD to see if the protein would return to its original state upon heme removal. Both centrifugal filtration and typical dialysis were used to filter samples in case one method was more effective than the other

(**Figure 3.2**). Each filtration method showed a peak shift from 210 nm to 203 – 204 nm, and a decrease in signal at the broad 222 nm band, indicating that the protein had indeed reverted to its mostly unstructured, random coil state. This shows that a simple sample preparation step could reduce the structural effect of heme binding in a purified protein. However, the overall CD signal decreased compared to the 15 heme traces and especially the 0 heme traces, which shows that both of these methods induce significant and undesirable sample loss.
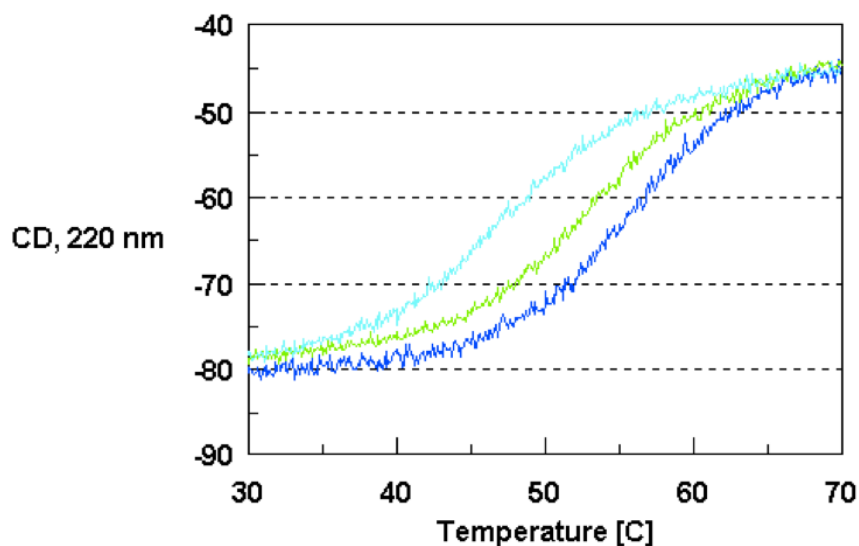
Figure 3.3.[20] *Example of protein melting curves generated using circular dichroism. Each color represents the same protein in a different buffer, demonstrating how protein environment can affect thermal stability.*

The effect of heat on rc*Pf*HRP2-heme binding was also investigated by monitoring the CD spectra at different temperatures. Typical proteins with defined structures tend to denature and lose those structures with the addition of heat, and protein stability can be affected by binding small molecules, thus affecting the denaturation process. Since rc*Pf*HRP2 seems to gain structure by binding heme, we wanted to see if heating the complex would disrupt that binding and revert the protein structure. CD can be used to find the melting temperature of a protein due

43

to the sharp structural transition in the protein, which is easily visible when monitoring CD signal at one wavelength.[21] These experiments can also be used to determine if factors such as buffer type, salt concentration, and other small molecules affect the thermal stability of the protein of interest. For example, **Figure 3.3**[20] depicts the same recombinant protein in three different buffers subjected to the same temperature scan. The melting point, at roughly the halfway point of each transition curve, changes depending on the buffer components and their effects on the thermal stability of the protein.
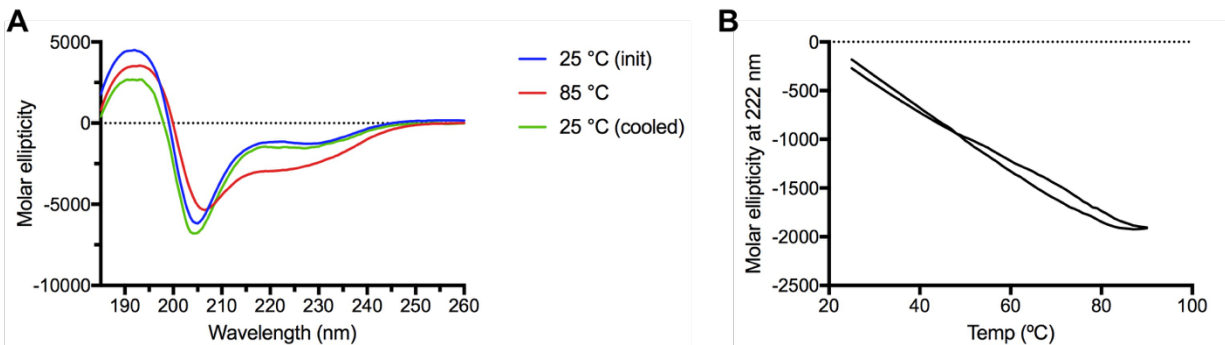
Figure 3.4. *A) Full CD spectra for ITG rcPfHRP2 at room temperature and 85℃. B) CD signal for ITG rcPfHRP2 at 222 nm monitored over a temperature scan from 25℃ to 85℃.*

To determine the effects of heat on the structure of rc*Pf*HRP2, full CD spectra were taken of a sample of ITG rc*Pf*HRP2 without heme at room temperature and at 85°C (**Figure 3.4A),** to determine which wavelength to monitor in a more detailed temperature scan. There was a noticeable change in signal intensity at 222 nm, which is also a common wavelength to monitor in CD temperature scans, so it was chosen for further study. The protein was then subjected to a gradual change in temperature, with CD signal at 222 nm being recorded after every 1°C change (**Figure 3.4B**). This temperature scan showed no sharp melting transition, however, indicating

that any structural changes observed by CD in this case are gradual and not the result of large-scale melting. These experiments were then repeated on rc*Pf*HRP2 samples bound to 15 molar equivalents of heme (**Figure 3.5**). Again, slight difference in CD signal at 222 nm was observed when the sample was heated to 85°C, so this wavelength was chosen for gradient monitoring. The temperature scan at 222 nm showed more variation in the heme-bound protein than the heme-naïve sample, but it still did not contain sharp inflection points indicating a sharp structural transition temperature. Both experiments with the heme-bound protein indicate that heat will not disrupt the binding of rc*Pf*HRP2 and heme.
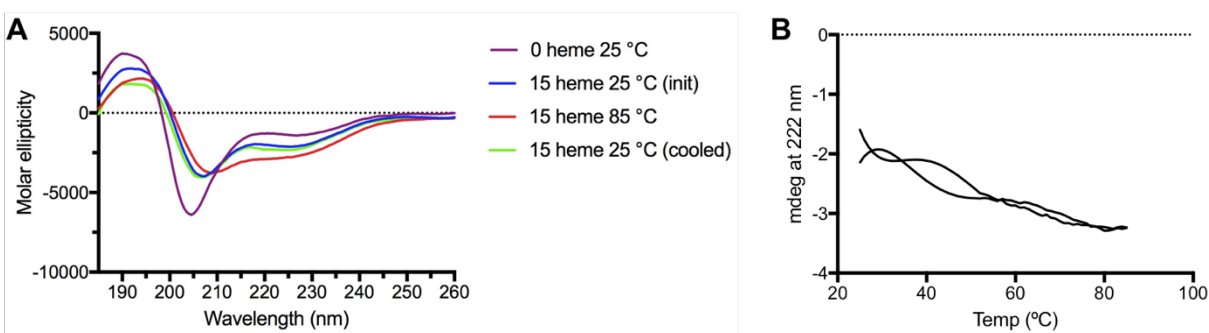
Figure 3.5. *A) Full CD spectra for ITG rcPfHRP2 with 15 molar equivalents heme at room temperature and 85 °C. B) CD signal for ITG rcPfHRP2 with 15 molar equivalents heme monitored at 222 nm over a temperature scan from 25 °C to 85 °C.*

Furthermore, it is worth noting that these structural changes to rc*Pf*HRP2 upon heme binding are only observable when an untagged protein variant is used. Many commercially-available rc*Pf*HRP2 variants, such as that from CTK Biotech and AbD Serotec/Bio-Rad, contain either a glutathione transferase (GST) or partial maltose-binding protein (MBP) fusion tag. The GST tag is ~26 kDa, which is nearly the same size as the ~30 kDa *Pf*HRP2 portion of the fusion protein, and the partial MBP tag is ~ 9 kDa, roughly one-third the size of *Pf*HRP2. When CD

spectra are taken of these variants, the mostly α-helical structure of the tag overwhelms the

spectra, and it is impossible to see any structural changes as the result of heme addition to the

solution (**Figure 3.6**). These tags can be cleaved from the protein of interest, but this step also

requires further column purification which can result in protein loss.
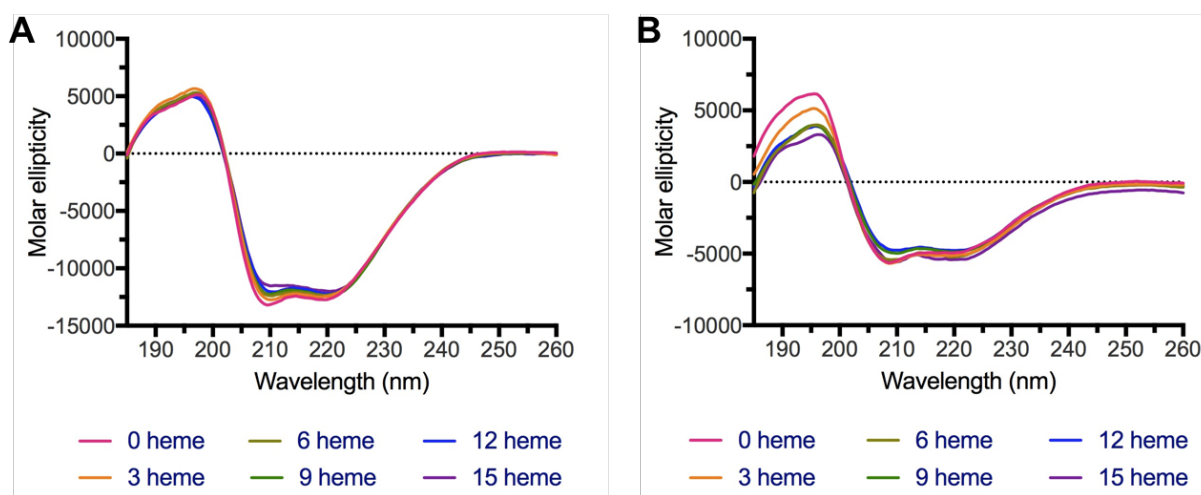
Figure 3.6. *Heme titrations in phosphate buffer of A) CTK Biotech rcPfHRP2 containing a GST tag and B) AbD Serotec rcPfHRP2 containing a partial MBP tag.*

Control experiments replacing heme with Zn(II)PPIX were performed to ensure that

these structural changes were specific to heme addition. Zn^{2+} has a well-documented affinity for

*Pf*HRP2, as it was used in an affinity column format to isolate native *Pf*HRP2 when the protein

was first identified.[22] Furthermore, our lab currently uses Zn^{2+}-conjugated magnetic beads to

quickly purify *Pf*HRP2 from blood culture samples. Therefore, we decided that using Zn^{2+} bound

in the same porphyrin ring as heme would be a suitable control to determine whether the protein

was interacting solely with the iron center of heme, or if the binding was unique to the larger

heme molecule. The control CD spectra show no change to rc*Pf*HRP2 structure upon addition of

Zn(II)PPIX (**Figure 3.7A**), which means that the structural shifts above are a result of the unique

heme binding to the protein. Further control experiments were run by adding 100 mM NaOH

directly to ITG rc*Pf*HRP2 in PB without heme present to ensure that the spectral changes

produced above were not the result of protein dilution. As expected, the spectra did not change

with the addition of NaOH alone (**Figure 3.7B**).
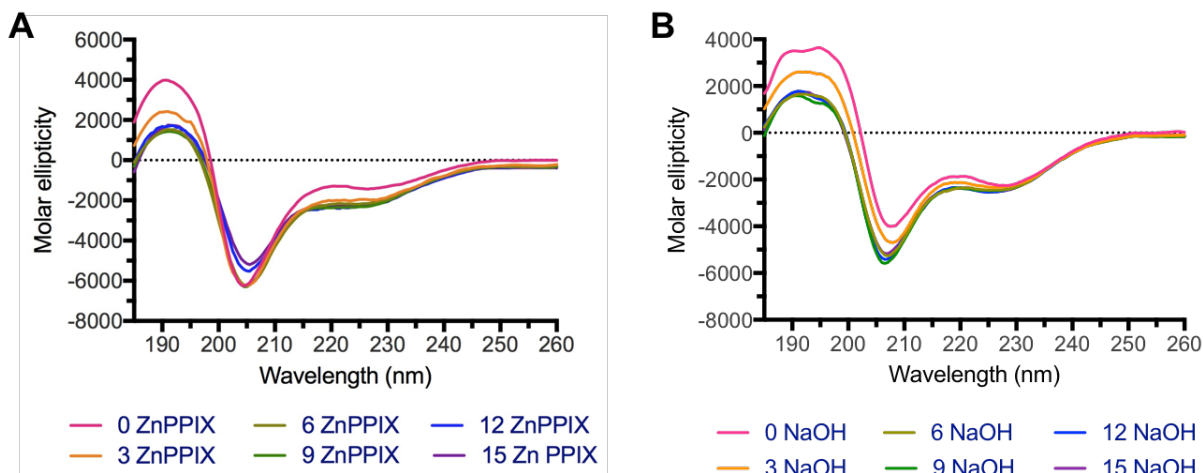
Figure 3.7. *Control experiments showing the titration of A) ZnPPIX and B) the same volume of 100 mM NaOH into ITG rcPfHRP2 in PB.*

Effect of heme-protein binding on RDT performance

      After confirming that heme binds to rc*Pf*HRP2 in a way that alters the three-dimensional

structure of the protein, we investigated how these changes affect RDT performance with the

protein. Three different RDT brands were tested using duplicate sample sets of various

rc*Pf*HRP2 concentrations in PBS. One sample set contained no additional heme, and the other

sample set was pre-incubated with 10.64 molar equivalents of heme relative to the protein

concentration. For all three RDT brands, a clear drop in signal was observed for those samples

which were pre-incubated with heme compared to the control samples (**Figure 3.8A-C**).

Furthermore, one RDT brand was tested with varying levels of heme pre-incubated with samples

of one rc*Pf*HRP2 concentration (**Figure 3.8D**). These experiments show a steady drop in RDT

signal with increasing heme equivalents added to the protein sample. These results indicate that

the change in rc*Pf*HRP2 structure caused by heme binding can affect the protein's ability to bind

to antibodies on RDTs. Because all heme levels tested in **Figure 3.8** were below the saturation

level of 15 equivalents relative to protein, we can assume that most of the heme added to these

samples was bound by the protein and was not free in solution to disrupt the antibody binding in

other ways.
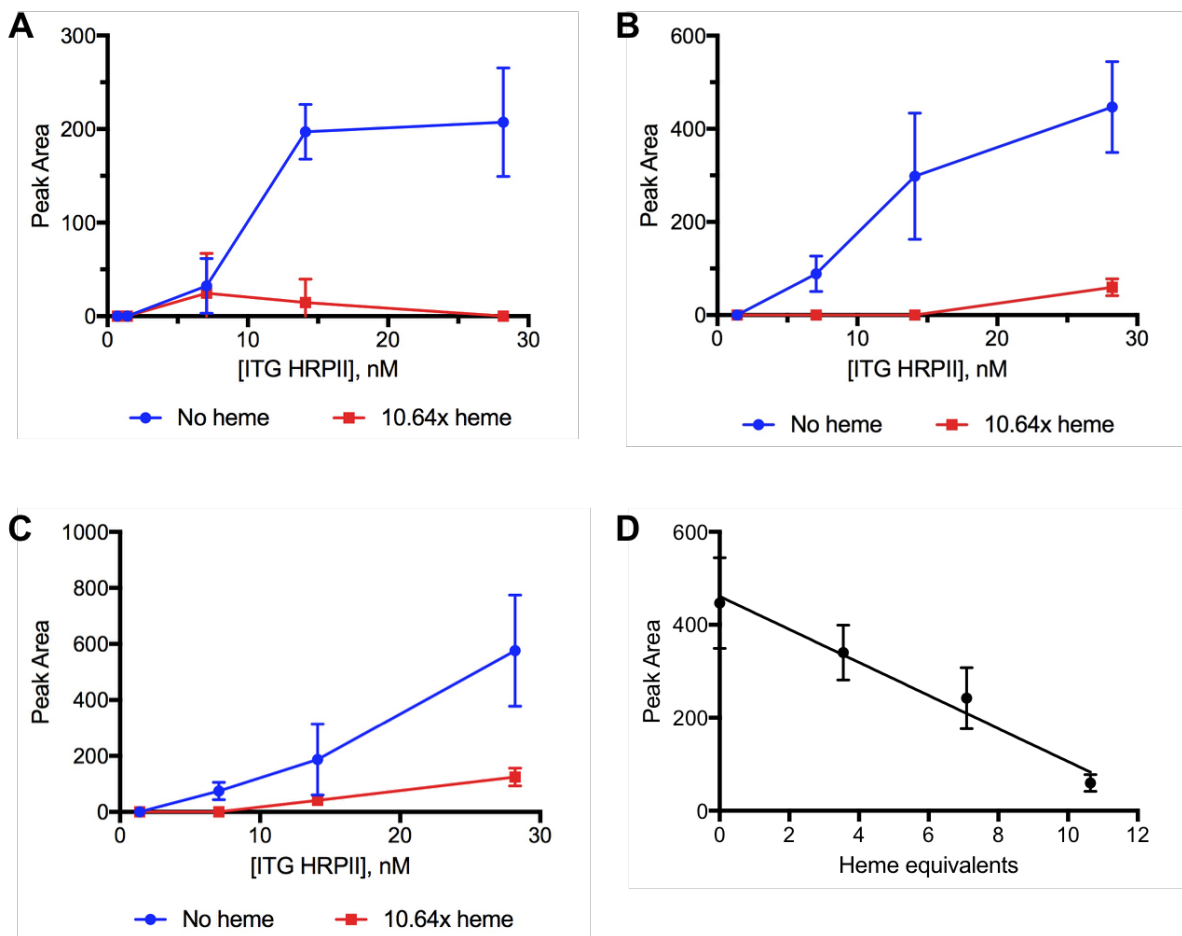
Figure 3.8. *Effect of heme binding on rcPfHRP2 RDT signal for A) Paracheck-Pf RDTs, B) SD Bioline Malaria Ag Pf RDTS, and C) ICT Malaria Pf RDTs. D) Varying heme concentration with constant rcPfHRP2 on SD Bioline Malaria Ag Pf RDTs.*

The protein concentrations used in these experiments would correspond to the protein levels found in malaria patients with high parasitemia loads, based on ELISA quantification of *Pf*HRP2 found in our in-lab parasite culture. Similarly, the corresponding heme concentrations tested are within the typical range for free heme in parasitized blood samples, as quantified by past lab members. However, it is important to note that we do not observe these drastic signal differences when rc*Pf*HRP2 is spiked into whole blood, and we do not expect such a large heme-binding effect in native parasitized samples. This is because blood contains several other heme-binding proteins, such as human serum albumin (HSA)[23], which will bind some percentage of free heme in blood, making it unavailable for binding with *Pf*HRP2. However, it is still possible for free heme to bind to *Pf*HRP2 and change its structure, thus interfering with antibody-based detection assays such as RDTs. Diagnostic tests run on patients with high levels of circulating *Pf*HRP2 and some amount of heme binding interference would probably still yield a positive result. For patients with low parasitemia loads and low circulating *Pf*HRP2 concentrations, even a small heme-binding interference could mean the difference between a diagnostic test showing a positive or negative result. A false negative from the heme binding interference would lead to delayed treatment and potentially a worse outcome for the patient.

Effect of heme-protein binding on ELISA performance

An ELISA format was used to further probe the effect of heme-induced structural changes on rc*Pf*HRP2-antibody binding. This *Pf*HRP2 ELISA was developed in our lab and is quite reliable for recombinant and native protein detection.[16] Its performance was re-evaluated with ITG rc*Pf*HRP2 in buffer before further experiments were run because we had not previously

used the ITG recombinant variant with this assay before. (**Figure 3.9A**) Of particular interest

was the dynamic range with this variant, since further experiments would depend on a reliable

standard curve. Since the standard curve is linear up to 5 pM of ITG rc*Pf*HRP2, three test

concentrations below this value were chosen to evaluate the effects of heme binding on ELISA

performance. Samples of 0.5 pM, 1 pM, and 3 pM ITG rc*Pf*HRP2 were incubated with varying

amounts of heme for 15 minutes before being added to the prepared ELISA plate. Once the

ELISA was completed, the apparent rc*Pf*HRP2 concentration was calculated for each sample

using the standard curve. The apparent concentration was compared with the actual known

protein concentration added to that well to calculate the percentage of protein successfully bound

to the ELISA antibodies. All protein concentrations tested showed a decrease in ELISA

performance after incubation with 5 molar equivalents of heme, with only 40 – 50 % of protein

detected (**Figure 3.9B**).
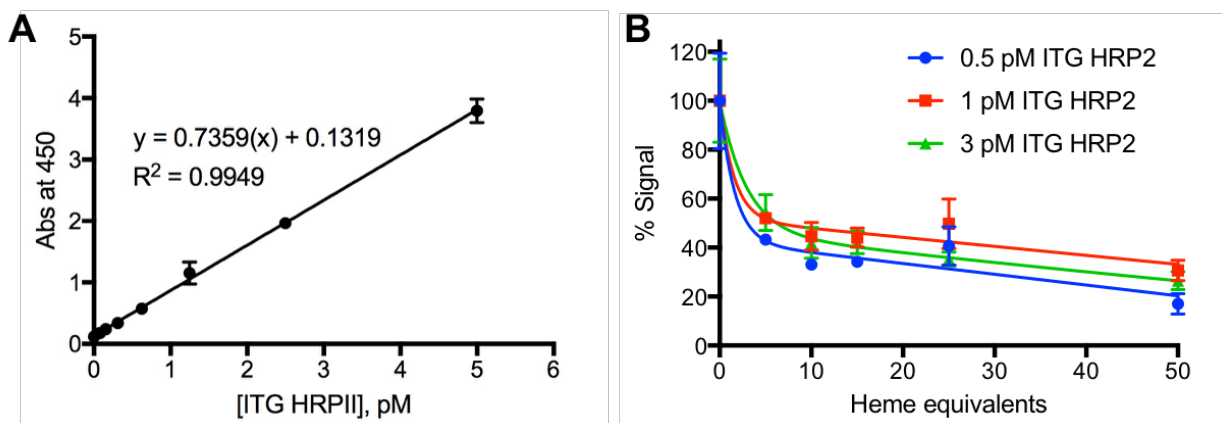
Figure 3.9. *A) ELISA standard curve using ITG rcPfHRP2 as standard antigen and B) Effect of heme-rcPfHRP2 binding on ELISA signal for several rcPfHRP2 concentrations and varying heme equivalents.*

The ELISA format allowed us to probe higher heme concentrations than those used in the previous RDT and CD experiments. While a heme:protein ratio of 25:1 or 50:1 is not necessarily biologically relevant, it does allow us to understand how the assay performs when there is an excess of free heme in solution. Rc*Pf*HRP2 is saturated with heme after 15 equivalents have been added, and this changes the protein structure so that the apparent concentration detected by ELISA is roughly 40% of the actual protein concentration. If more heme is added, however, the apparent protein concentration does not continue to drop until 50 molar equivalents of heme have been added. This indicates that the heme is probably not interfering directly with the antibodies in the assay, only the rc*Pf*HRP2 structure that allows the antibodies to bind to it.

Again, such drastic binding interference is not expected in parasitized blood samples, but it is more likely that heme binding in blood does dampen the signal of rc*Pf*HRP2 assays to some smaller degree. Unfortunately, it is impossible to use CD to investigate native or recombinant *Pf*HRP2 in a complex protein-rich matrix such as blood, so a complete picture of heme-induced structural changes has not yet been achieved. Future work can instead focus on rc*Pf*HRP2 spiked into whole blood, or isolated native *Pf*HRP2. While native protein can be isolated from blood using protocols developed in our lab[16], it is not to the scale or purity standards that would be necessary for CD analysis.

Conclusion

This chapter explored the structural changes of rc*Pf*HRP2 when bound to heme and the practical effects of these changes on antibody-based assays to detect the protein. Heme binds to rc*Pf*HRP2 at a saturating ratio of 15:1, shifting the protein structure from a predominantly random-coil form to a helical structure. These structural changes adversely affect rc*Pf*HRP2

binding to antibodies in RDT and ELISA formats, and they appear to be reversible with diafiltration. Future work depends on the ability to successfully isolate pure native *Pf*HRP2 from culture or patient samples, which past lab members have proven is difficult to do at adequate purity and scale for these experiments.

These results have implications in future assay development. As the community continues to develop more and more sensitive diagnostic assays, every possible hindrance must be removed, including assay binding interference caused by heme. The sample filtration discussed above may be one solution to this issue, but it has not been tested on real-world samples. Heme-induced structural changes for rc*Pf*HRP2 may also lead assay developers to investigate assays that do not rely on antibody binding, such as the assay described in the previous chapter, or to focus on a different biomarker altogether, such as DNA biomarkers discussed in later chapters.

Acknowledgements

References

(1)   The malERA CGoDD. *PLoS Med.* **2011**, *8*, e1000396.

(2)   Laishram, D. D.; Sutton, P. L.; Nanda, N.; Sharma, V. L.; Sobti, R. C.; Carlton, J. M.; Joshi, H. *Malar. J.* **2012**, *11*, 29.

(3)   Vinetz, J. M.; Gilman, R. H. *Am. J. Trop. Med. Hyg.* **2002**, *66*, 639–640.

(4)   Bousema, T.; Okell, L.; Felger, I.; Drakeley, C. *Nat. Rev. Microbiol.* **2014**, *12*, 833–840.

(5)   UNITAID. *Malaria Diagnostics Technology and Market Landscape, 2014*; 2014.

(6)   World Health Organization; Special Programme for Research and Training in Tropical Diseases; Foundation for Innovative New Diagnostics; Centers for Disease Control and Prevention. *Malaria Rapid Diagnostic Test Performance: Results of WHO Product Testing of Malaria RDTs: Round 3 (2010 - 2011).*; 2011.

(7)   World Health Organization. *Malaria rapid diagnostic test performance: results of WHO product testing of malaria RDTs: round 6 (2014-2015)*; 2015.

(8)   Baker, J.; McCarthy, J.; Gatton, M.; Kyle, D. E.; Belizario, V.; Luchavez, J.; Bell, D.; Cheng, Q. *J. Infect. Dis.* **2005**, *192*, 870–877.

(9)   Baker, J.; Ho, M. F.; Pelecanos, A.; Gatton, M.; Chen, N.; Abdullah, S.; Albertini, A.; Ariey, F.; Barnwell, J.; Bell, D. **2010**.

(10)   Koita, O. A.; Doumbo, O. K.; Ouattara, A.; Tall, L. K.; Konare, A.; Diakite, M.; Diallo, M.; Sagara, I.; Masinde, G. L.; Doumbo, S. N.; Dolo, A.; Tounkara, A.; Traore, I.; Krogstad, D. J. *Am. J. Trop. Med. Hyg.* **2012**, *86*, 194–198.

(11)   Gamboa, D.; Ho, M.-F.; Bendezu, J.; Torres, K.; Chiodini, P. L.; Barnwell, J. W.; Incardona, S.; Perkins, M.; Bell, D.; McCarthy, J.; Cheng, Q. *PLoS One* **2010**, *5*, e8091.

(12)   Pandey, A. V.; Babbarwal, V. K.; Okoyeh, J. N.; Joshi, R. M.; Puri, S. K.; Singh, R. L.; Chauhan, V. S. *Biochem. Biophys. Res. Commun.* **2003**, *308*, 736–743.

(13)   Sullivan, D. J.; Gluzman, I. Y.; Goldberg, D. E. *Science (80-.).* **1996**, *271*, 219–222.

(14)   Desakorn, V.; Dondorp, A. M.; Silamut, K.; Pongtavornpinyo, W.; Sahassananda, D.; Chotivanich, K.; Pitisuttithum, P.; Smithyman, A. M.; Day, N. P. J.; White, N. J. *Trans. R. Soc. Trop. Med. Hyg.* **2005**, *99*, 517–524.

(15)   Schneider, E. L.; Marletta, M. A. *Biochemistry* **2005**, *44*, 979–986.

(16)   Davis, K. M.; Swartz, J. D.; Haselton, F. R.; Wright, D. W. *Anal. Chem.* **2012**, *84*, 6136–6142.

(17)   Karnaukhova, E.; Rutardottir, S.; Rajabi M., M.; Rosenlöf, L. W.; Alayash, A. I.; Åkerström, B. *Front. Physiol.* **2014**, *5*, 1–11.

(18)   Greenfield, N.; Fasman, G. D. *Biochemistry* **1969**, *8*, 4108–4116.

(19)   Kelly, S. M.; Jess, T. J.; Price, N. C. *Biochim. Biophys. Acta - Proteins Proteomics* **2005**, *1751*, 119–139.

(20)   Alliance Protein Laboratories Inc. Circular Dichroism http://www.ap-lab.com/circular_dichroism.htm (accessed Feb 8, 2017).

(21)   Greenfield, N. J. *Nat. Protoc.* **2006**, *1*, 2527–2535.

(22)   Panton, L. J.; McPhie, P.; Maloy, W. L.; Wellems, T. E.; Taylor, D. W.; Howard, R. J. *Mol. Biochem. Parasitol.* **1989**, *35*, 149–160.

(23)   Kamal, J. K. A.; Behere, D. V. *Indian J. Biochem. Biophys.* **2005**, *42*, 7–12.

CHAPTER IV

DEVELOPMENT OF AUTOMATED DEVICES FOR THE EXTRACTION AND PCR
AMPLIFICATION OF MALARIA DNA FROM SURROGATE PATIENT SAMPLES

Introduction

Current point-of-care diagnostics for malaria rely on the presence of protein biomarkers
*Pf*HRP2 and *Plasmodium* lactate dehydrogenase (*p*LDH) to work effectively. These proteins and
their unique characteristics offer many advantages in a diagnostic setting, but they are not
without their faults. For example, *p*LDH is an essential enzyme produced by all *Plasmodium*
parasites, so it is unlikely to suffer gene deletions, and it can be used as a diagnostic in any
geographic area regardless of the prevalence of particular parasite species.[1,2] Furthermore, it does
not persist in the body after parasites have been cleared, unlike *Pf*HRP2, which can persist for
weeks even after the patient has been cured.[3-6] However, *p*LDH can be difficult to work with
because it is easily denatured, and rapid diagnostics tests for the protein are not as sensitive as
those for *Pf*HRP2.[7-9] *Pf*HRP2 is a convenient diagnostic protein for several reasons, including
those explored in the previous two chapters. Its histidine-rich structure allows for the use of
metal-based chemistry for both isolation and detection of the protein, and its lack of a defined
three-dimensional structure makes it very stable at high temperatures, as noted previously in this
dissertation.[10,11] Biologically, the protein persists in patients long after parasite clearance, making
it a poor biomarker for monitoring treatment effectiveness.[3,4,6] It is also a common gene deletion
in parasites in certain geographical areas, such as South America, making it an unreliable
biomarker in general.[12-14] So, while both *Pf*HRP2 and *p*LDH have been important biomarkers in

the modern fight against malaria, it is clear that we need to incorporate other biomarkers into the diagnostic strategy as we move towards malaria elimination.

DNA is commonly used as a biomarker for human pathogens due to its versatility and specificity. For malaria, the presence of any DNA sequence specific to the parasite in a patient sample can be used for diagnosis. DNA can also provide much more information than a positive or negative diagnosis. Sequence variation between *Plasmodium* species can be used to determine the particular species infecting the patient, thus informing treatment since different drugs are used to treat different species of *Plasmodium*.[8,15,16] Furthermore, genetic information can change the treatment between two patients infected with the same *Plasmodium* species. Mutations in the K13 propeller gene in *Plasmodium falciparum* have been found to lead to artemisinin resistance, indicating that identifying only the parasite species may not be enough to effectively treat the patient.[17,18] DNA also provides practical advantages to protein biomarkers. It is relatively stable even at room temperature at basic pH, provided the solution is not contaminated with DNase. Specific sequences can be captured from samples simply by using synthetic, cheaply available complementary DNA, without the need for expensive, time-consuming antibody production that hinders several protein diagnostics.

Of course, DNA is not a perfect biomarker for pathogens, and it has drawbacks of its own. Specific malaria DNA sequences are often present at much lower concentrations than protein biomarkers in patient samples, so a target amplification step is often needed before the DNA biomarker can be detected.[19,20] The most reliable DNA amplification method is polymerase chain reaction (PCR), which requires expensive equipment and reagents and extensively-trained technicians to perform. These requirements make PCR a viable diagnostic technique in modern, well-equipped diagnostic labs or hospitals, but they are some of the largest hindrances to the use

of DNA as a biomarker in low-resource settings. Furthermore, PCR is often inhibited by compounds commonly found in patient samples, such as the hemoglobin in blood.[21] This means that DNA biomarkers must be extracted from the sample matrix before detection can occur, adding another lengthy, manual step to the diagnostic process. Silica-based extraction techniques are frequently used to capture all nucleic acids in a sample, but they are most commonly used as centrifugal columns which require expensive centrifuges to purify a sample.

Silica-functionalized magnetic beads are an attractive alternative to column-based DNA extractions because the only additional equipment they require for use is an external magnet. Magnetic beads are easy to manipulate manually in small sample tubes with a hand-held magnet, or they can also be easily integrated into high-throughput automated extraction devices.[22–26] These devices are typically well plate- or chip-based, and they use an external magnet to either keep the beads stationary within a plate or move the beads through an array of processing solutions. Plate-based devices require complex fluid pumping and movable robotics, and are forced by design into batch-based processing.[22] In this device design, multiple samples are processed in parallel on a plate, and an entire plate is usually filled before processing. These systems work very well in high-throughput laboratories, but they are inefficient in low sample number settings. Magnetic beads have been used in chip devices to eliminate the need for fluid pumping, but the format requires multiple solution outlets and precise fluid manipulations.[26] An ideal DNA extraction device for a low-resource setting would not require complex fluidics or robotics, but would instead consist of a simple, flexible design made of components that are both easy to program and easy to repair.

This chapter describes the development of a magnetic bead-based protocol to extract malaria DNA from blood, and its adaptation into two automated devices that can be used to

57

simplify the extraction and detection workflow. The first roller-based device requires offline PCR analysis, but the second axle-based device incorporates PCR thermocycling as the final step. The first device (**Figure 4.1A**) consists of a circular plastic cartridge that rests on both a roller controlled by a programmable motor, and a support bar containing six neodymium magnets. To perform an extraction, the sample is incubated with magnetic beads to capture the biomarker of interest, and then it is then loaded into a length of small-diameter plastic tubing containing preloaded processing solutions. This length of tubing is wrapped around the device cartridge and as the cartridge rotates, the biomarker-bound magnetic beads are transferred through the processing solutions by the stationary external magnet. Biomarker extraction in this format is enabled by our previously described surface tension valves, or immiscible fluid separators, which are used to sequentially array processing solutions within a single length of small-diameter tubing.[10,27–29] The second device follows a similar design, but with a cassette fixed on a central rotation axle (**Figure 4.1B**). This design also allows us to incorporate the electronics necessary for PCR thermocycling and optical detection in-tube directly after DNA extraction.

This simple format for both of these devices has advantages over other biomarker extraction procedures because multiple biomarker classes can be extracted on the same device, simply by using different bead surface chemistries and processing solutions. The devices require little power and are simple to operate. The performance of these devices were validated for the extraction of malaria DNA using a panel of surrogate patient samples prepared by the Program for Appropriate Technology in Health (PATH).
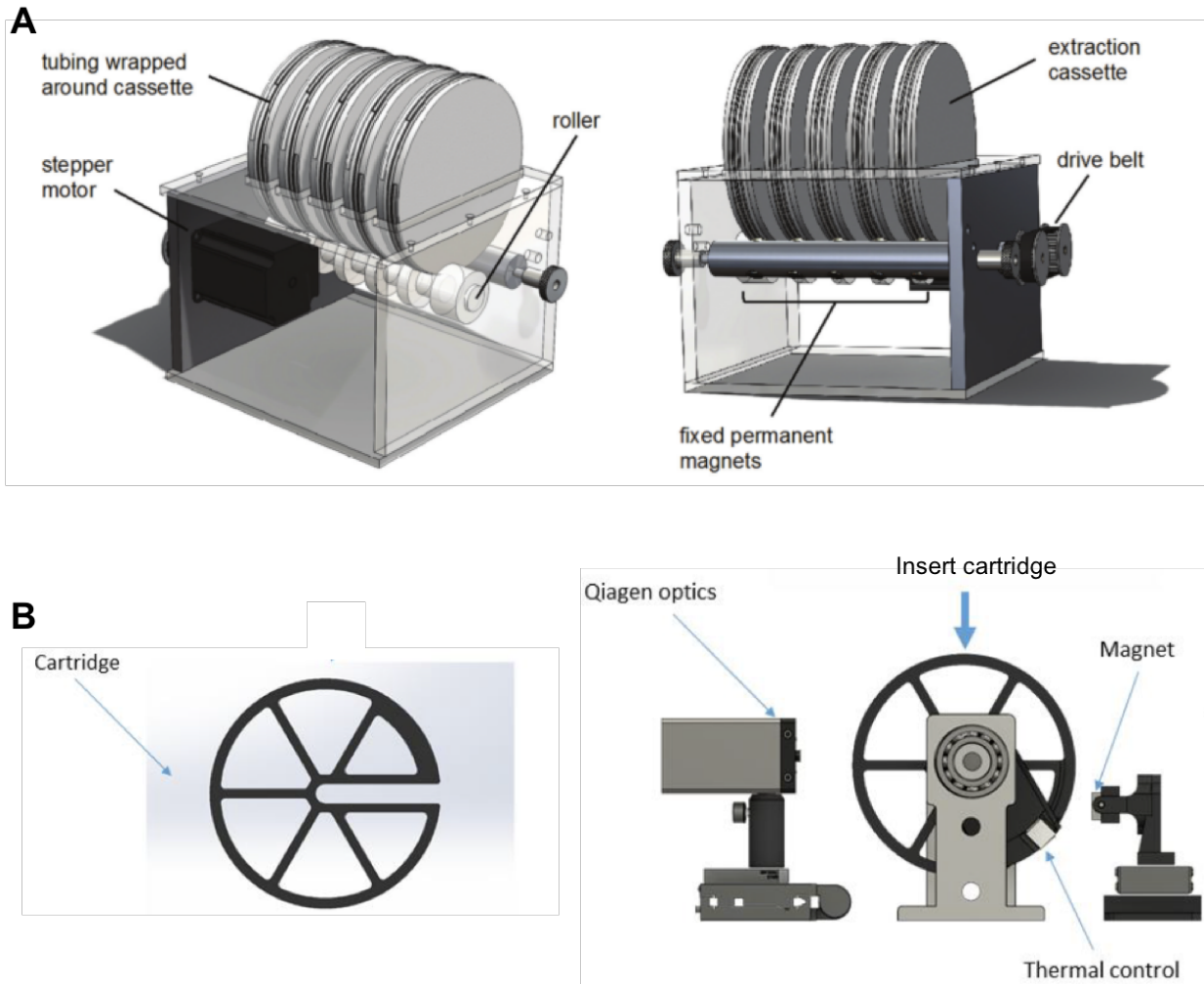
Figure 4.1. *A) Roller-based automated biomarker extraction device, which requires off-line PCR analysis. B) Axle-based automated biomarker extraction and detection device, which includes heating and optical detection elements allowing the user to run PCR in the same extraction tube directly after DNA extraction.*

Materials and Methods

Materials for DNA biomarker extraction tube

Plasmodium falciparum (malaria parasite) infected sample panels were prepared and provided by PATH. Primers, probes, and reference standard templates were purchased from Integrated DNA Technologies. SuperScript III RT/Platinum TAQ mix (Cat # 11732-088) and Dynabeads MyOne Silane magnetic beads (Cat # 37002D) were purchased from Life

Technologies. Quanta PerfectA 2x mastermix was purchased from VWR (Quanta Biosciences, Cat # 84010). Filtration swabs (Cat # 5001.02) were purchased from Salimetrics Inc. Fluorinated ethylene propylene (FEP) tubing was purchased from McMaster Carr (Cat # 2129T11 and # 9369T46). Hemato-Seal tube sealing compound (Cat # 02-678) was purchased from Fisher Scientific. All other materials and reagents were purchased from Sigma Aldrich or Fisher Scientific.

Materials for roller-based device fabrication

The Arduino UNO Rev3 programmable controller was purchased from Arduino (Cat # A000066). The stepper motor drive controller (Cat # STR4), stepper motor (Cat # HT23-401), and power supply (Cat # PS150A24) were purchased from Applied Motion Products. Cylindrical magnets were purchased from SuperMagnetMan (Cat # Cyl0360 N40). The components were assembled using aluminum components made in-house by the Vanderbilt Physics and Astronomy Machine Shop. The plastic cassettes were designed and printed in-house using SolidWorks software and a NovaCopy ProJet HD 3000 Plus 3D printer.

Design and operation of the roller-based automated biomarker extraction device

The automated biomarker extraction device was designed to transport magnetic beads through a series of processing solutions contained within 1.6 mm i.d. tubing by rotating an extraction cassette (i.e., a plastic disc with extraction tubing wrapped around the circumference) past a fixed magnet using a simple stepper motor (**Figure 4.1A**). The cassette is a plastic disc that is 14 cm in diameter and 1.9 cm thick, with a continuous channel on the outer edge to secure the assay tubing around the disc circumference. In this design, individual cassettes are placed

onto a rotating shaft to drive the rotation of the cassettes past a second shaft containing fixed magnets. As the disc rotates, the magnetic beads within the assay tubing are held in place by the magnets while the processing solutions contained in the assay tubing move past the beads. An open-top roller-drive design was chosen over an axle-drive design to facilitate asynchronous, random-access loading and processing of independent cassettes on the device.

The Arduino UNO Rev3 programmable controller was used to send logical input commands to the motor controller to regulate the direction, speed, and timing of the drive motor. The Arduino code was developed to allow the operator to input desired rotational distance and velocity. Two timing gears and a ribbed belt attach the motor to a roller on which the cassettes sit. As the roller rotates, friction between the roller and the cassettes causes the cassettes to rotate past the panel of fixed magnets. The rotation processes magnetic beads through the array of solutions within the tubing.

Materials for axle-based device fabrication

The Arduino UNO Rev3 programmable controller was purchased from Arduino (Cat # A000066). The stepper motor drive controller (Cat # STR4), stepper motor (Cat # HT23-401), and power supply (Cat # PS150A24) were purchased from Applied Motion Products. Cubic magnets were purchased from SuperMagnetMan (Cat # Cyl0360 N40). The Qiagen ESELog USB Fluorescence reader (Cat # 9002069) was purchased from Qiagen. The Peltier heating element (Cat # VT-31-1.0-1.3) was purchased from TE Technology. The TDK Lambda Z+ Power Supply (Cat # Z36-6-U) was purchased from TDK Lambda. The Omega TC, K-type small gauge 0.05" thermocouple (Cat # 5TC-TT-K-36-36) was purchased from Omega. The components were assembled using aluminum components made in-house by the Vanderbilt

Physics and Astronomy Machine Shop. The plastic cassettes were designed and printed in-house using SolidWorks software and a NovaCopy ProJet HD 3000 Plus 3D printer.

Design and operation of the axle-based automated biomarker extraction device

As in the device described above, the axle-based extraction device was designed to transport magnetic beads through a series of processing solutions contained within 1.6 mm inner diameter (ID) tubing by rotating an extraction cartridge past a fixed magnet using a simple stepper motor (**Figure 4.1B**). The cartridge is 3D printed in ABS-equivalent plastic with a diameter of 7 inches. The cartridge has a cut-out to allow it to fit onto an axle to enable top-down loading onto the axle, and a continuous channel on the outer edge to secure the assay tubing around the cartridge circumference. The cartridge contains a copper tube (7.525 mm ID, ½-inch long) into which the end of the assay tube is threaded where the detection chamber is located. Once the cartridge is loaded onto the axle, this copper tube interfaces with the Peltier device to provide a uniform thermal distribution around the circumference of the amplification chamber in the assay tube during PCR. Another identical copper tube is located beneath the other one into which a 1-inch long FEP tube is inserted that contains water and is capped at both ends. This "witness tube" interfaces the same Peltier device when the cartridge is loaded on the instrument. A resistance temperature detector (RTD) is contained within the witness tube and is connected to the temperature controller to enable monitoring of the fluid temperature. By monitoring the temperature of the witness tube, the temperature of the fluid in the assay tube can be estimated for temperature feedback and control purposes without having to directly access the fluid in the assay tube. The magnet is encased in a spring-loaded plastic holder which maintains

constant pressure between the magnet and the assay tube when the cartridge is fitted onto the axle.

The Arduino UNO Rev3 programmable controller is used to send logical input commands to the motor controller to regulate the direction, speed, and timing of the drive motor. The Arduino code was developed to require minimal input from the user, so that the cartridge always starts the program in the same position. The motor drives the axle, and the rotation processes magnetic beads through the array of solutions within the tubing, depositing the beads in the PCR solution and pulling them back out after a short elution time. Once the extraction portion of the assay is complete, the instrument begins PCR thermocycling. The Peltier heats the solutions until the witness tube registers 95 °C, and then it switches off and allows the witness tube and assay tube to cool down to 56 °C, when it begins heating again. This is repeated for 45 cycles, or the operator can stop the reaction early. At the end of each cycle, when the witness tube temperature reads 56 °C, the Qiagen fluorescence detector reads the EvaGreen fluorescence.

Nucleic acid quantification by qPCR

Nucleic acids extracted from the PATH panel samples were quantified by qPCR as appropriate according to protocols adapted by PATH from an existing study.[30] The primer/probe sequences and cycling conditions are provided in **Table 4.1**. DNA from malaria parasite was amplified via qPCR using Quanta PerfectA 2x mastermix in 25 μL reaction volumes. Final primer concentration was 800 nM for each primer and final probe concentration was 150 nM. For quantification, each reaction was performed in parallel with a standard curve prepared by serially diluting synthetic DNA amplicons in TE buffer. The sequence of the amplified gene was purchased from Integrated DNA Technologies (IDT). Ten-fold dilutions were prepared from 10^7

copies/μL to 10 copies/μL. No template controls (NTC) were also performed with no DNA

added. Thermal cycling was performed using the Roche LightCycler 96, and cycle threshold (Ct)

values were calculated using the provided software.

Table 4.1. *Primer and probe sequences for PCR of extracted P. falciparum DNA. The probe is only used for off-line PCR after manual on roller-based device extraction, as the in-tube PCR uses EvaGreen dye for detection.*

Forward Primer	5' – ACA TGG CTA TGA CGG GTA ACG – 3'
Reverse Primer	5' – TGC CTT CCT TAG ATG TGG TAG CTA – 3'
Probe	5' – FAM-TCA GGC TCC CTC TCC GGA ATC GA-BHQ1 – 3'
Biomarker Template	5' – ACA TGG CTA TGA CGG GTA ACG GGG AAT TAG AGT TCG ATT CCG GAG AGG GAG CCT GAG AAA TAG CTA CCA CAT CTA GGA AGG CA – 3'

Manual and roller-based extraction of Plasmodium falciparum DNA from human blood culture

For manual and roller-based device extractions, assay tubing was prepared in a 43 cm

length of 2.36 mm i.d. FEP tubing. The tubing was loaded by pipetting 50 μL elution buffer (10

mM Tris pH 8.0, 1 mM EDTA, 0.05% Tween-20), 300 μL 70% ethanol, and 300 μL chaotropic

wash buffer (80% ethanol, 640 mM guanidine thiocyanate, 1.6 mM Tris pH 8.0, 160 μM EDTA,

0.08% Triton X-100) into one end. Each solution was separated from the next by a ~6 mm air

valve.

A 100 μL sample of malaria parasite-infected human blood culture (5% hematocrit) or

pooled whole blood spiked with synthetic DNA was combined with 300 μL lysis buffer (4 M

guanidine thiocyanate, 10 mM Tris HCl pH 8.0, 1 mM EDTA, 0.5% Triton X-100) and

incubated at room temperature for 10 minutes with occasional vortexing to lyse red blood cells.

The lysed samples were then filtered using one-fourth of a Salimetrics swab, and the sample was

expressed from the swab by using a 5 mL plastic syringe. After the addition of 100 μL of 100%

isopropanol and 7.5 x 10^8 silica-coated magnetic beads (25 μL suspension) to the filtered sample, it was incubated for 3 minutes at room temperature. Following nucleic acid adsorption, the tube contents were pipetted into the end of the preloaded tubing, both ends were sealed with tube sealing compound, and the assay was completed using both a manual magnetic bead-based extraction method and the two-speed automated extraction method.

For manual processing, the beads were collected within the sample chamber using a 1-inch neodymium magnet. The beads were slowly pulled across the air valve into the first wash chamber. The magnet was moved back and forth quickly along the wall of the tubing to mix the beads within the first wash chamber for 30 seconds. The beads were then pulled into the second wash chamber and mixed the same way for 30 seconds. Finally, the beads were pulled into the elution chamber, where they were mixed for 3 minutes using the magnet. The beads were then removed from the elution chamber, and the DNA in the final solution was quantified by qPCR as described above.

For automated processing on the roller-based device, the tubing was loaded on the extraction cassette, and extraction was carried out as described above. After 5 minutes of automated extraction, the tubing was removed from the cassette and the DNA in the final solution was quantified by qPCR as described above.

Axle-based extraction of Plasmodium falciparum DNA from human blood culture

For the axle-based device, extraction tubing was prepared in the same way as above, but omitting the 50 μL elution buffer. The sample was then prepared and mixed with silane magnetic beads as above, and pipetted into the upstream end of the preloaded tubing. Next, 20 μL PCR-grade mineral oil was pipetted into the downstream end of the tube, leaving a 6 mm air valve

between the oil and 70% ethanol wash. The oil was followed with 50 μL PCR reaction mix

(**Table 4.2**) pipetted into the downstream end, with no air gap between the oil and PCR mix. The

downstream end of the tubing was sealed with a Teflon tape-wrapped polypropylene screw, so

that the screw was in contact with the edge of the PCR solution. The upstream end of the tubing

was sealed with Hemato-Seal Capillary Tube Sealant.

Table 4.2. *Components of the in-tube PCR reaction and their concentrations.*

Component	Volume per 50 μL reaction	Final Concentration
5X KAPA2G Buffer	10 μL	1X
MgCl$_2$ (25 mM)	3 μL	1.5 mM
dNTP mix (10 mM each)	1 μL	200 μM
Forward primer (10 μM)	2 μL	400 nM
Reverse primer (10 μM)	2 μL	400 nM
KAPA2G polymerase (5 units/μL)	0.5 μL	2.5 units/reaction
EvaGreen (20 mM)	2 μL	800 μM
PCR grade water	29.5 μL	-

Witness tube preparation

A 30 mm length of FEP tubing was cut to make a "witness" tube for temperature

calibration. This tube was loaded with 20 μL PCR-grade mineral oil and 50 μL water to mimic

the PCR chamber of the actual assay tube. This witness tube was also sealed with a Teflon tape-

wrapped polypropylene screw and sealant clay to mimic the assay tube. The witness tube was

inspected before every PCR run to ensure the integrity of the chambers, and replaced if needed.

Loading the tubes onto the axle-based device

The witness tube was loaded into the inner groove of the copper heat block, and a

thermocouple plugged into the instrument was threaded through the clay sealant and submerged

in the water chamber to report the temperature to the instrument. The PCR assay tube was loaded

onto the instrument by threading the upstream (clay-sealed) end through the outer groove of the

copper heat block, and pulling the tubing through the copper block until the polypropylene screw

stopped it. This places the PCR solution inside the copper heating block. The tubing was then

pressed snugly into the groove around the diameter of the cassette.

Validation using surrogate patient sample panels from PATH

   The efficacy of the roller-based and axle-based extraction devices were tested using a

panel of surrogate malaria patient samples prepared and validated by PATH. Each panel

contained human blood culture spiked with concentrations of parasite corresponding to a

biologically relevant low, medium, or high level of infection, or 0.001%, 1%, and 5%

parasitemia respectively. Negative control samples containing no pathogen were also provided.

The sample panels tested are listed in **Table 4.3**. The sample panel was received frozen on dry

ice and stored at -80 °C until used.

Table 4.3. *Detailed composition of mock patient sample panel, diluted from high-parasitemia culture with normal blood diluted to a similar red blood cell concentration. All final samples are 5% hematocrit and stabilized with Glycerolyte 57.*

Spike	% Parasitemia	Infected cells/μL
High	5 %	$6 - 9 \times 10^4$
Medium	1 %	$0.8 - 2.5 \times 10^4$
Low	0.001%	8 - 20
Negative	0	0

Data analysis for the axle-based device

   The axle-based extraction and PCR device does not have data analysis software, so a

manual method of determining cycle thresholds for validation was needed. During the

amplification reaction, fluorescence was recorded after each cycle when the witness tube temperature reached 56°C. This fluorescence vs. cycle data was recorded and plotted as an amplification curve. The first ten cycles of each run were averaged to obtain the background signal, which was then subtracted from the raw fluorescence readings. Cycle threshold (Ct) values were defined as the cycle when the slope of the measured fluorescence ($dF/dCycle$) reached its maximum.[31]

Results and Discussion

Manual extraction optimization

Before this work was undertaken, our laboratory had used functionalized magnetic beads to isolate nucleic acids from sample matrices such as urine,[28] synthetic sputum,[32] and nasal swabs,[27] but not blood. The malaria biomarker *Pf*HRP2 had been isolated from blood using magnetic beads,[10] but it was clear that nucleic acids were quickly becoming a preferred biomarker for malaria diagnosis for the reasons explained above. Therefore, a new nucleic acid extraction protocol was developed for silane-coated beads that would allow DNA to be extracted from blood samples.

Studies first focused on optimizing the lysis and wash conditions to maximize the extraction efficiency of malaria DNA from whole blood. Preferred lysis conditions would not require the use of unnecessary PCR inhibitors, extensive heating, or long incubation times. Typical silica-based DNA extraction kits utilize proteinase K for lysis, but this enzyme requires heating for optimal activity, so it was eliminated after preliminary tests showed a negligible effect on extraction efficiency. Triton X-100 was chosen as a lysis detergent instead of sodium dodecyl sulfate (SDS) because it is not a PCR inhibitor like SDS. Finally, guanidinium

68

thiocyanate (GuSCN) served to denature proteins and to act as a chaotropic agent to drive DNA adsorption to the silica-coated beads. In order to determine the efficacy of these lysis conditions, they were tested using the extraction cassette described above using in-house 5% parasitemia culture, and subsequently analyzed via qPCR. A high level of parasite DNA (1.26×10^6 copies/μL) was detected after extraction, which indicated that the parasites were effectively lysed using the lysis buffer.

In order to calculate actual extraction efficiency, the synthetic parasite DNA sequence to be amplified was spiked into whole blood at a concentration of 1×10^4 copies/μL and subjected to several optimization experiments. First, an effective post-lysis, pre-silica adsorption filtration method needed to be identified in order to reduce later bead aggregation due to cell debris from the sample. Glass wool is typically an effective blood filtration material,[10] but it was not an option since the silica surface would bind the parasite DNA before it reached the magnetic beads. Instead, a polymer saliva collection swab in a 5 mL plastic syringe was used to filter lysed blood samples before introducing the silica-coated magnetic beads. This filtration method resulted in an increase in extraction efficiency from unfiltered samples and an increase in ease of bead handling due to lack of cell debris (**Figure 4.2A**).

Further extraction optimization was performed on filtered samples by adding either a second chaotropic wash step to remove excess protein, a second ethanol wash step to remove PCR inhibitors, or by increasing the elution volume to ensure that all DNA was being eluted from the beads (**Figure 4.2B**). Percent recovery of spiked DNA was very low for all methods, but was not unexpected. Silica adsorption isolates all nucleic acids from a sample, and whole blood contains human DNA from the white blood cells. This means that the spiked parasite DNA makes up a small percentage of total nucleic acids present in the blood sample, and it is likewise

only a small percentage of the nucleic acids bound to the beads. These three optimization tests did not increase extraction efficiency, so the original extraction device design was used to extract the samples provided by PATH.
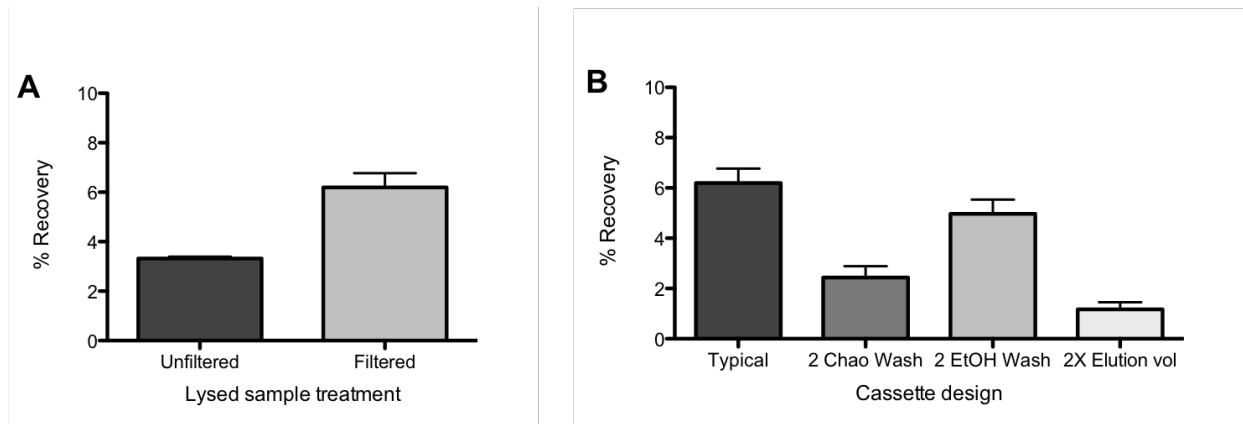

Figure 4.2. *Optimization of DNA extraction cassette. A) Recovery of DNA for unfiltered and filtered samples. B) Recovery of DNA for typical cassette design (1 wash each type, 50 µL elution) compared to other designs.*

As a way to validate our tubing-based extraction method with standard samples, we extracted DNA from parasite culture samples provided by PATH for this purpose. These samples contained 5% hematocrit in growth media, with standardized parasitemia levels of 0.001%, 1%, and 5%, along with uninfected samples. These percentages corresponded to 8 – 20 parasites/µL, $0.8 – 2.5 \times 10^4$ parasites/µL, and $6 – 9 \times 10^4$ parasites/µL, respectively, according to the provided sample descriptions. All sample concentrations were extracted with our manual method using n = 9 extractions per concentration. qPCR amplification and detection showed that *P. falciparum* DNA is present at detectable levels after extraction with the manual extraction device, even in low parasitemia infections with 8 – 20 parasites/µL (**Figure 4.3**, black bars). Positive signal was

obtained for negative samples, which indicates contamination either during the off-line PCR or during the tubing preparation.
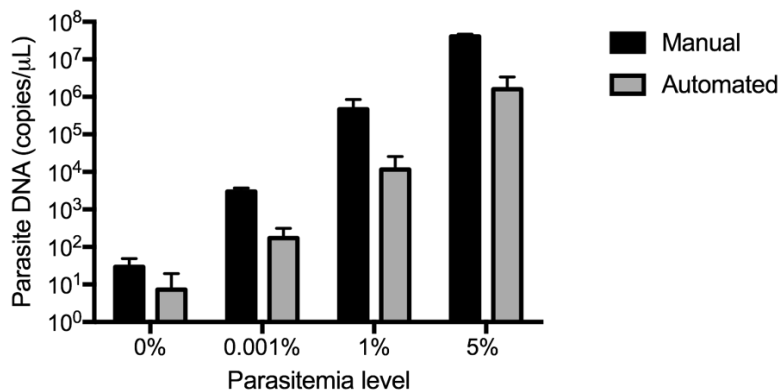

Figure 4.3. *Panel sample DNA extractions using the manual method and roller-based device, with off-line PCR run in a LightCycler 96.*

Roller-based device validation

The extraction works well in a manual format, but it is not well-suited to a low-resource environment due to the careful handling and manipulation required to successfully operate the device. Training and practice are necessary to extract malaria DNA using this extraction tubing setup, and it is difficult to handle more than three extraction tubes at one time if one is extracting multiple samples. For these reasons, we decided to adapt the handheld extraction tube into an automated extraction device that still adhered to parameters required in a low-resource setting, namely that it be simple to operate and require little electrical power. The roller-based device developed for this purpose features an asynchronous sample loading design that allows for samples to be added to and removed from the device at any time while it is running. This is particularly appealing in settings that receive low sample numbers, as it removes the requirement to batch samples. Users can add or remove individual assay cartridges from the device

71

asynchronously, without stopping or otherwise impacting the processing of other assays. To operate the device, the user wraps the cassette around the circumference of a plastic disc, which is then placed onto the rollers. The magnetic beads within the cassette are pulled through the extraction tubing as the plastic disc rotates past a fixed external magnet (**Figure 4.1A**). The device was programmed with two "steps," using the first step to slowly pull the beads a short distance within the cassette and the second step to quickly rotate the cassette 705° before stopping, collecting the beads, and repeating the two steps. The quick rotation step serves to spread and mix the beads throughout the chamber in which they are contained, thus washing the beads within the wash solutions and elution chamber.

We used the roller-based device to repeat the DNA extractions above, using the same PATH panel samples so that we could compare the roller-based extraction device with a manual extraction. All sample concentrations from PATH were extracted with n = 9 per concentration as before, and analyzed using offline qPCR after the purified sample was excised from the extraction tubing. In general, the automated device recovered only slightly less *P. falciparum* DNA than the manual method, but the DNA was still detected at acceptable levels using qPCR (**Figure 4.3**, gray bars). These results indicated that this automated DNA extraction device could be further extended to incorporate PCR, thus resulting in a fully automated sample-to-answer diagnostic instrument.

Axle-based device PCR optimization

Adding PCR to the automated extraction device required adding a chamber to the extraction tubing set-up, changing or adding several mechanical elements of the instrument, and changing the PCR chemistry. First, the extraction tubing would now contain a PCR reaction

mixture as the final chamber (**Figure 4.4A**), instead of a buffer elution chamber (**Figure 4.4B**). This would allow the DNA to elute from the beads directly into the PCR reaction mixture. The removable plastic disc of the previous automated device became a fixed component of the instrument, and it was powered by an axle through the center of the disc instead of resting on rollers. These changes enabled the addition of a heat block to the disc and an LED fluorimeter to the instrument, both of which would be difficult or impossible to incorporate using the removable plastic disc from the roller-based device. The reaction temperature was monitored using a "witness tube," or a short piece of tubing containing water and oil to mimic the PCR chamber, placed directly beside the reaction tube in the heating block. The temperature of the water was monitored using a wire thermocouple threaded through the sealing clay and submerged in the water. By design, thermocycling on the axle-based device would proceed by heating the copper heat block until the reaction mixture reached 95°C, then passive cooling would be used to bring the reaction temperature down to 56°C. Modern PCR instruments hold these reaction temperatures for a set amount of time, typically from 30 to 60 seconds. In an effort
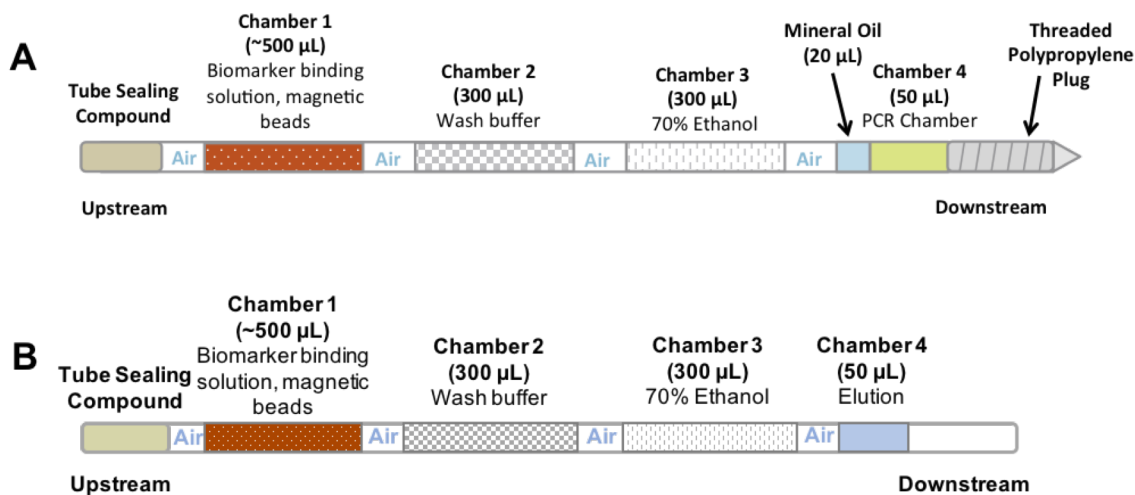

Figure 4.4 *Final tubing arrays for use with A) the manual extraction method and roller-based extraction device, and B) the axle-based extraction device with PCR.*

to save reaction time and to make the device simpler to program, however, we chose not to incorporate "hold" times into our instrument. This meant that the PCR chemistry of our all-in-one assay had to change from the assay previously used above.

The new in-line PCR assay was optimized to allow for 1 second hold times at each thermocycling step by using the same PCR primers and biomarker targets as above, but using a different polymerase specifically suited to fast cycling times. Several polymerases claiming to allow fast cycling were tested in a RotorGeneQ PCR instrument, first using typical cycling hold times of 30 and 60 seconds for the 95°C and 56°C steps, respectively. When these hold times were gradually shortened to 15 and 30 seconds each, then 5 and 10 seconds each, then 1 second each, the only polymerase able to amplify the DNA was KAPA2G Fast polymerase (**Figure 4.5**). This polymerase was used in all subsequent axle-based device experiments, and the in-line PCR portion of the assay only takes 15 minutes.
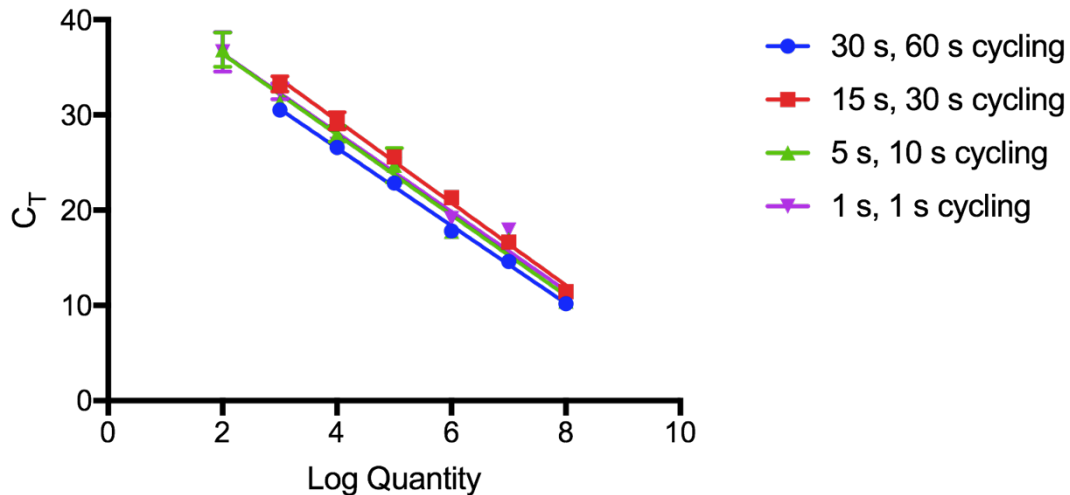

Figure 4.5. *Parasite DNA qPCR standard curve using KAPA2G Fast polymerase with progressively shorter cycling hold times.*

Another crucial consideration for in-line PCR was to prevent the PCR reaction mixture from evaporating within the tubing. The extraction tubing chambers are separated by short volumes of air, and applying heat to the PCR chamber caused the reaction mixture to evaporate and then condense in the air valve nearest to the chamber. To avoid this problem, the PCR reaction mixture was separated from the air valve by mineral oil, and the end of the tubing was sealed with a plastic screw directly behind the PCR chamber (**Figure 4.4A**). At both ends of the PCR chamber, extreme care was taken to ensure that no air bubbles were introduced because air bubbles expand with heat, interfering with the PCR reaction.
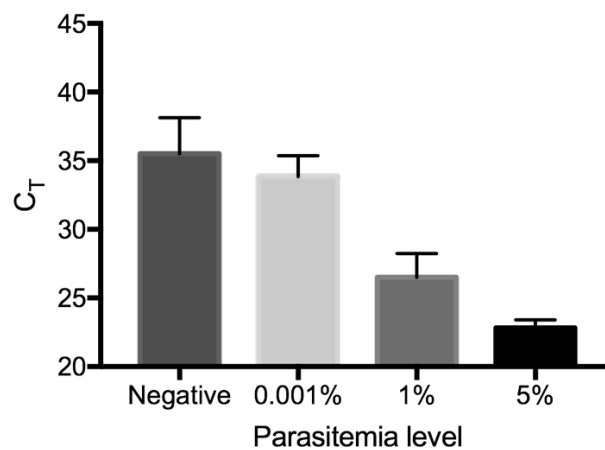

Figure 4.6. *Panel sample results using the axle-based extraction and PCR device.*

Axle-Based Device Validation

Once the reaction and mechanical parameters were worked out, the axle-based design was validated using the same PATH panel samples that were used with the roller-based device and the manual extractions. The device was able to extract, amplify, and detect *Plasmodium falciparum* DNA from blood culture samples of 5%, 1%, and 0.001% parasitemia with n = 3 for each concentration (**Figure 4.6**). The average Ct values calculated for the positive blood culture

samples provided by PATH were statistically significant from one another. However, the Ct

values for the 0.001% parasitemia and negative samples were not statistically different. This

result was not surprising when compared with previous results, reported above, that show the

negative and 0.001% parasitemia samples amplifying with similar Ct values. However, the

calculated Ct values for these experiments cannot be directly compared to those calculated for

the roller-based device and the manual extractions, because these Ct values were calculated

manually without the assistance of LightCycler software and a different polymerase was used.

The average total time to result for this device, including benchtop preparation steps, was

85 minutes. If this device were to become publicly available, however, much of the benchtop

preparation could be eliminated by manufacturing the extraction tubes in bulk. Excluding these

benchtop steps, the extraction and PCR assay together require 66 minutes on average. In
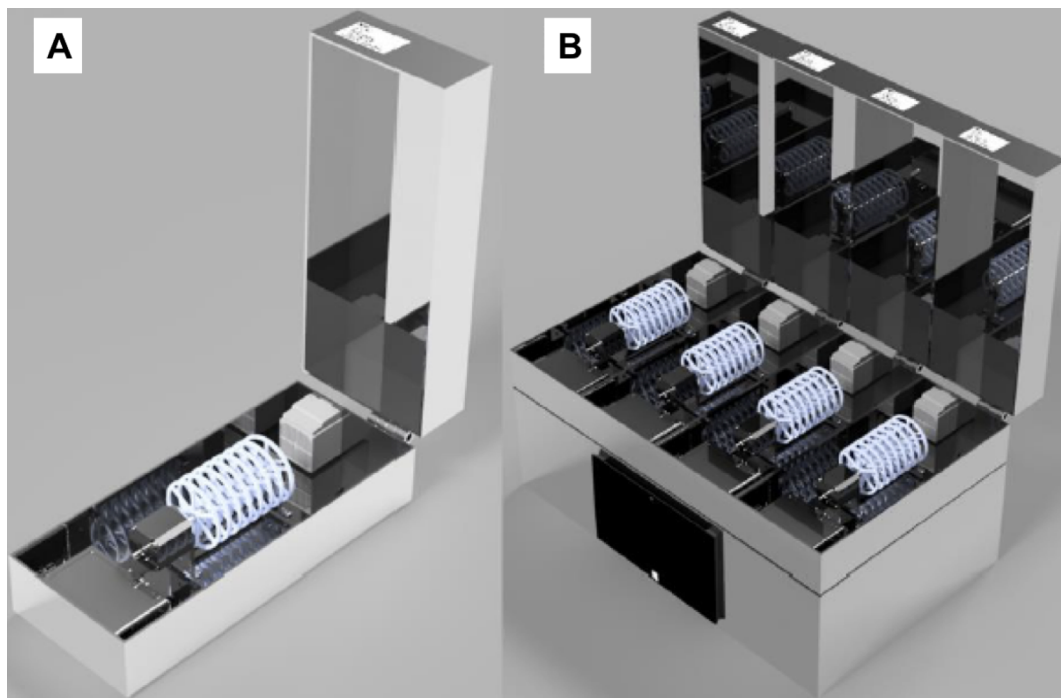

Figure 4.7. *A rendered concept showing the scaled-up axle-based integrated extraction and PCR device. A) One axle with 8 cartridges and B) Four axle modules in one instrument.*

comparison, a typical column-based DNA extraction requires roughly 30 minutes, and the original PCR assay in a LightCycler 96 requires roughly 30 minutes to set up and 108 minutes to run. This means taking a sample from DNA extraction to PCR detection using typical laboratory methods requires a total of 168 minutes, nearly twice the time it takes to achieve the same result with our fully integrated device. It is important to note that in its current state, our integrated axle-based device can only process one sample at a time, while a typical PCR instrument can amplify 96 samples or more at one time. However, our current device is a prototype which can be scaled up to process many samples at once by placing multiple cartridges on one axle, and controlling several axles with one instrument (**Figure 4.7**).

Conclusion

This chapter has covered the development of a bead-based method for extracting malaria DNA from blood samples, and the incorporation of PCR detection in-line with the extraction process. The final integrated device combines the chemistry of DNA extraction and PCR amplification with engineering to operate the device and detect the amplified DNA. The final device halves the sample-to-answer time of a typical extraction and PCR process, and is more amenable to a low-resource setting than typical PCR. This instrument can distinguish between high, medium, and low parasitemia samples, although the negative panel samples do yield positive results at times. Further validation using actual clinical samples would be necessary before this device could reach market, and this would also help determine a Ct cutoff value for calling positive and negative samples.

Overall, this device could help make PCR a more accessible technique in low-resource areas, but it will still require a certain level of infrastructure support. The instrument does not

require high levels of electricity, but it does require electricity. It also requires a data processing in its current form. Although software development could make this easier for users to perform, it would be very difficult for an untrained clinician to correctly analyze and interpret the data without the instrument making the positive or negative call itself. With further development, these improvements could be made, but ultimately it is not simple to transfer PCR from a high-resource laboratory setting to a low-resource rural clinic setting. DNA detection in diagnostics has the potential to provide a large amount of clinically relevant information, but other detection methods besides PCR must be developed in order to use DNA diagnostics at the point of care. The next chapter of this dissertation works towards this goal by describing a PCR-free method to amplify DNA so that it can be detected using a rapid diagnostic test.

Acknowledgements

the fabrication, circuitry, coding, and software development. Francesca Solinas and Megan Pask performed much of the in-tube PCR optimization, and helped prepare samples for the roller-based device validation. Hali Bordelon provided guidance and advice when I initially started to develop the manual DNA extraction protocol, and Patricia Russ provided data analysis advice.

References

(1)   Jain, P.; Chakma, B.; Patra, S.; Goswami, P. *Biomed Res. Int.* **2014**.

(2)   Makler, M. T.; Piper, R. C.; Milhous, W. K. *Parasitol. Today* **1998**, *14*, 376–377.

(3)   Mayxay, M.; Pukrittayakamee, S.; Chotivanich, K.; Looaresuwan, S.; White, N. J. *Trans. R. Soc. Trop. Med. Hyg.* **2001**, *95*, 179–182.

(4)   Iqbal, J.; Siddique, A.; Jameel, M.; Hira, P. R. *J. Clin. Microbiol.* **2004**, *42*, 4237–4241.

(5)   Oduola, A. M. J.; Omitowoju, G. O.; Sowunmi, A.; Makler, M. T.; Falade, C. O.; Kyle, D. E.; Fehintola, F. A.; Ogundahunsi, O. A. T.; Piper, R. C.; Schuster, B. G.; Milhous, W. K. *Exp. Parasitol.* **1997**, *87*, 283–289.

(6)   Moody, A. *Clin. Microbiol. Rev.* **2002**, *15*, 66–78.

(7)   Hendriksen, I. C. E.; Mtove, G.; Pedro, A. J.; Gomes, E.; Silamut, K.; Lee, S. J.; Mwambuli, A.; Gesase, S.; Reyburn, H.; Day, N. P. J.; White, N. J.; von Seidlein, L.; Dondorp, A. M. *Clin. Infect. Dis.* **2011**, *52*, 1100–1107.

(8)   Baird, J. K.; Valecha, N.; Duparc, S.; White, N. J.; Price, R. N. *Am. J. Trop. Med. Hyg.* **2016**, *95*, 35–51.

(9)   World Health Organization; Special Programme for Research and Training in Tropical Diseases; Foundation for Innovative New Diagnostics; Centers for Disease Control and Prevention. *Malaria Rapid Diagnostic Test Performance: Results of WHO Product*

Testing of Malaria RDTs: Round 3 (2010 - 2011).; 2011.

(10) Davis, K. M.; Swartz, J. D.; Haselton, F. R.; Wright, D. W. *Anal. Chem.* **2012**, *84*, 6136–6142.

(11) Davis, K. M.; Bitting, A. L.; Wright, D. W. *Anal. Biochem.* **2014**, *445*, 60–66.

(12) Gamboa, D.; Ho, M.-F.; Bendezu, J.; Torres, K.; Chiodini, P. L.; Barnwell, J. W.; Incardona, S.; Perkins, M.; Bell, D.; McCarthy, J.; Cheng, Q. *PLoS One* **2010**, *5*, e8091.

(13) Koita, O. A.; Doumbo, O. K.; Ouattara, A.; Tall, L. K.; Konare, A.; Diakite, M.; Diallo, M.; Sagara, I.; Masinde, G. L.; Doumbo, S. N.; Dolo, A.; Tounkara, A.; Traore, I.; Krogstad, D. J. *Am. J. Trop. Med. Hyg.* **2012**, *86*, 194–198.

(14) World Health Organization (WHO). *World Malaria Report 2016*; 2016.

(15) Global Malaria Progamme. *Control and Elimination of Plamodium Vivax Malaria - A Technical Brief*; 2015.

(16) World Health Organization. *World Malaria Report 2015*; 2015.

(17) Isozumi, R.; Uemura, H.; Kimata, I.; Ichinose, Y.; Logedi, J.; Omar, A. H.; Kaneko, A. *Emerg. Infect. Dis.* **2015**, *21*, 490–492.

(18) Straimer, J.; Gnadig, N. F.; Witkowski, B.; Amaratunga, C.; Duru, V.; Ramadani, A. P.; Dacheux, M.; Khim, N.; Zhang, L.; Lam, S.; Gregory, P. D.; Urnov, F. D.; Mercereau-Puijalon, O.; Benoit-Vical, F.; Fairhurst, R. M.; Menard, D.; Fidock, D. A. *Science (80-.).* **2015**, *347*, 428–431.

(19) Niemz, A.; Ferguson, T. M.; Boyle, D. S. *Trends Biotechnol.* **2011**, *29*, 240–250.

(20) Dineva, M. A.; Mahilum-Tapay{, L.; Lee, H. .

(21) Al-Soud, W. A.; Radstrom, P. *J. Clin. Microbiol.* **2001**, *39*, 485–493.

(22) Smit, M. L.; Giesendorf, B. A. J.; Heil, S. G.; Vet, J. A. M.; Trijbels, F. J. M.; Blom, H. J.

Biotechnol. Appl. Biochem. **2000**, *32*, 121–125.

(23)   Sur, K.; McFall, S. M.; Yeh, E. T.; Jangam, S. R.; Hayden, M. A.; Stroupe, S. D.; Kelso, D. M. *J. Mol. Diagnostics* **2010**, *12*, 620–628.

(24)   Berry, S. M.; Regehr, K. J.; Casavant, B. P.; Beebe, D. J. *J. Lab. Autom.* **2012**, *18*, 206–211.

(25)   Siddiqui, H.; Nederbragt, A. J.; Jakobsen, K. S. *Clin. Biochem.* **2009**, *42*, 1128–1135.

(26)   Han, N.; Shin, J. H.; Han, K.-H. *RSC Adv.* **2014**, *4*, 9160.

(27)   Bordelon, H.; Adams, N. M.; Klemm, A. S.; Russ, P. K.; Williams, J. V; Talbot, H. K.; Wright, D. W.; Haselton, F. R. *ACS Appl. Mater. Interfaces* **2011**, *3*, 2161–2168.

(28)   Bordelon, H.; Russ, P. K.; Wright, D. W.; Haselton, F. R. *PLoS One* **2013**, *8*, e68369.

(29)   Adams, N. M.; Olmsted, I. R.; Haselton, F. R.; Bornhop, D. J.; Wright, D. W. *Nucleic Acids Res.* **2013**, *41*, e103.

(30)   Gama, B. E.; Silva-Pires, F. do E. S.; Lopes, M. N. R.; Cardoso, M. A. B.; Britto, C.; Torres, K. L.; de Mendonça Lima, L.; de Souza, J. M.; Daniel-Ribeiro, C. T.; de Fátima Ferreira-da-Cruz, M. *Exp. Parasitol.* **2007**, *116*, 427–432.

(31)   Choi, G.; Song, D.; Shrestha, S.; Miao, J.; Cui, L.; Guan, W. *Lab Chip* **2016**, *16*, 4341–4349.

(32)   Creecy, A.; Russ, P. K.; Solinas, F.; Wright, D. W.; Haselton, F. R. *PLoS One* **2015**, *10*, e0130260.

CHAPTER V

PROGRESS TOWARD THE DEVELOPMENT OF A BIO-BARCODE-BASED RAPID
DIAGNOSTIC TEST FOR THE DETECTION OF MALARIA DNA

Introduction

As described and demonstrated in the previous chapter, nucleic acid biomarkers have the
potential to be a superior diagnostic target for malaria when compared to protein biomarkers.
Parasite-specific DNA is present in any sample containing parasite, since it does not rely on
complicated expression pathways like protein biomarkers do. Nucleic acid testing for malaria
can also yield much more information than testing for protein biomarkers. It is possible to design
assays that detect genetic sequences conserved by all species of malaria, or sequences that are
specific to one particular species.[1–5] Detecting gene deletions and mutations are also important
for determining drug resistance,[6] which can inform treatment and allow for faster patient
recovery times. All of this genetic information is not only useful on a per-patient basis, but it is
also useful in larger epidemiological and mapping studies, such as those tracking malaria species
and drug resistance distributions over large areas.

However, the current state of nucleic acid testing is not perfect, and it faces several
hurdles for malaria diagnostics. The source of these hurdles is the relatively low concentration of
nucleic acid biomarkers compared to protein biomarkers. While parasites produce protein
biomarkers such as *Pf*HRP2 throughout their life cycle, DNA biomarkers are limited by the
amount of genetic material contained in a single parasite which does not increase with time. For
example, the 18S SSU rRNA gene is commonly detected for malaria diagnostics because there
are typically 5 or more copies of the gene per parasite. In patients with low parasite levels, such

as 100 parasites/μL blood, this equates to $\sim$ 500 copies/μL of the biomarker gene, or 0.83 fM. The most reliable way to detect such low concentrations of DNA is to use PCR, such as in the previous chapter. However, PCR presents a second hurdle for nucleic acid diagnostics for malaria. While there are a variety of well-developed and dependable PCR methods, the technique is mostly reserved for diagnosis in a reference lab due to the equipment and skill necessary to perform an assay. Until recently, alternative nucleic acid testing strategies for malaria had not been explored because PCR was so dependable on its own. This meant that nucleic acid testing was reserved for well-equipped laboratories and point-of-care testing was limited to protein-based diagnostics.

However, in the past several years it has become clear that point-of-care testing can benefit from the additional diagnostic information and sensitivity that nucleic acid testing can provide over protein assays. Some work has focused on translating lab-based DNA detection assays to the field. Recently, several alternative assays such as loop-mediated isothermal amplification (LAMP) have been developed as a replacement for PCR in order to simplify the equipment and technique required.[7–9] LAMP is not a perfect substitute for PCR, since it requires more primers than PCR, increasing the risk of false positive amplification. However, the isothermal capabilities of LAMP make it a good candidate for simple, field-deployable instrumentation. For example, PATH has developed a thermos-like device to contain loop-mediated isothermal amplification (LAMP) reaction tubes, which are heated by an exothermic chemical reaction similar to that used to heat military MREs (Meals Ready-to-Eat).[10] Other efforts have focused on developing a rapid diagnostic test for malaria DNA similar to those used for malaria protein biomarkers. However, due to the low abundance of nucleic acid biomarkers as described above, many DNA-based RDTs still require some sort of enzymatic amplification,

such as LAMP, before the test is run.[11–13] Some groups have even integrated the LAMP reaction into the RDT design.[14] While this design works well, an even better device would eliminate the need for an enzymatic reaction to amplify target DNA to detectable levels.

One possible method for amplifying target DNA without requiring an enzymatic reaction is known as the bio-barcode assay. In this assay developed by the Mirkin group,[15] target DNA is hybridized to a magnetic bead that was pre-functionalized with a short, complementary DNA capture oligo. After washing away unbound sample matrix, the bead/target complex is incubated with AuNPs pre-functionalized with a "barcode" tag DNA sequence and a different short capture oligo sequence that is also complementary to the target DNA. The final complex sandwiches the target DNA between the capture magnetic bead and the tagging "barcode" AuNP (**Figure 5.1**). After stringent washing, the barcode DNA is released by dithiothreitol (DTT) or heat and can be detected in a number of ways. The barcode DNA sequence provides enzyme-free amplification because there are up to 200 barcode sequences per AuNP, so for every one target sequence captured there can be 200 barcode sequences detected. While this amplification is not on the same scale as PCR or LAMP, it can be enough amplification to make the change from a negative to a positive signal in colorimetric detection assays.
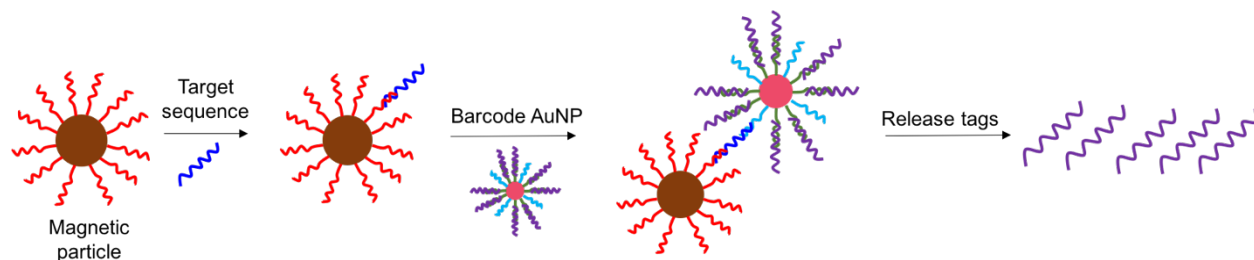

Figure 5.1. *The bio-barcode assay for DNA detection. This assay was originally used for the detection of proteins using antibodies to capture the target biomarker but was then adapted for DNA using short oligos to capture a target DNA sequence.*

Typically, bio-barcode assays have been coupled with scanometric readouts, where the released barcode sequences are re-captured onto a glass slide functionalized with spots of complementary capture oligo.[15,16] Then, AuNPs functionalized with another short complementary DNA sequence are added to the slide and allowed to hybridize to the immobilized barcode DNA. The AuNPs provide a visible spot on the glass slide, which can be further enhanced by silver staining.[16] This scanometric detection method is relatively simple to perform in a laboratory setting, but it would be difficult to use as a point-of-care diagnostic in a low-resource setting because it requires careful manipulation and a controlled-humidity environment to be successful.
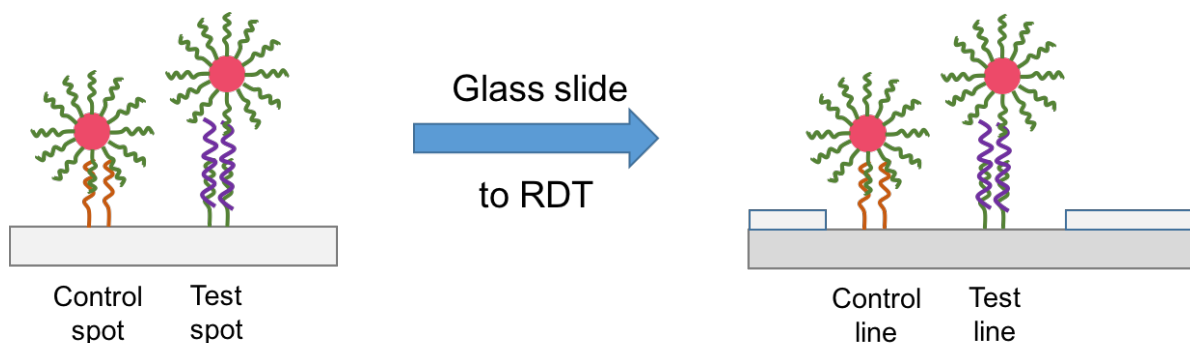

Figure 5.2. *The scanometric detection method for bio-barcode assays compared to the proposed RDT detection method.*

Instead of using glass slides to detect the barcode DNA, the bio-barcode assay format would combine perfectly with an RDT detection strategy for DNA biomarkers (**Figure 5.2**). The bio-barcode amplification would overcome the hurdle of low target DNA concentrations, while the RDT detection strategy would enable point-of-care clinicians to continue using a familiar, simple, self-contained diagnostic device. To our knowledge, the bio-barcode assay has not been used as an amplification strategy for RDTs before. While the amplification assay will add several pre-processing steps to the RDT workflow, our work in the previous chapter[17,18] indicates that in

the future, these steps could be incorporated into a simple device to reduce the number of complicated steps for the clinician. This chapter discusses the efforts towards combining the bio-barcode assay with a novel DNA barcode-detecting RDT.

Materials and Methods

Materials and Reagents

Table 5.1. *List of DNA sequences used for the bio-barcode assay and LFA in this chapter.*

| Function	Name	Sequence
Magnetic bead capture	Thio-RevFP	5'-CGT TAC CCG TCA TAG CCA TGT T$_{10}$ -thio -3'
Target biomarker	PATH sequence	5'-ACA TGG CTA TGA CGG GTA ACG GGG AAT TAG AGT TCG ATT CCG GAG AGG GAG CCT GAG AAA TAG CTA CCA CAT CTA AGG AAG GCA -3'
Amplification AuNP capture	Thio-RP	5'-thio- T$_{10}$ TGC CTT CCT TAG ATG TGG TAG CTA -3'
Barcode AuNP capture	Thio-BarP	5'-GCT AGT GAA CAC AGT TGT GT-T$_{10}$-thio -3'
Barcode sequence	Barcode	5'-ACA CAA CTG TGT TCA CTA GCG TTG AAC GTG GAT GAA GTT G-3'
LFA test line	Biotin-BarP	5'-biotin-T10-CAA CTT CAT CCA CGT TCA AC-3'
LFA control line	Biotin-controlP	5'-ACA CAA CTG TGT TCA CTA GC-A$_{10}$-Biotin-3'
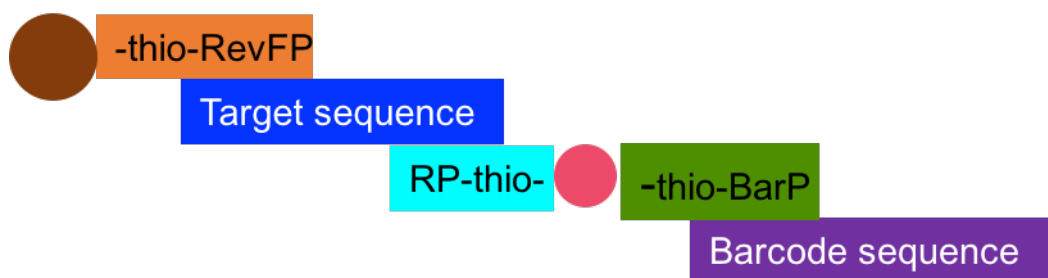
Figure 5.3. *Hybridization scheme for the bio-barcode amplification of the target sequence. The brown circle represents the magnetic bead, and the pink circle represents the AuNP.*

Dynabeads M-270 Amine functionalized magnetic beads (Cat # 14307D) and Dynabeads

MyOne Streptavidin T1 magnetic beads (Cat # 65601) were purchased from ThermoFisher

Scientific. All DNA sequences were custom ordered from Integrated DNA Technologies (**Table

5.1, Figure 5.3**). Sulfo-SMCC, no-weigh format (Cat # 22622) and EZ-Link Maleimide-PEG2-

Biotin (Cat # 21901BID) were purchased from ThermoFisher Scientific. Amicon Ultra 3K

MWCO filters were purchased from Millipore (Cat # UFC500324). Unconjugated 40 nm gold

nanoparticles were purchased from Ted Pella (Cat # 15707-5). FF120HP nitrocellulose

membrane with 10 mil polystyrene backing (Cat # 10547001) and CF7 high-flow wicking pads

(Cat # 8117-2250) were purchased from Whatman. G041 glass fiber conjugate/sample pads were

purchased from EMD Millipore (Cat # GFCP 203000). All other buffers and reagents were

purchased from either Sigma-Aldrich or Fisher Scientific.

Instrumentation

Absorbance and fluorescence measurements were taken using a Synergy H4 microplate

reader, using a Take3 micro-volume plate as needed. Lateral flow assay reagents were deposited

onto test strips using a BioDot AD1520 Aspirate/Dispense platform, and the individual test strips

were cut using a BioDot CM4000 membrane cutter. RDT signal measurements were taken using

a Qiagen ESEQuant Lateral Flow Reader.

Reduction of dithiol bonds on thiolated DNA sequences

Thiolated DNA was received lyophilized and protected as a dithiol, which had to be

reduced before use. The dithiol reduction was accomplished by adding 1 mL 100 mM

dithiothreitol (DTT) in 0.1 M dibasic phosphate, pH 8.3, to each tube of dried DNA. Each tube

was vortexed to fully dissolve the DNA pellet and incubated on a rotisserie for 1 hr. The reduced thio-DNA was purified using Amicon Ultra 3K MWCO centrifugal filters. 500 μL sample was added to each filter, and centrifuged at 14,000 x g for 30 mins. The concentrated sample remaining in the filter was then washed twice by the addition of 500 μL TE buffer, pH 8 followed by centrifugation at 14,000 x g for 30 mins. After the second wash, the filter was inverted into a new collection tube and centrifuged at 1,000 x g for 3 mins to collect the purified, concentrated thio-DNA. Each aliquot was diluted with 500 μL TE buffer, pH 8, and the concentration was determined by the absorbance at 260 nm using a Take3 micro-volume plate in a BioTek Synergy H4 plate reader. Purified thio-DNA was stored in small aliquots at -80°C.

Functionalization of amine-coated magnetic beads

A 200 μL suspension of Dynabeads M-270 amine magnetic beads were added to a microcentrifuge tube and mixed with 1 mL conjugation buffer (100 mM Na-phosphate buffer, pH 7.4, 150 mM NaCl, 0.01% Tween-20). The supernatant was removed, and the beads were washed again with 1 mL conjugation buffer. After the supernatant was removed, the beads were resuspended in 188 μL conjugation buffer. No-weigh sulfo-SMCC was prepared to a final concentration of 10 mg/mL according to the manufacturer's instructions. 12 μL of 10 mg/mL sulfo-SMCC was added to each tube of magnetic beads and incubated at room temperature for 30 mins on rotisserie. The reaction solution was removed from the beads, and the beads were washed twice with 500 μL conjugation buffer before being resuspended in the original volume of 200 μL conjugation buffer.

The maleimide-activated beads were then incubated with 2 μL of 176 μM thio-RevFP capture oligo for 2 hrs at room temperature on rotisserie. Excess maleimide sites on the beads

were then passivated by adding 2 μL of 500 mM cysteine in water to each tube of beads. After incubating for 15 mins on rotisserie, the beads were washed three times with 500 μL conjugation buffer and resuspended in a final 200 μL volume of conjugation buffer.

Functionalization of streptavidin-coated magnetic beads

Thio-RevFP capture oligo was functionalized with a biotin moiety using EZ-Link maleimide-PEG2-biotin reagent. First, 200 μL of 176 μM thio-RevFP capture oligo was buffer exchanged into PBS, pH 7 using Zeba 7K MWCO Spin Desalting columns according to the manufacturer's instructions. Final DNA recovery was quantified by the absorbance at 260 nm using a Take3 micro-volume plate in a BioTek Synergy H4 plate reader. EZ-Link maleimide-PEG2-biotin was reconstituted according to manufacturer's instructions to a final concentration of 20 mM. 35.2 μL of 20 mM maleimide-PEG2-biotin (>20-fold excess) was added to 200 μL thio-RevFP and incubated on rotisserie at room temperature for 2 hrs. Excess maleimide-PEG2-biotin was removed using Zeba 7K MWCO Spin Desalting columns according to the manufacturer's instructions. Final biotin-thio-RevFP DNA concentration was determined by the absorbance at 260 nm using a Take3 micro-volume plate in a BioTek Synergy H4 plate reader. Small volume aliquots were stored at -80°C.

200 μL Dynabeads MyOne Streptavidin T1 beads were placed in a microcentrifuge tube, and washed three times with 1 mL 1X binding and wash buffer (1XBW buffer) (5 mM Tris buffer, pH 8, 0.5 mM EDTA, 1M NaCl, 0.1% Tween-20). Beads were resuspended in 800 μL 1XBW buffer, and 12.8 μL of 125 μM biotin-thioRevFP capture oligo was added to the beads. The beads were incubated on a rotisserie at room temperature for 15 mins before being washed three times with 1 mL 1XBW buffer and resuspended in 200 μL of 1XBW buffer. Excess

streptavidin sites were passivated by adding 8 μL of 1 mg/mL D-biotin to the beads, which were then incubated on a rotisserie at room temperature for 15 minutes. The beads were washed three times with 200 μL 1XBW buffer and resuspended in a final volume of 200 μL 1XBW buffer.

Magnetic bead biomarker capture optimization

The amount of target DNA required to saturate the surface of the DNA-conjugated M-270 amine beads was determined by incubating 50 μL aliquots of magnetic beads in triplicate with 100 μL of various concentrations of FAM-target DNA in conjugation buffer for 1 hr in the dark. The supernatant was removed and saved to quantify the amount of unbound FAM-target DNA. The beads were washed three times with 100 μL conjugation buffer (100 mM Na-phosphate buffer, pH 7.4, 150 mM NaCl, 0.01% Tween-20) and resuspended in 100 μL TE + 0.05% Tween-20 buffer. The bead solution was heated at 95°C for 10 mins with occasional vortexing, and the supernatant of eluted FAM-target DNA was removed. The concentrations of the unbound and eluted FAM-target DNA were determined by reading FAM fluorescence (λ_{ex} = 495 nm, λ_{em} = 520 nm) using a Take3 micro-volume plate in a BioTek Synergy H4 microplate reader.

The time required to maximize target DNA binding to the surface of the beads was determined by incubating 20 μL aliquots of DNA-conjugated M-270 amine beads with 100 μL of 150 nM FAM-target DNA for various amounts of time. The supernatant was removed and saved to quantify the amount of unbound FAM-target DNA. The beads were washed three times with 100 μL conjugation buffer (100 mM Na-phosphate buffer, pH 7.4, 150 mM NaCl, 0.01% Tween-20) and resuspended in 100 μL TE + 0.05% Tween-20 buffer. The bead solution was heated at 95°C for 10 mins with occasional vortexing, and the supernatant of eluted FAM-target

DNA was removed. The concentrations of the unbound and eluted FAM-target DNA were determined by reading FAM fluorescence (λ_{ex} = 495 nm, λ_{em} = 520 nm) using a Take3 micro-volume plate in a BioTek Synergy H4 microplate reader.

Barcode gold nanoparticle functionalization

40 nm citrate-coated gold nanoparticles (AuNPs) were split into 1 mL aliquots. To each aliquot, 1 μL Tween-20 was added and vortexed. Each aliquot was brought to a final concentration of 0.4 μM thio-barcode primer and 0.004 μM thio-PATH reverse primer. If fluorescently-tagged AuNPs were desired, each aliquot was brought to a final concentration of 0.4 μM FAM-Barcode DNA. For DNA loading quantification, each aliquot was also brought to a final concentration of 0.004 μM FAM-PATH DNA. If the AuNPs did not require a fluorescent tag, each aliquot was brought to a final concentration of 0.4 μM Barcode DNA. After all DNA additions had been made, the AuNPs were left to incubate in the dark on a rotisserie overnight. The next day, all aliquots were buffer adjusted to 10 mM Na-phosphate buffer, pH 7. Then all aliquots were brought to a concentration of 0.1 M NaCl and allowed to incubate for 3 hrs in the dark on a rotisserie. All aliquots were then brought to a concentration of 0.2 M NaCl, and after another 3 hr incubation they were brought to a final concentration of 0.3 M NaCl. The AuNPs were then allowed to incubate overnight in the dark on a rotisserie. Excess DNA was removed by centrifuging the AuNPs at 5,000 x g for 30 mins, after which the supernatant was removed. The AuNPs were then washed three times by resuspending the particles in 1 mL of PBS + 0.1% Tween-20 (PBST) and centrifuging at 5,000 x g for 30 minutes, removing the supernatant after each wash. After the final wash, the particles were resuspended in PBST to the desired volume and concentration.

LFA gold nanoparticle functionalization

Thiolated DNA was reduced, purified, and stored as described above. 40 nm citrate-coated gold nanoparticles (AuNPs) were split into 1 mL aliquots. To each aliquot, 1 μL Tween-20 was added and vortexed. Each aliquot was brought to a final concentration of 187 nM thio-Barcode primer DNA, and was left to incubate on a rotisserie overnight in the dark. The same salt-aging and purification procedures were performed as above. After the final wash step, the AuNP pellets were resuspended in the residual buffer and combined into one tube. AuNP concentration was determined using absorbance at 520 nm, and AuNPs were diluted to a final working concentration of 1.5 nM using PBS with 5% BSA, 0.25% Tween-20, and 10% sucrose (LFA AuNP buffer).

Quantification of DNA loading on gold nanoparticles

A small volume of concentrated FAM-DNA labeled AuNPs was added to a 500 μL solution of 0.1 M dithiothreitol (DTT) in 0.1 M dibasic Na-phosphate, pH 8.3, so that the final AuNP concentration was 0.15 nM. This solution was incubated in the dark on a rotisserie for at least 2 hrs, until the solution changed from pink to clear. The sample was then centrifuged at 14,000 x g for 30 mins to remove any debris from the solution. FAM fluorescence was measured (λ_{ex} = 495 nm, λ_{em} = 520 nm) using a BioTek Synergy H4 microplate reader. Fluorescence was compared to a standard curve prepared using the same FAM-labeled DNA sequences in the same DTT solution background. DNA loading in strands per nanoparticle was calculated by dividing the nanomolar FAM DNA concentration by the AuNP concentration of 0.15 nM.

Barcode gold nanoparticle blocking experiments

Optimal conditions for tagging magnetic bead-bound target DNA with barcode-conjugated AuNPs were investigated using barcode AuNPs conjugated with FAM-barcode DNA. First, 20 μL magnetic beads were incubated with target DNA or blank buffer as described above. After 3 washes with PBST, the beads were resuspended in 100 μL blocking buffer and 50 μL of 250 pM FAM-barcode AuNPs were added to the tube. Various buffers such as PBST, PBST with low salt, PBST with 5% BSA, and PBST with 1 mg/mL salmon sperm DNA were tested to block nonspecific binding of the AuNPs to the magnetic beads. The AuNPs were incubated for 1 hr with the beads, before the bead-AuNP complex was washed 5 times with blocking buffer. The bead-AuNP complex was then resuspended in 50 μL TE buffer + 0.05% Tween-20 and heated for 10 mins at 95°C with mixing to ensure complete FAM-barcode elution. FAM fluorescence was then measured (λ_{ex} = 495 nm, λ_{em} = 520 nm) using a Take3 micro-volume plate in a BioTek Synergy H4 microplate reader.

LFA fabrication

The BioDot AD1520 Aspirate/Dispense system was used to deposit test and control line solutions onto a Whatman FF120HP nitrocellulose membrane with 10 mil polystyrene backing to form the LFA. Each solution contained 100 μM biotinylated DNA and 30 μM streptavidin in PBS + 0.1% Tween-20, incubated at room temperature for 30 mins before deposition onto the LFA membrane. Line solutions were deposited at a speed of 1 μL/cm of nitrocellulose membrane, or 40 nL drops deposited continuously at a 400 μm pitch. The membrane was dried at 40°C, and was not blocked unless otherwise noted. EMD Millipore GFCP 203000 glass fiber conjugate/sample pads were cut into 1.9 cm x 20 cm strips and blocked by immersing in 50 mM

borate buffer pH 9 with 1% BSA, 1% polyvinyl pyrrolidinone (PVP), and 0.25% Triton X-100, and were dried at 40°C. Whatman CF7 high-flow wicking pads were used without any pretreatment. The LFA was assembled by attaching the wicking pad and blocked conjugate pad to the opposite ends of the nitrocellulose membrane adhesive backing card (**Figure 5.4**), making sure that each pad overlapped the nitrocellulose membrane. Early experiments were performed without the use of a conjugate pad, and for these "half-strips" the backing card meant to hold the conjugate pad was cut off so the LFA consisted only of nitrocellulose membrane and wicking pad. A CM4000 guillotine membrane cutter was used to cut the assembled LFA into test strips 4 mm wide. If the test strips were "whole" strips containing a conjugate pad, then 5 μL of 1.5 nM (OD 10) LFA AuNPs (or "conjugate") in LFA AuNP buffer was pipetted onto the middle of the conjugate pad and allowed to dry at 37°C for 1 hr. The test strips were then stored in foil pouches with desiccant until use.
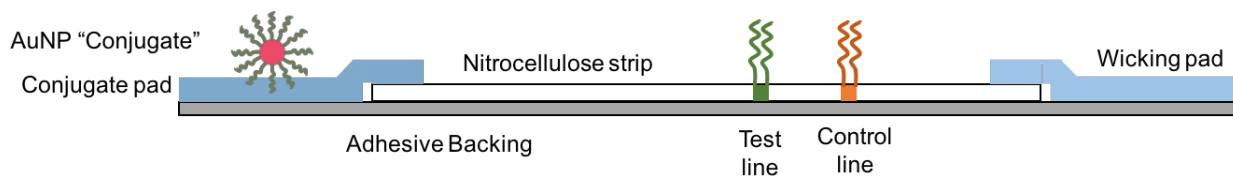

Figure 5.3. *Side view of a complete RDT as fabricated in-house. Control and test lines are in color for illustration only.*

LFA optimization experiments

LFA design and running conditions were first optimized using half-strips, which did not contain a conjugate pad. For these tests, 5 μL of sample and 5 μL 1.5 nM AuNP conjugate were added to either a test tube or a well in a 96-well microplate, and the LFA half-strip was placed into the well like a dipstick, with the nitrocellulose membrane contacting the liquid in the well

and with the wicking pad up in the air. Once the sample and AuNP conjugate had been wicked

into the test strip, running buffer was added to the well in 50 μL aliquots as needed. The strips

were allowed to develop for 20 minutes before being visualized. Experiments with "full" test

strips were run by pipetting 5 μL of sample onto the spot of dried AuNPs on the conjugate pad,

along with 50 μL to 100 μL running buffer, as needed. The strips were allowed to develop for 20

minutes before being visualized. Experiments were run with a variety of sample, running, and

AuNP buffers to choose the optimal conditions. Positive controls were run using 50 nM barcode

DNA in buffer as sample, and negative controls were run using blank buffer as sample. Optimal

conditions were chosen by visual inspection as those which minimized false positives and

"smearing" of the AuNPs across the test strip, while allowing for strong positive control signal.

Results and Discussion

Target DNA binding to amine magnetic beads

After the amine-coated magnetic beads were functionalized with thio-RevFP capture

DNA sequence, their binding capabilities were assessed. First, 50 μL of beads were incubated

with 100 μL of various concentrations of FAM-labeled target DNA (FAM-PATH) for 1 hr with

mixing in order to determine the maximum amount of target DNA that could be captured by the

beads. FAM fluorescence of the sample was measured before and after bead incubation, and the

percent sample captured by the beads was calculated. Above 200 nM target DNA, the percent

captured by the beads begins to decrease, indicating that above this concentration the beads

become saturated with target DNA (**Figure 5.5A**). Next, the kinetics of binding were

investigated to determine the optimal incubation time for beads in a sample. To conserve beads,

this experiment was performed using 20 μL of beads incubated at various timepoints with 150
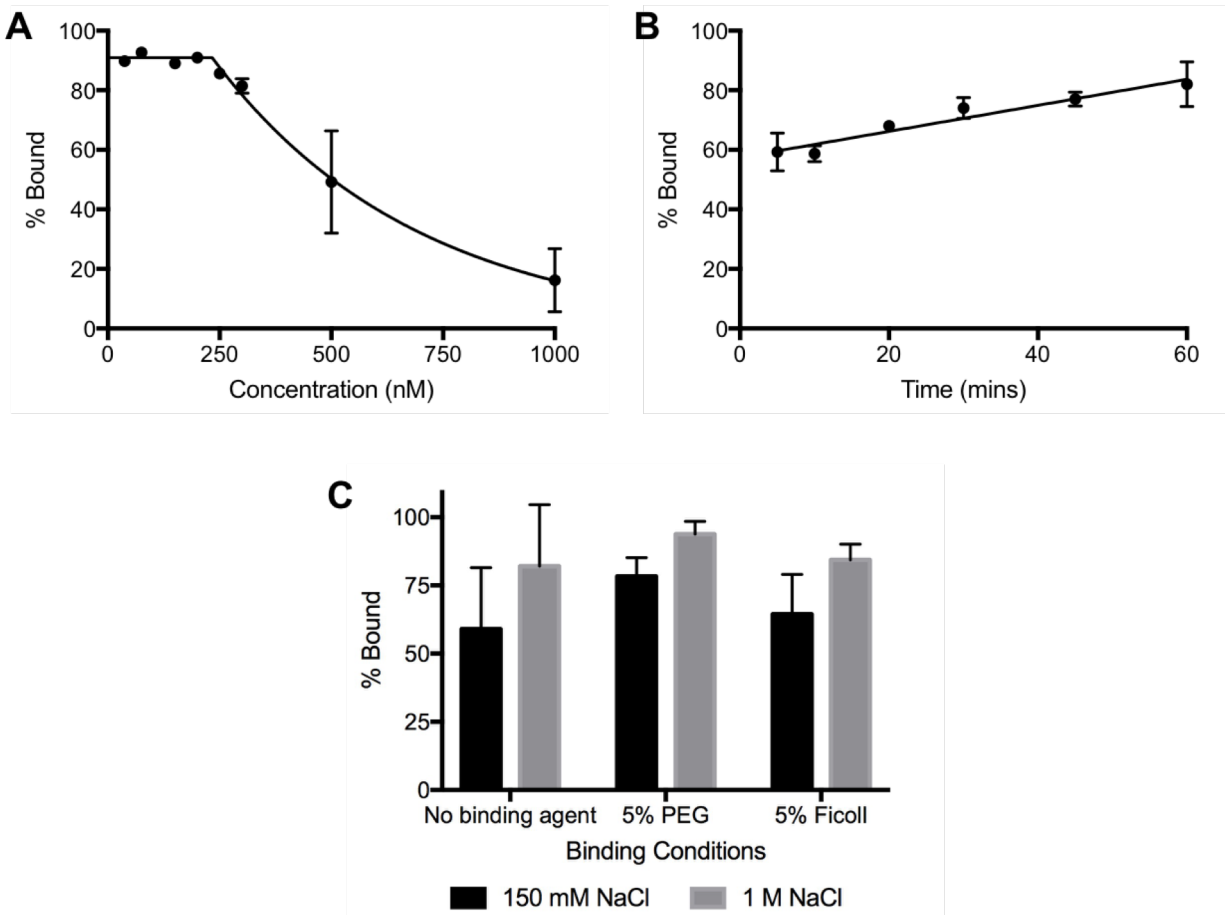
Figure 5.5. *Percent target DNA bound to functionalized magnet beads A) after 1 hr with 50 µL beads and various starting concentrations of target DNA; B) with 20 µL beads and 150 nM target DNA over various incubation times; and C) after 10 mins with 20 µL beads, 150 nM target DNA, and various hybridization accelerators in the binding buffer.*

nM FAM-target DNA and mixing. Again, FAM fluorescence of the sample was measured before and after beads incubation so the percent of sample captured could be calculated. Even with continuous mixing of the sample to ensure the beads did not settle, maximum target binding did not occur until 1 hr incubation (**Figure 5.5B**). This is not ideal for the first step of a point-of-care assay, especially one that is meant to replace time-consuming PCR.

In order to increase the target binding kinetics, we decided to alter the binding buffer components. Hybridization rate accelerators such as polyethylene glycol (PEG) and ficoll are

used in many molecular biology applications to decrease the time needed for DNA hybridization.[19] These polymers exclude water from solvating the DNA strands, which effectively makes it "look" like the single stranded DNA is at a higher concentration than it truly is. This effective increase in DNA concentration also increases the hybridization rate. PEG and ficoll were tested as hybridization rate accelerators in the binding buffer, along with a higher concentration of NaCl to further stabilize DNA duplexes once they were formed on the beads. These experiments were performed with 20 μL functionalized beads, 100 μL of 150 nM FAM-target DNA and a 10 minute incubation time instead of 1 hour. Our results show that increasing the concentration of salt alone is enough to increase target binding from 58% to 82% in 10 minutes, but with high variation (**Figure 5.5C**). Combining a higher 1M NaCl concentration with 5% PEG added to the conjugation buffer allowed us to bind 94% of our target DNA in 10 minutes while also reducing the variability. This conjugation buffer was used in all further experiments as the incubation buffer for the bead-target complex.

AuNP incubation optimization

Sandwiching captured target DNA with barcode-functionalized AuNPs is a crucial step in this assay. However, nonspecific binding of the barcode AuNPs to the magnetic beads quickly became a large hurdle to be overcome. Functionalized magnetic beads that were not bound to target DNA captured as many barcode AuNPs as magnetic beads that were bound to target DNA. This gave the assay a signal to noise ratio of 1, where a positive sample could not be distinguished from a negative one. Several blocking conditions were investigated to reduce the nonspecific binding of AuNPs to magnetic beads, including conjugation buffer with low salt, PBST, BSA, and salmon sperm DNA.

Initial barcode AuNP binding experiments used the same 1 M NaCl, 5% PEG conjugation buffer to incubate the AuNPs and beads as was used to capture the target DNA from solution. This gave high background signal, but this was not unexpected due to the nature of the buffer. Lower salt concentrations were tested to reduce the stability of nonspecific DNA hybridization in an effort to reduce the background signal but when this also reduced the positive signal when target DNA was introduced (**Figure 5.6A**). Buffer with 575 mM salt was used going forward to test further blocking conditions with 1% BSA or 1 mg/mL salmon sperm DNA. Neither incubation buffer produced an acceptable signal to noise ratio (**Figure 5.6B**).
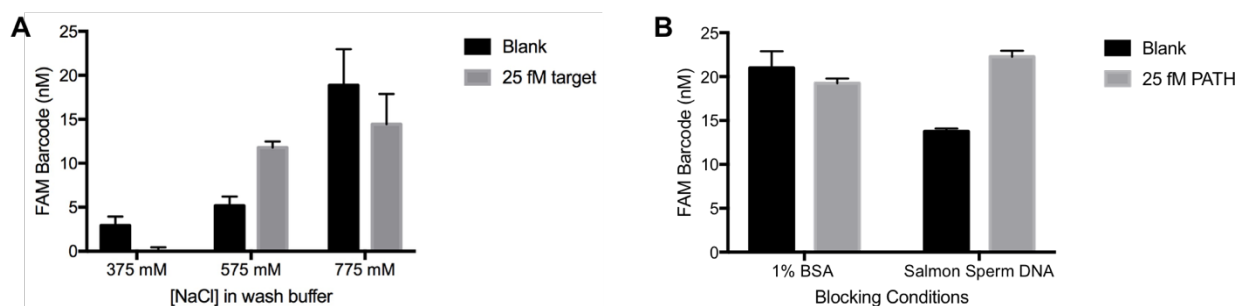
Figure 5.4. *FAM-labeled barcode DNA signal after different blocking conditions were used to screen nonspecific barcode-AuNP binding to functionalized amine magnetic beads. A) Varying NaCl concentration in AuNP incubation and wash buffer; B) The addition of 1% BSA and 1mg/mL salmon sperm DNA to 575 mM NaCl wash buffer.*

Next, streptavidin-coated magnetic beads were used as a base for the assay instead of amine-coated magnetic beads, because unbound free amines on the bead surface could have been interacting electrostatically with the barcode AuNPs. It is easy to passivate unbound binding sites on streptavidin beads with biotin while it is difficult to fully passivate the surface of amine-coated beads. These beads were tested with both positive and negative samples, incubated with barcode AuNPs in PBST, PBST with 5% BSA, and PBST with 1 mg/mL salmon sperm DNA
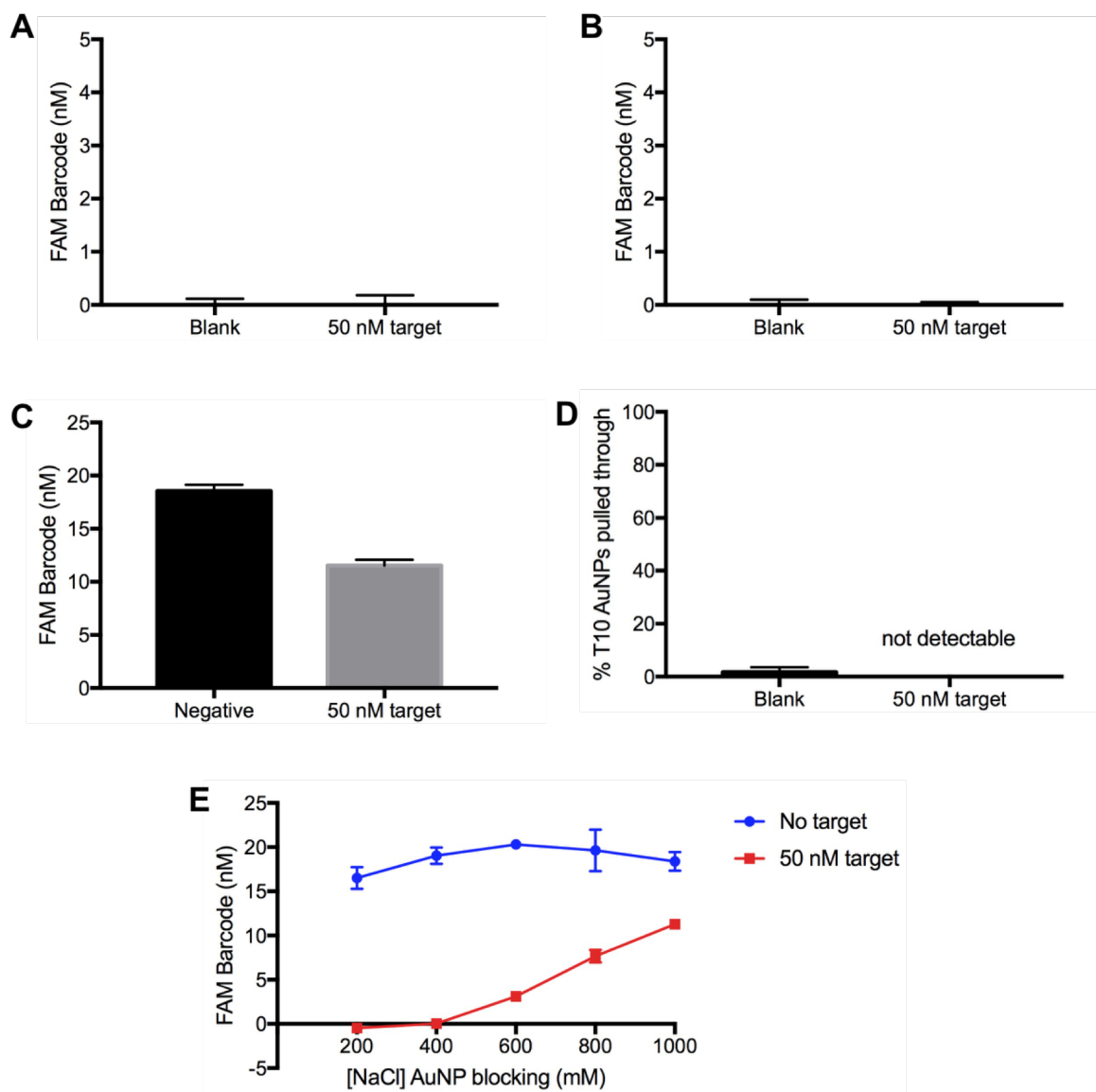
Figure 5.7. *Several blocking conditions were tested to reduce nonspecific binding of barcode AuNPs to streptavidin magnetic beads. A) PBST + 0.1% Tween-20 (PBST); B) PBST + 5% BSA; C) PBST + 1 mg/mL salmon sperm DNA. D) T10 AuNPs used in place of barcode AuNPs. E) Varying the NaCl concentration in PBST to encourage specific DNA hybridization.*

(**Figure 5.7A, B, and C**). Again, none of these conditions produced any signal to noise ratio to be useful, with some even producing no signal relative to pure buffer. Furthermore, several concentrations of NaCl in the PBST incubation buffer were tested to find a concentration to encourage specific binding (**Figure 5.7E**), but none of the concentrations tested produced a favorable result. To investigate this issue of nonspecific signal further, AuNPs functionalized

solely with short sequences of 10 thymine residues (T10 AuNPs) were tested in this assay

instead of barcode AuNPs. In this experiment, it appears that T10 AuNPs bind to streptavidin

magnetic beads only minimally (**Figure 5.7D**), so the specific DNA sequences used in this assay

may be to blame for the high background signal and low target signal. In order to mitigate this

issue, entirely new target sequences will have to be selected.

LFA optimization

Table 5.2. *Optimized experimental conditions for the lateral flow barcode detection assay.*

Experimental Condition	Values tested	Optimum value
LFA AuNP buffer	PBST; 5% BSA; 0.25% Tween-20; Denhardt's solution; 5% BSA, 0.25% Tween-20, 10% sucrose	5% BSA, 0.25% Tween-20, 10% sucrose
Nitrocellulose blocking	None; TBS pH 7.4, 0.015% casein, 0.3% PVP, 0.05% Tween-20	No blocking
Conjugate pad material	Whatman glass fiber, Millipore glass fiber	Millipore Glass fiber
Conjugate pad blocking	None; 50 mM borate buffer pH 9, 1% BSA, 1% PVP, 0.25% Triton X-100	50 mM borate buffer pH 9, 1% BSA, 1% PVP, 0.25% Triton X-100
Running buffer ionic strength	4X, 1X, 1/2X, 1/4X SSC	4X
Running time	10 min, 20 min, 30 min	20 min

Lateral flow assay (LFA) components and conditions were optimized empirically to

obtain the best limit of detection and dynamic range possible. This was achieved by choosing

conditions that minimized background binding of LFA AuNPs to the nitrocellulose membrane

while also allowing the assay sandwich to form effectively at the test and control lines. We

aimed to design a test that would detect barcode DNA that had been eluted into a water and

Tween-20 solution, preferably only using 5 μL of this eluted sample as this is a typical sample
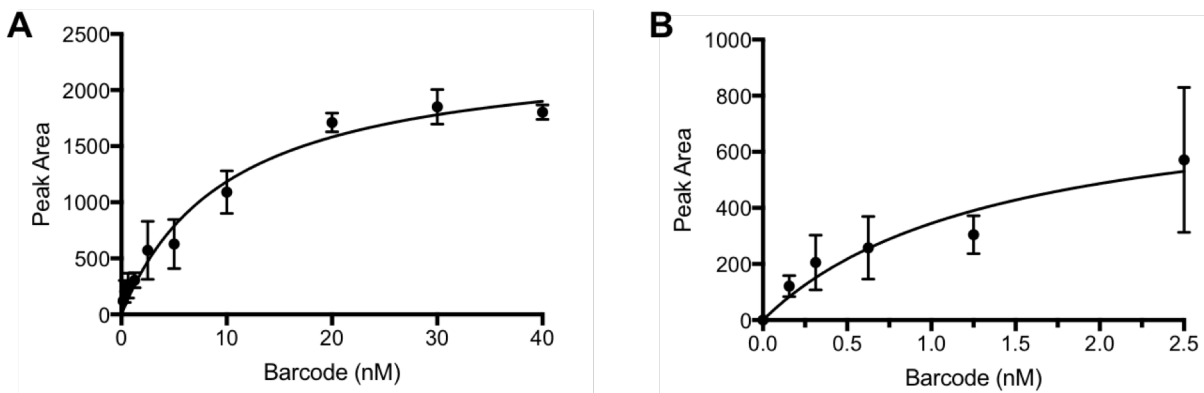
Figure 5.5. *A) The full binding curve using the optimized LFA to detect barcode DNA in buffer B) Zoomed-in binding curve from 0 – 2.5 nM showing the limit of detection of 0.156 nM barcode DNA in buffer.*

volume for commercial LFAs. In order to achieve this goal, the use of a conjugate pad was required to allow salts and blocking agents to be dried into the pad. If a half-strip (no conjugate pad) was used, mixing the water sample with LFA AuNPs in a test well caused the AuNPs to aggregate, which causes the test to lose all function. The components optimized for this assay were LFA AuNP buffer, nitrocellulose blocking, conjugate pad material, conjugate pad blocking, and running buffer composition, as summarized in **Table 5.2** above.

Once the conditions and parameters for the LFA were optimized, various concentrations of barcode DNA were diluted in PBS + 0.5% Tween-20 and run on the test to determine an approximate limit of detection (**Figure 5.8**). The optimized LFA can detect barcode DNA as low as 0.156 nM, which in theory would equate to roughly 2×10^7 barcode AuNPs being pulled through the assay to elution. This also equates, in theory, to 2×10^7 copies of target malaria DNA being captured by the magnetic beads. In a 100 μL sample, this would translate to an original biomarker concentration of 2×10^5 copies/μL minimum if all copies of the biomarker are bound by the beads. This is a very feasible concentration of this target DNA sequence in a malaria sample, corresponding to about 1% parasitemia in standardized cultures. Ideally this LFA would

101

be further optimized to further decrease the limit of detection to allow for the diagnosis of lower parasitemia patients.

Conclusion

This assay has produced new knowledge for the laboratory in terms of LFA optimization. The LFA for barcode DNA detection is the first full LFA developed in our laboratory, and holds great promise for future applications. The detection binding for this LFA is also entirely DNA hybridization-based, and therefore eliminates issues associated with antibody stability. If the AuNP binding in the bio-barcode assay can be optimized, then the entire bio-barcode-RDT assay will be functional as a low-resource method to detect malaria DNA in patient samples. Furthermore, any of the DNA sequences can be changed to suit future needs; different biomarker sequences for other diseases may be targeted by the capture beads and different sequences can be targeted by the LFA. Furthermore, the assay could be multiplexed to detect multiple malaria species or multiple diseases by using different barcode sequences for each target. Also, if a particular DNA or RNA sequence is present in a sample in high enough abundance, it is possible that the current DNA LFA sequences and buffer conditions could be modified to detect that biomarker from a patient sample without requiring the bio-barcode portion.

Furthermore, we have decreased the time it takes to isolate specific sequences of DNA. Previous work by our collaborators[20] showed that sequence-specific DNA isolation can take up to 3 hours to isolate 80% of a sample, making this type of DNA isolate seem unfeasible in a diagnostic setting. This work has shown that with the right buffer conditions, DNA can be isolated by sequence-specific hybridization in as little as 10 minutes, which opens the door for assays such as the bio-barcode assay that do not rely on downstream PCR for target-specific

detection. The roadblock of nonspecific AuNP binding still stands, but further work on this assay can be performed to minimize this binding.

Acknowledgements

References

(1) Gama, B. E.; Silva-Pires, F. do E. S.; Lopes, M. N. R.; Cardoso, M. A. B.; Britto, C.; Torres, K. L.; de Mendonça Lima, L.; de Souza, J. M.; Daniel-Ribeiro, C. T.; de Fátima Ferreira-da-Cruz, M. *Exp. Parasitol.* **2007**, *116*, 427–432.

(2) Rougemont, M.; Van Saanen, M.; Sahli, R.; Hinrikson, H. P.; Bille, J.; Jaton, K. *J. Clin. Microbiol.* **2004**, *42*, 5636–5643.

(3) Nwakanma, D. C.; Gomez Escobar, N.; Walther, M.; Crozier, S.; Dubovsky, F.; Malkin, E.; Locke, E.; Conway, D. J. *J. Infect. Dis.* **2009**, *199*, 1567–1574.

(4) Perandin, F.; Manca, N.; Calderaro, A.; Piccolo, G.; Galati, L.; Ricci, L.; Medici, M. C.; Arcangeletti, M. C.; Snounou, G.; Dettori, G.; Chezzi, C. *J. Clin. Microbiol.* **2004**, *42*, 1214–1219.

(5)   Putaporntip, C.; Buppan, P.; Jongwutiwes, S. *Clin. Microbiol. Infect.* **2011**, *17*, 1484–1491.

(6)   Isozumi, R.; Uemura, H.; Kimata, I.; Ichinose, Y.; Logedi, J.; Omar, A. H.; Kaneko, A. *Emerg. Infect. Dis.* **2015**, *21*, 490–492.

(7)   Polley, S. D.; González, I. J.; Mohamed, D.; Daly, R.; Bowers, K.; Watson, J.; Mewse, E.; Armstrong, M.; Gray, C.; Perkins, M. D.; Bell, D.; Kanda, H.; Tomita, N.; Kubota, Y.; Mori, Y.; Chiodini, P. L.; Sutherland, C. J. *J. Infect. Dis.* **2013**, *208*, 637–644.

(8)   Oriero, E. C.; Geertruyden, J.-P. Van; Nwakanma, D. C.; D'Alessandro, U.; Jacobs, J. *Expert Rev. Mol. Diagn.* **2015**, *7159*.

(9)   Han, E. T.; Watanabe, R.; Sattabongkot, J.; Khuntirat, B.; Sirichaisinthop, J.; Iriko, H.; Jin, L.; Takeo, S.; Tsuboi, T. *J. Clin. Microbiol.* **2007**, *45*, 2521–2528.

(10)   Singleton, J.; Osborn, J. L.; Lillis, L.; Hawkins, K.; Guelig, D.; Price, W.; Johns, R.; Ebels, K.; Boyle, D.; Weigl, B.; LaBarre, P. *PLoS One* **2014**, *9*, e113693.

(11)   Rohrman, B. A.; Leautaud, V.; Molyneux, E.; Richards-Kortum, R. R. *PLoS One* **2012**, *7*.

(12)   Yongkiettrakul, S.; Jaroenram, W.; Arunrut, N.; Chareanchim, W.; Pannengpetch, S.; Suebsing, R.; Kiatpathomchai, W.; Pornthanakasem, W.; Yuthavong, Y.; Kongkasuriyachai, D. *Parasitol. Int.* **2014**, *63*, 777–784.

(13)   Mens, P. F.; de Bes, H. M.; Sondo, P.; Laochan, N.; Keereecharoen, L.; van Amerongen, A.; Flint, J.; Sak, J. R. S.; Proux, S.; Tinto, H.; Schallig, H. D. F. H. *J. Clin. Microbiol.* **2012**, *50*, 3520–3525.

(14)   Rodriguez, N. M.; Wong, W. S.; Liu, L.; Dewar, R.; Klapperich, C. M. *Lab Chip* **2016**.

(15)   Nam, J.-M.; Stoeva, S. I.; Mirkin, C. A. *J. Am. Chem. Soc.* **2004**, *126*, 5932–5933.

(16)   Taton, T. A.; Mirkin, C. A.; Letsinger, R. L. *Science* **2000**, *289*, 1757–1760.

(17)   Bitting, A. L.; Bordelon, H.; Baglia, M. L.; Davis, K. M.; Creecy, A. E.; Short, P. A.;

Albert, L. E.; Karhade, A. V.; Wright, D. W.; Haselton, F. R.; Adams, N. M. *J. Lab.*

Autom. **2016**, *21*, 732–742.

(18)   Russ, P. K.; Karhade, A. V; Bitting, A. L.; Doyle, A.; Solinas, F.; Wright, D. W.;

Haselton, F. R. *J. Lab. Autom.* **2016**, *21*, 590–598.

(19)   Gerstein, A. S. *Molecular Biology Problem Solver: A Laboratory Guide*; Gerstein, A. S.,

Ed.; Wiley, 2004.

(20)   Adams, N. M.; Bordelon, H.; Wang, K. K. A.; Albert, L. E.; Wright, D. W.; Haselton, F.

R. *ACS Appl. Mater. Interfaces* **2015**, *7*, 6062–6069.

CHAPTER VI

CONCLUSION AND PERSPECTIVES

This dissertation encompasses work performed in the advancement of both protein- and DNA-based malaria diagnostics. As malaria control efforts mature into malaria elimination efforts, sensitive and accurate point-of-care diagnostics will be extremely important tools. Most current point-of-care diagnostics detect protein biomarkers such as *Pf*HRP2 or *p*LDH. These tests can accurately diagnose symptomatic infections, but become more unreliable at low parasite densities, when the patient typically does not present symptoms. These tests can also be degraded by heat and humidity because they are antibody-based. As an alternative, the malaria community has recently focused its efforts on DNA-based diagnostics that are accessible in a low-resource setting. DNA can provide more diagnostically-relevant information than protein, and it is more stable than protein in typical working conditions. It can also be amplified using a variety of enzymatic reactions, if necessary, although these reactions are often technically demanding and not well-suited to low-resource settings. The work presented here sought to improve upon these issues with protein and DNA diagnostics in several ways.

First, a fluorescent detection method for *Pf*HRP2 was described that relies on a transition metal compound rather than enzyme-tagged antibodies to produce signal. This system is more stable than an antibody-based detection system, and was incorporated into an on-bead sandwich assay similar to an ELISA. The on-bead assay work best in a laboratory setting, but it could also potentially be incorporated into a field diagnostic for *Pf*HRP2. The "switch-on" fluorescence capabilities could be used in conjunction with a UV pen light or a portable fluorimeter to read

fluorescence, and the mixing of the iridium reagent and *Pf*HRP2 could be accomplished by any number of easy-to-use devices, including a "glow stick" device. In the next chapter, the structure of rc*Pf*HRP2 in the presence of heme was investigated using circular dichroism. Heme binding causes the protein to adopt a more helical structure than its typical unstructured form, and this shift in structure also adversely affects the protein's ability to bind to antibodies on RDTs and in ELISAs. The effects of heme could be further investigated on native *Pf*HRP2 to ensure that these results are not unique to the recombinant protein. If they are not replicated by the native protein, then this brings up important questions about using recombinant *Pf*HRP2 as a standard in diagnostic assays.

Work then transitioned to focus on DNA-based diagnostics due to the valuable information that DNA biomarkers can provide, and the large unmet need for point of care DNA diagnostic tests. Because sample preparation can be a bottleneck for DNA diagnostics, initial work focused on simplifying the DNA extraction process into an automated format. This device was then expanded to include PCR in-line with the extraction to eliminate the manipulation and technical difficulties of setting up an external PCR reaction. In a low-resource setting, this would allow an unskilled operator to input a raw sample into the device and receive a reliable PCR result without performing any technically-demanding procedures. These devices work well, but still rely on PCR amplification and data analysis to obtain a result. In the next chapter, a DNA-based RDT was developed to bring DNA diagnostics to the point of care. The RDT uses DNA hybridization to form a "sandwich" similar to a typical antibody-based RDT, which could allow the RDT to be customized to detect nearly any sequence of DNA simply by changing the capture and detection DNA sequences attached to the RDT membrane and detection AuNPs. This RDT was optimized to detect a "barcode" DNA sequence, as part of the bio-barcode assay. The bio-

barcode assay is a way to amplify target DNA by hybridizing the capture target to a gold nanoparticle tagged with hundreds of barcode DNA sequences. When the barcode sequences are released, the signal from one target DNA strand is amplified to a level detectable by the RDT. The particular bio-barcode assay developed in this chapter has issues with nonspecific binding of barcode AuNPs in a negative sample, so unfortunately the two aspects of this assay were never combined with good results. However, redesigning the capture sequences to target a different malaria DNA sequence may reduce nonspecific binding and increase the signal to noise ratio, thus allowing the two aspects of this assay to be combined as a low-resource DNA-based RDT.

Overall, this work follows the transition in the malaria diagnostics community from protein-based methods to DNA-based methods. Protein still has its uses in RDTs, especially because these tests are already familiar to clinicians and are monitored by WHO for quality purposes. There is still ongoing research, especially in our research group, to improve upon current protein diagnostics and to develop new protein-based assays for the point of care. The first half of this dissertation focused on improving protein diagnostics with a new metal-based assay and by further understanding the protein biomarker and its structure. However, DNA diagnostics can provide a wealth of clinically relevant information, and there is currently a shortage of new point-of-care DNA diagnostic techniques. In order to bring the value of DNA diagnostics to low-resource settings, the malaria diagnostic community needs to move beyond PCR amplification methods and investigate new combinations of techniques to amplify DNA so that it can be detected with low-resource, point-of-care technology. The second half of this dissertation sought first to make PCR more accessible for low-resource settings, and then sought to develop a new assay that could be read using a point-of-care RDT.

In the future, our research group will pursue both protein-based and DNA-based diagnostics with the ultimate goal of providing user-focused diagnostics to low-resource settings. Ultimately, the best diagnostic is one that can be easily used and understood by the person administering it. In most of the world, the person administering a diagnostic test is most likely not a doctor or even a trained clinic worker, so we seek to develop tests that can be understood by laypeople. This requires a long, iterative development process, but I believe our laboratory can make great strides in this area. We are focused on user-friendly designs and are willing to test devices in the field, then bring them back to Vanderbilt to make changes based on what was observed during the field trials, and test them in the field again. We can only effectively accomplish our goal by making changes based on data and observations, and we have the capacity to do so with our collaborators in Macha, Zambia. It is my hope that the work described here will contribute to and act as a stepping stone for future protein-based and DNA-based diagnostic assays for malaria.

The DNA diagnostic work presented here also has applications outside the malaria community. DNA-based diagnostics can be used for any pathogenic disease – those caused by bacteria, viruses, or other microorganisms. In these cases, the disease-causing agent has its own genetic code distinct from the human host, and this genetic material can be detected as a biomarker. The presence of certain genetic sequences can confirm disease and also inform treatment, making DNA an attractive target for low-resource diagnostics development. This means that with effective development, one DNA test format can be applied to a multitude of diseases, such as tuberculosis, Zika virus, Ebola, and any type of bacterial infection. Adapting a DNA test for a different disease can also be done very quickly, simply by changing the DNA sequences in the test to be complementary for a disease-specific target sequence. Some re-

optimization of the test may be necessary, but all of this could reasonably be accomplished within a couple of months. In comparison, developing new antibodies to use in immunoassays can take several months to a year, which is less desirable. A fast turnaround time to develop a diagnostic assay is especially important for emerging diseases such as Zika and Ebola, due to the devastation that can be caused without proper diagnosis and treatment. Due to this versatility of DNA diagnostics and the wealth of information they can provide, developing low-resource DNA-based tests is of great interest to the greater infectious disease community. The techniques used in this work show great promise in this regard, and with further development I hope that we can see the widespread use of low-resource DNA tests in the near future.

SUPPORTING INFORMATION: CHAPTER II
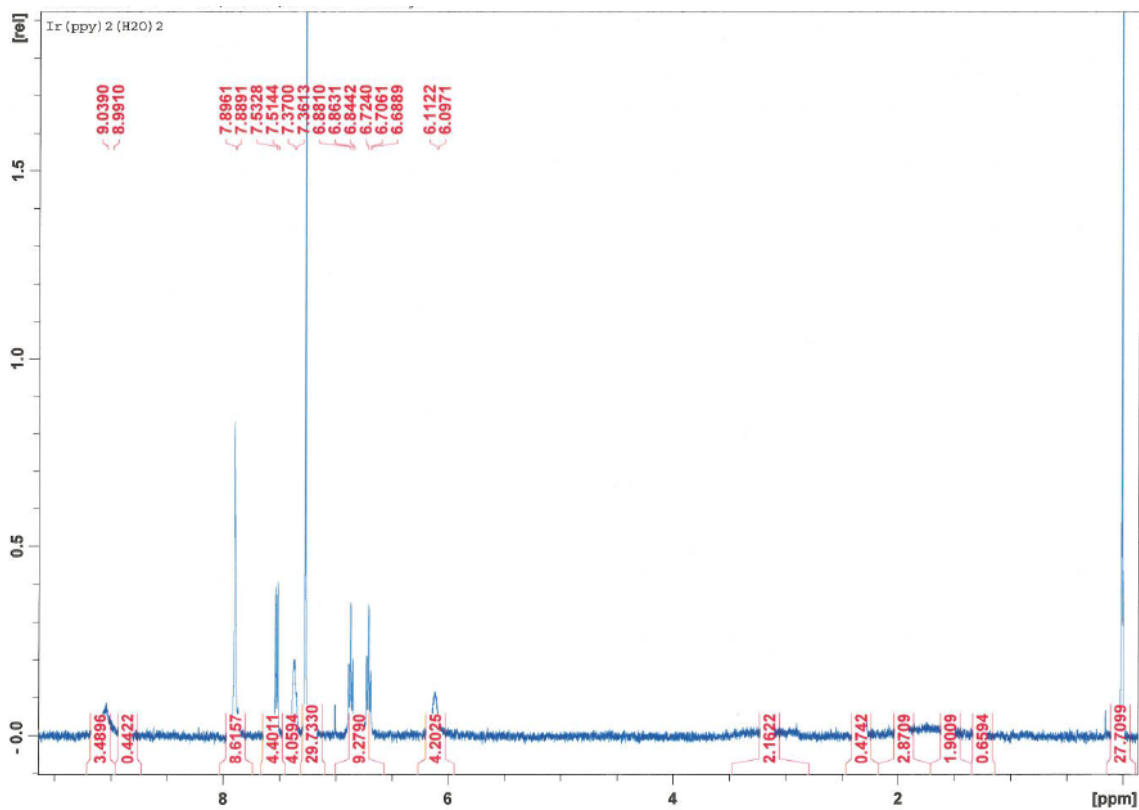
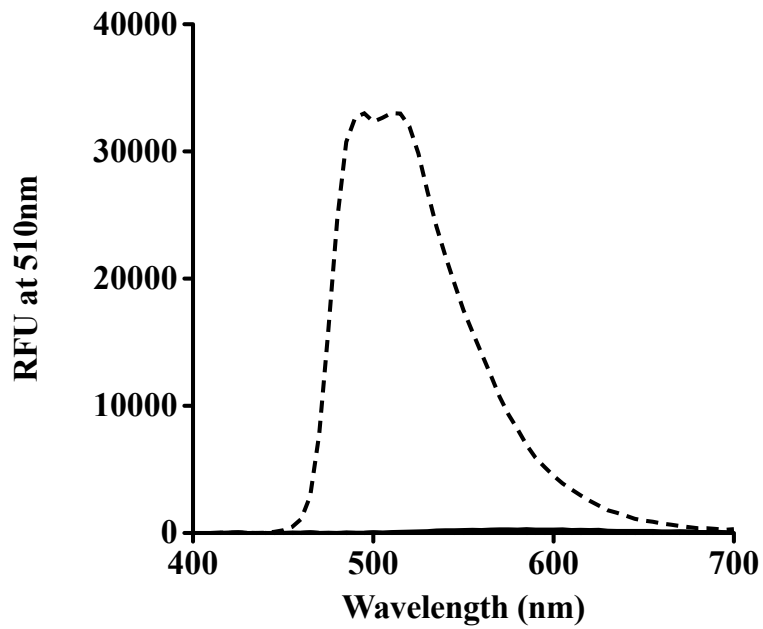***Supporting Information Figure II.1.*** *^{1}H NMR of **Ir1**.*
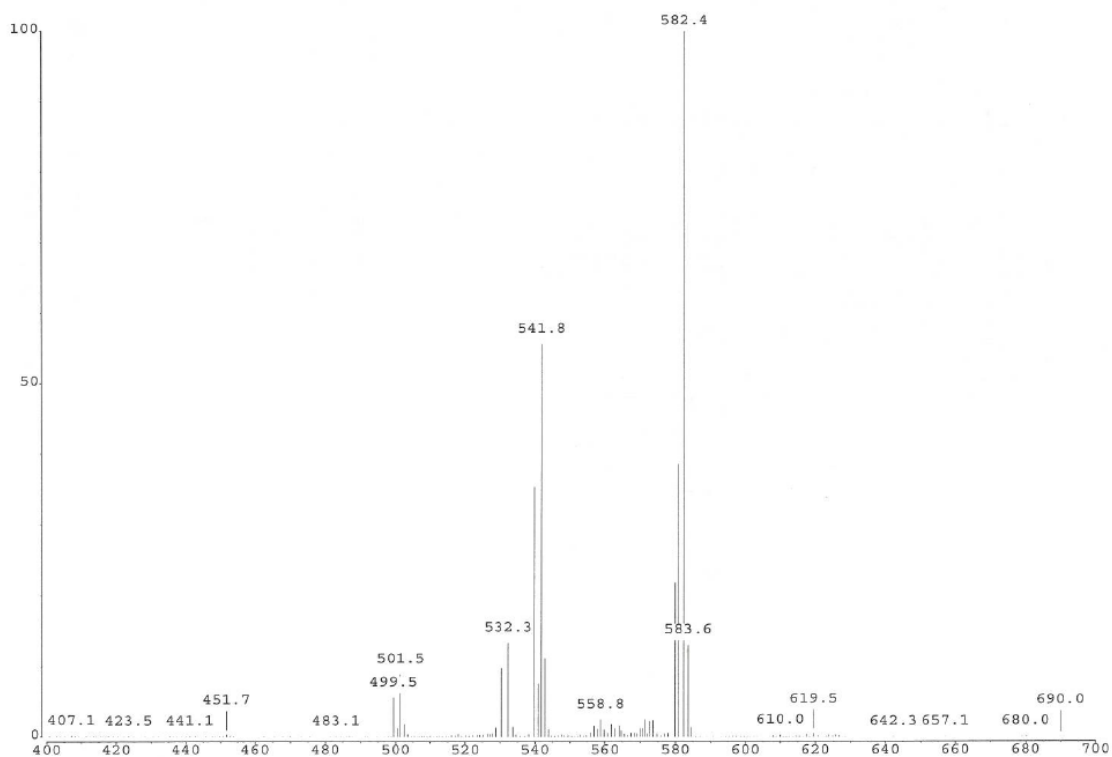
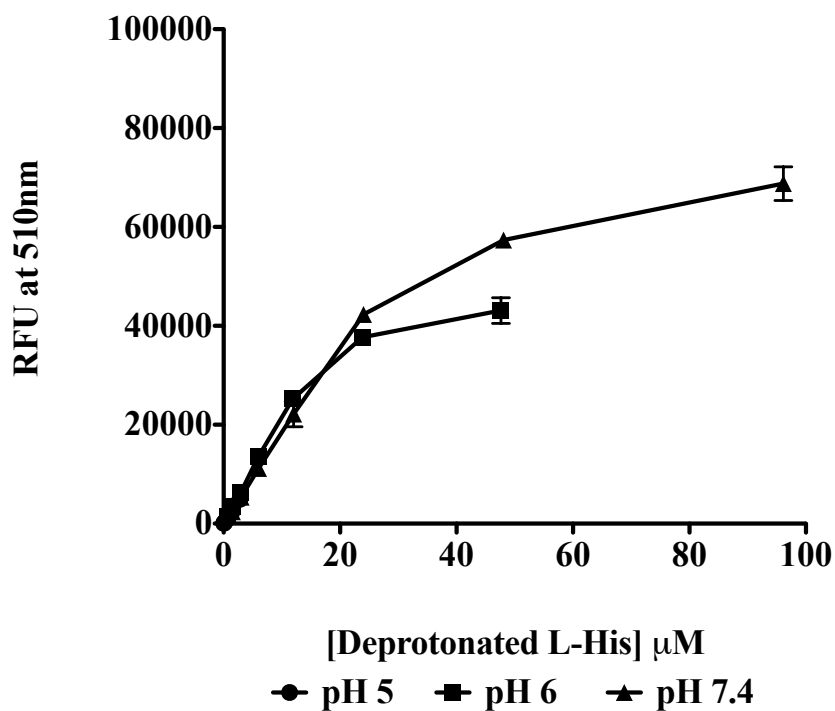***Supporting Information Figure II.2.*** *ESI-MS of* **Ir1***.*
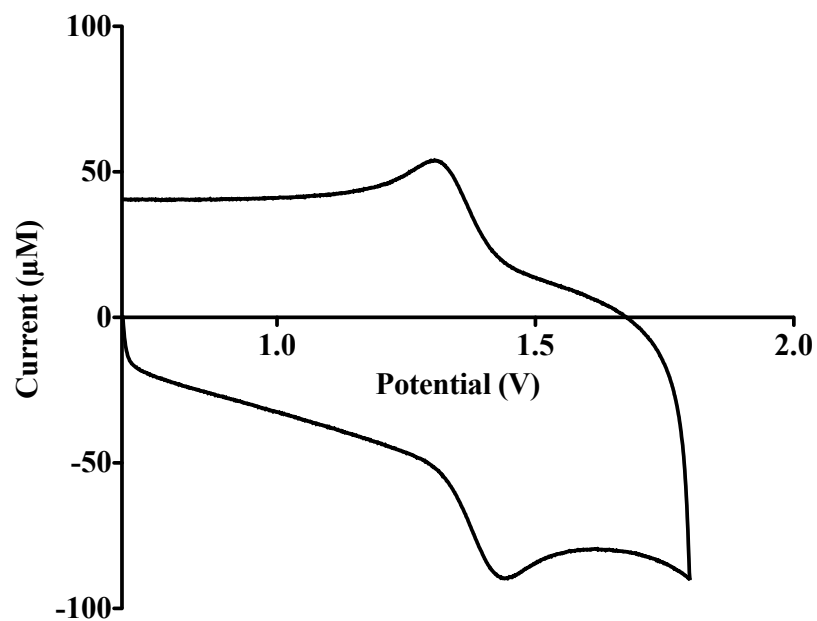
Supporting Information Figure III.3. *Cyclic Voltammetry of **Ir1**.*
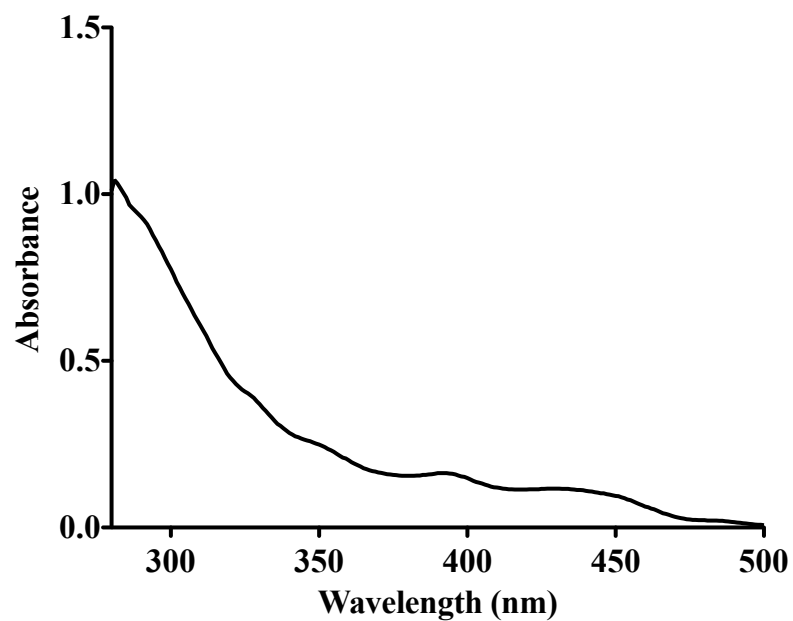
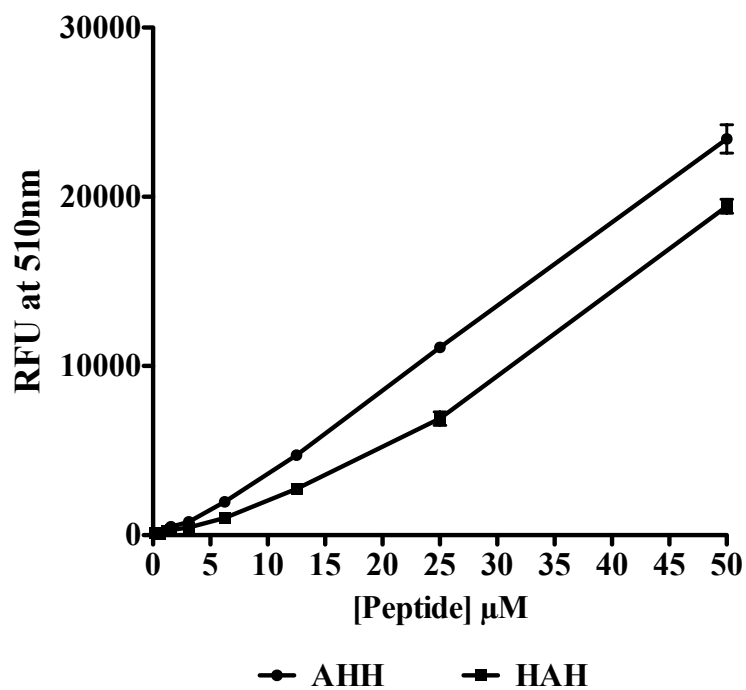***Supporting Information Figure II.4.*** *UV-Visible spectrum of 100μM **Ir1** in MeOH.*

Supporting Information Figure II.5. *Amino Acid selectivity of 50μM **Ir1** with 10μM solutions of amino acids in 100mM HEPES buffer with 137 mM NaCl (HBS). Ala, Asp, Cys, Ile, Lys, Phe, Ser, Trp and Val were all negligible. Histidine is shown as a dashed line.*
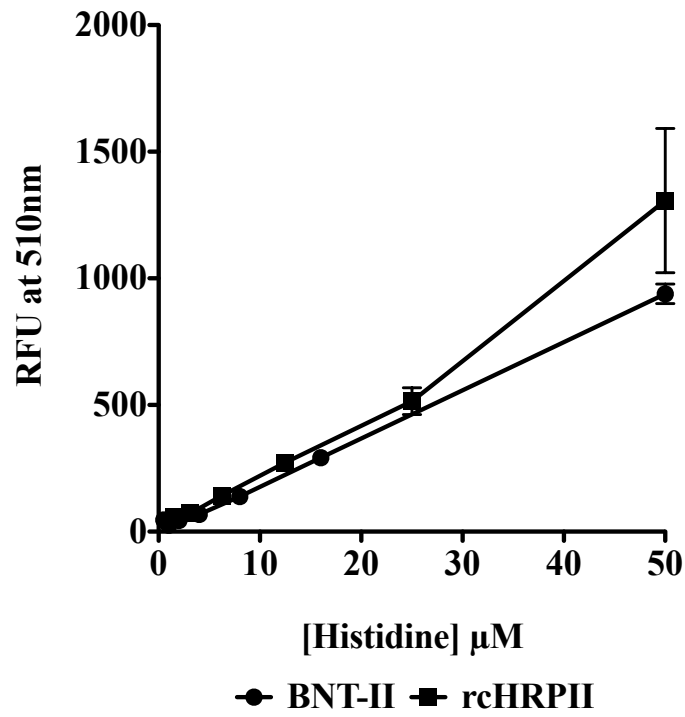
Supporting Information Figure II.6. *Signal intensity of L-His with 50 µM **Ir1** as a function of concentration of deprotonated histidine at each pH.*

| Sample	Quantum Yield
Ir1	<0.1%
Ir1/L-His	7.0%
Ir1/BNT-II	8.3%

Supporting Information Figure II.7. *Quantum yield of 50 µM **Ir1** with 400 µM L-His and 100 µM BNT-II in HBS. Quinine sulfate was used as the reference compound (Φ=0.546 in 0.5M H₂SO₄; λex=366nm).*

115

Supporting Information Figure II.8. *Signal intensity of tripeptides AHH and HAH with 50 μM **Ir1** in HBS. Tripeptides were allowed to incubated with **Ir1** for 10 minutes before measuring signal at 510 nm (365 nm ex). $Slope_{AHH} = 456 \pm 9$. $Slope_{HAH} = 356 \pm 19$. While the two curves are statistically different, this data shows that **Ir1** can bind both adjacent and split histidine residues within the AHHAHHAAD motif of PfHRP2.*
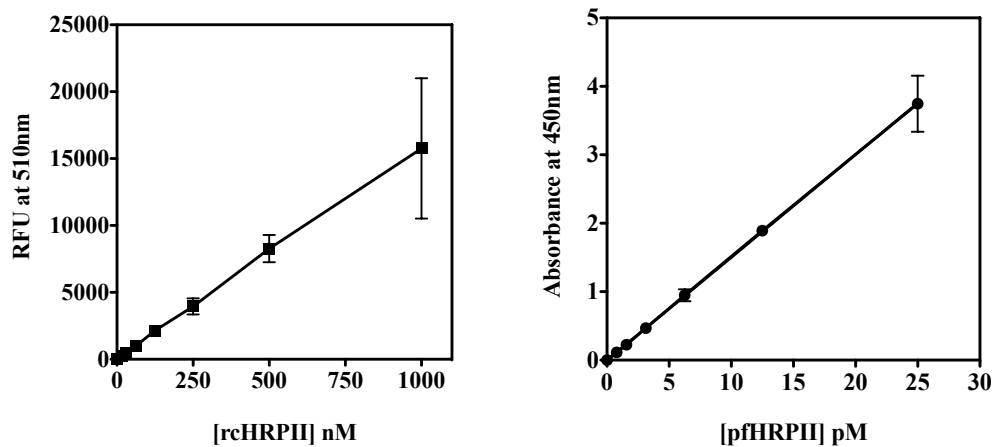
Supporting Information Figure II.9. *Correlation between relative fluorescence signal intensity and concentration of total histidine in BNT-II and rcHRP2 with 50 µM **Ir1** in HBS*.
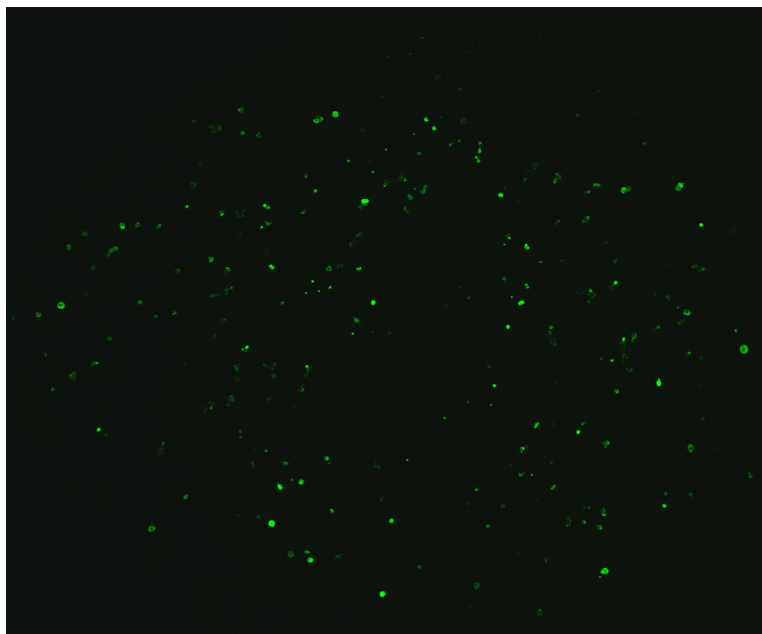
Supporting Information Figure II.10. *Visualization of **Ir1** signal with 100 μM BNT-II bound to the surface of 50 μM NI(II)NTA agarose particles deposited on a glass slide. Fluorescence was imaged under fluorescence microscopy (Nikon TE2000U inverted fluorescence microscope).*
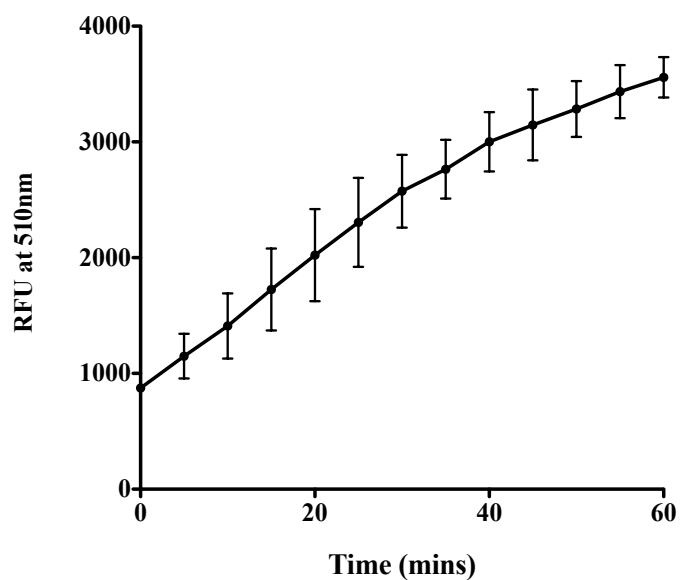
Supporting Information Figure II.11. *Signal generated from 50 μM **Ir1** coordinating to 100 nM rcHRP2 bound to the surface of 50 μm Ni(II)NTA agarose particles over 60 minutes.*

Supporting Information Figure II.12*. Side by side comparison of the linear range of our on-bead **Ir1** assay (left graph) and a traditional ELISA (right graph) for the detection of PfHRP2. The slope of the line for the on-bead assay and ELISA are 15.93 ± 0.13 and 0.1502 ± 0.0003, respectively.*